Application of Visible Light Absorbing Catalysts Basing on Silver Salts in Blue-green Algal Toxic Metabolites (Microcystins) Removal

May 2013

Xin WANG

Application of Visible Light Absorbing Catalysts Basing on Silver Salts in Blue-green Algal Toxic Metabolites (Microcystins) Removal

A Dissertation Submitted to

the Graduate School of Life and Environmental Sciences,

the University of Tsukuba

in Partial Fulfillment of the Requirements

for the Degree of Doctor of Philosophy in Biotechnology

(Doctoral Program in Bioindustrial Sciences)

Xin WANG

Abstract

As the increasing human activities, organic pollution has become an urgent issue needing to be tackled. Microcystins (MCs), produced by various cyanobacteria such as *Microcystis*, *Anabaena*, *Oscillatoria* and *Nostoc* species, are a group of potent hepatotoxins for humans and wildlife. The MCs-related issues are of increasing concern all over the world. There are more than 90 microcystin variants among which MC-LR, MC-YR and MC-RR are three common toxic variants and MC-LR possesses the most toxic effect. Moreover, MCs exhibit a stable property against physicochemical and biological factors including temperature, sunlight and enzymes. Photocatalysis for which solar light can be employed greatly arouses the attention of wastewater researchers as solar light is a type of costless, durable and pollution free resource. Although titania has been employed as a typical photocatalyst to remove MCs owing to its excellent stability and high photoactivity under ultraviolet (UV) light, the majority of studies tend to exploit visible-sensitive material to remove MCs due to visible light accounts for about 42% of solar light. Recently, Silver phosphate (Ag_3PO_4), a novel visible light sensitive photocatalyst, has been reported to be highly efficient in splitting water and removing organic pollutants compared with traditional catalysts such as WO_3, $TiO_{2-x}N_x$, $BiVO_4$. However, it's a pity that this material has a character of self-photocorrosion. In this study, a series of experiments were conducted, attempting to alleviate the photo-corrosion of Ag_3PO_4 and achieve a highly efficient and relatively stable photocatalyst for successive application in degrading MCs under simulated solar light irradiation.

The first attempt is to prepare Ag/Ag_3PO_4 heterojunction. The results clearly indicated that MC-LR was much more easily degraded by the Ag/Ag_3PO_4 catalysts than Ag_3PO_4 alone owing to the change of Ag_3PO_4 morphology and deposition of Ag nanoparticles (NPs) on Ag_3PO_4 after

irradiation treatment. It is also indicated that the photocatalic efficiency of Ag/Ag_3PO_4 was affected by catalyst dosage and light intensity, respectively. Besides, the oxidation of the microcystins over this heterojunction catalyst was observed to exhibit rather differently with the removal efficiency following the trend: MC-YR > MC-RR > MC-LR. One more aspect worth noticing was that the ratio of Ag NPs and Ag_3PO_4 for the best photocatalytic activity of the Ag/Ag_3PO_4 heterojunction in degrading MC-LR was not the one for the most stable state of it.

The continual dissolved Ag_3PO_4 was thought to be the main reason for the unstable state of Ag/Ag_3PO_4. Therefore, another hybrid $AgBr/Ag_3PO_4$ was prepared by producing a low solubility film of AgBr surrounding Ag_3PO_4. The $AgBr/Ag_3PO_4$ was observed to possess much greater photocatalytic efficiency in degrading MCs under simulated solar light condition. However, the photo-corrosion phenomenon cannot be avoided during photocatalysis under simulated solar light irradiation, since AgBr was also a type of photo-corrosive silver salt, although Ag_3PO_4 was relatively stable in this heterojunction.

Thus, titania (TiO_2) of which the photocatalytic activity can be accelerated by Ag^0 was then combined with the hybrid $AgBr/Ag_3PO_4$ by *in situ* deposition method. This heterojunction $AgBr/Ag_3PO_4/TiO_2$ is expected to alleviate the decrease of photocatalytic capacity of $AgBr/Ag_3PO_4$ caused by the loss of AgBr during photocatalytic process. The results clearly indicated that $AgBr/Ag_3PO_4/TiO_2$ possessed higher photocatalytic capacity than $AgBr/Ag_3PO_4$ in degrading MCs under the simulated solar light condition, which was attributed to the increased surface area and the combined action among Ag nanoparticles (NPs), AgBr, Ag_3PO_4 and TiO_2. In addition, $AgBr/Ag_3PO_4/TiO_2$ heterostructured photocatalyst was observed to be more stable than unsupported $AgBr/Ag_3PO_4$ in successive photocatalysis under simulated solar light

condition. Furthermore, $AgBr/Ag_3PO_4/TiO_2$ kept high photocatalytic activity in degrading MC-LR under various conditions (e.g., pH, anions, cations and humic acid).

This heterostructured $AgBr/Ag_3PO_4/TiO_2$ catalyst not only possesses great photocatalytic activity under simulated solar light irradiation, but also significantly decreases the loading of noble metal Ag from 72 wt% to 53 wt%, thereby significantly reducing the cost for the practical application of $AgBr/Ag_3PO_4$ photocatalyst. Therefore, this photocatalyst would be required, and possesses greatly potential application in the photocatalytic field.

Contents

Chapter 1 Introduction

1.1. Background

1.1.1. Origin and distribution of blue-green algae

Blue-green algae (cyanobacteria), which are one of the largest and most important groups of bacteria on earth, have the distinction of being the oldest known fossils, more than 3.5 billion years old. Although they are most closely related to bacteria, they contain chlorophyll and depend on sunlight to grow, like plants (Gupta *et al.*, 2013).

Many Proterozoic oil deposits are attributed to the activity of cyanobacteria (Parmar *et al.*, 2011). They are also important providers of nitrogen fertilizer in the cultivation of rice and beans (Gupta *et al.*, 2013). The cyanobacteria have also been tremendously important in shaping the course of evolution and ecological change throughout earth's history. The oxygen atmosphere that we depend on was generated by numerous cyanobacteria during the Archaean and Proterozoic Eras. The other great contribution of the cyanobacteria is the origin of plants (Gupta *et al.*, 2013). Sometime in the late Proterozoic, or in the early Cambrian, cyanobacteria began to take up residence within certain eukaryote cells, making food for the eukaryote host in return for a home. This event is known as endosymbiosis, and is also the origin of the eukaryotic mitochondrion (Parmar *et al.*, 2011).

Cyanobactera, as a naturally occurring part of the food chain, can be found in almost every terrestrial and aquatic habitat: In oceans, fresh water, even bare rock and soil. They can occur as planktonic cells or form phototrophic biofilms in fresh water and marine environments, they occur in damp soil, or even on temporarily moistened rocks in deserts.

Aquatic cyanobacteria are probably best known for the extensive and highly visible blooms that can form in both freshwater and the marine environment and can have the appearance of blue-green paint or scum.

1.1.2. Occurrence of blue-green algae bloom

The occurrence of cyanobacteria is natural and has occurred throughout history. Still, as the increasing human activities, cyanobacteria bloom in aquatic habitat has been a worldwide problem (Figure 1-1), which have resulted in widespread deterioration of the quality of surface water, especially in lakes and reservoirs (Wang *et al.*, 2011b). During the bloom, generally, a green layer of cyanobacteria will form on surface water as cyanobacteria are capable of floating up which are manipulated by gas vesicle in its cell (Damerval *et al.*, 1991). Most of cyanobacteria prefer living in warm aquatic habitat, which therefore resulting in the algal bloom mostly happening in summer.

The cyanobacteria were traditionally classified by morphology into five sections as: Chroococcales, Pleurocapsales, Oscillatoriales, Nostocales and Stigonematales. The most dominant bloom forming cyanobacterial genera responsible for these mass occurrences are: *Anabaena, Aphanazomenon, Cylindrospermopsis, Gloeotrichia, Oscillatoria, Rivularia, Lyngbya, Microcystis, Nostoc* and *Planktothrix* (Anagnostidis and komarek, 1985).

1.1.3. Main causes for cyanobacteria bloom

Eutrophication is widely proved to be the main reason for the outbreak of cyanobacteria, which often arises from anthropogenic pollution with nutrients, particularly the release of sewage effluents and agricultural run-off carrying fertilizers into natural waters (Cao *et al.*, 2011; Paerl, 2006; Sellner *et al.*, 2003; Wang *et al.*, 2011).

Among inorganic nutrients, nitrogen is of paramount importance as it accounts for 10% of the dry weight of cyanobacterial cells. Nitrate (NO_3^-) and ammonium (NH_4^+) are virtually universal sources of nitrogen for cyanobacteria, but urea or other organic nitrogenous compounds can be also used by some strains (Davidson *et al.*, 2012). Meanwhile, many, but not all, cyanobacteria are able to fix N_2. The process is carried out by the enzyme nitrogenase and is a costly one, involving the consumption of both ATP and reduction equivalents (supplied by ferredoxin).

Another essential nutrient for the growth of cyanobacteria was phosphate (Falkner *et al.*, 1984). Phosphate is incorporated via facilitated diffusion into the cell, where it is converted by photophosphorylation into the metabolized fraction (mainly polyphosphates). The bloom lasted as long as the phosphate concentration was above the threshold value of the algal material under the respective ecological condition. Algal growth cease when the phosphate concentration drops below the threshold value (Sellner *et al.*, 2003).

In additional, increasing inputs of N and P are often associated with declining silicon contributions due to a number of river management strategies such as dam construction, leading to lower available silicon for diatom production and greater contributions of non-siliconrequiring species like Phaeocystis, dinoflagellates, and prymnesiophytes (Sellner *et al.*, 2003).

1.1.4. Production of microcystins (MCs) by blue-green algae

Microcystins (MCs), produced by various cyanobacteria such as *Microcystis*, *Anabaena*, *Oscillatoria* and *Nostoc* species, are a group of potent hepatotoxins for humans and wildlife, which is of increasing concern all over the world (Rodr ǵuez *et al.*, 2008). There are more than 90 microcystin variants among which MC-LR, MC-YR and MC-RR are three common toxic

variants and MC-LR possesses the most toxic effect (Li *et al.*, 2009). MC-LR, in particular, is known to be produced by species belonging to the genera *Anabaena*, *Microcystis*, *Nostoc* and *Anabaenopsis*. And MC-YR is produced by *Microcystis aeruginosa* and *Hapalosiphon* spp.. MC-RR has been isolated from *Oscillatoria agardhii* and *Microcystis aeruginosa* (Dow and Swoboda, 2000; WHO, 2003).

1.1.5. Structure of MCs

MCs have a general structure comprised of five amino acids with minor variations (D-alanine, D-erythro-*b*methyl aspartic acid, D-glutamic acid, N-methyldehydroala methyldehydroalanine and Adda (3-amino-9-methoxy-2,6,8-trimethyl-10-phenyldeca- 4,6-dienoic acid)) and a pair of variable L-amino acids (Figure 1-2).

1.1.6. Hazards of MCs

Cyanobacterial toxins are naturally produced poisons stored in the cells of certain species of cyanobaceria. These toxins fall into various categories. Some are known to attack the liver (hapatotoxins) or the nerous system (neurotoxins); others simply irritate the skin. These toxis are usually released into water when the cells rupture or die (Oberholster *et al.*, 2004). Scientists are more concerned about hepatotoxins than neurotoxins, because neurotoxins are not considered to be as wide spread as hepatotoxins in water supplies. Microcystin has been reported to be a kind of hapatotoxins, associating with acute liver damage and possibly liver cancer in laboratory animals (Lora *et al.*, 2002). In mammals, MCs are selective for hepatic cells, irreversibly inhibiting serine/threonine protein phosphatease PP1 and PP2A (Hiripi *et al.*, 1998). In mice, the intraperitoneal LD_{50} values for MC-LR, -YR, and -RR are 50, 70, and 300-500 μg kg^{-1} of body weight, respectively, which suggesting the most toxic effect of MC-LR. Furthermore, studies collected for human poisoning assessment reveal that MC would cause acute and chronic effects

on humans and even death (Pouria *et al.*, 1998). As a result of the concerns about the harmful effect of MCs, the guidelines for these toxins have been defined by World Health Organization (WHO). In particular, a guideline value of 1 μg L^{-1} for MC-LR in drinking water has been issued (WHO, 1998).

Consequently, the cyanobacteria which can produce MCs would be dangerous to humans and animals. Because they bloom in freshwater and marine habitats, which may cause mass mortalities of fish and other animals.

1.2. Previous studies on MCs removal

MCs exhibit a stable property against physicochemical and biological factors including temperature, sunlight and enzymes (Harada *et al.*, 1996; Miao *et al.*, 2010; Okano *et al.*, 2006; Tsuji *et al.*, 1994). Conventional water treatment methods such as flocculation, coagulation, sedimentation and filtration are ineffective in removing dissolved (extracellular) MCs (Himberg *et al.*, 1989; Mouchet *et al.*, 1998; Chow *et al.*, 1999; Newcombe and Nicholson, 2004). Still, several attempts have been made to address the issue of MCs to date, including biological, physical and chemical treatments.

1.2.1. Present treatments for MCs removal

(1) Biological treatment

Biodegradation has been proved to be an efficient way to remove MCs. Many studies revealed that MCs can be naturally degraded by MCs degradation bacteria existed in bottom sediment in reservoir or lake (Eleuterio and Batista, 2010; Li *et al.*, 2011). The biodegradation pathway for MCs by single bacteria strain was described as a three-step process which involves linearisation of MC molecule, formation of a tetrapeptide and subsequent hydrolysis of these products

catalysed by three enzymes MlrA, MlrB and MlrC, respectively (Bourne *et al.*, 1996). Although biological treatment is a low cost method for MCs removal, the degradation efficiency is readily affected by environmental factors, such as pH, temperature and toxic coexisting ions (e.g. metal ions).

(2) Physical treatment

Adsorption by activated carbon and separation by membrane techniques have been prove to be two effective physical methods to remove MCs (Gijsbertsen-Abrahamse *et al.*, 2006; Ho *et al.*, 2011; Lambert *et al.*, 1996). However, the adsorption efficiency is greatly affected by the loading of coexisting organic chemicals (e.g. humic acid), which would shorten the service life of adsorbents and membrane.

(3) Chemical treatment

Advanced oxidation processes (AOPs) including chlorination, ozonation, hydrogen peroxide disinfect, electrolysis and photocatalysis etc. have been proved to be efficient to remove MCs (Ho *et al.*, 2006; Jacinto *et al.*, 2009; Kull *et al.*, 2004; Miao *et al.*, 2010; Pelaez *et al.*, 2010). However, most prominently, costs of most AOPs are too high, since a continuous input of expensive chemical reagents are required to maintain the operation of most AOPs system.

1.2.2. Photocatalysis

Photocatalysis for which solar light can be employed therefore greatly attracts the attention of wastewater researchers as solar light is a type of costless, durable and pollution free resource. Furthermore, photocatalysis is particularly suitable for the abatement of refractory organics including MCs since it offers possibilities of being applied as an immediate approach for target pollutants removal and being installed at remote locations.

During photocatalysis, electrons are stimulated and transit from valence band to conductive band, forming hole-electron pairs in catalyst. MCs can be oxidized by the hole (h^+) in valence band (Iainliu *et al.*, 2003; Triantis *et al.*, 2012). On the other hand, various oxygen radical species (e.g., •OH, $•O_2^-$, H_2O_2) are expected to form by oxidation of H_2O in valence band or reduction of O_2 by the electrons (Cao *et al.*, 2012 a). MCs are therefore further destructed by these radical (Iainliu *et al.*, 2003; Triantis *et al.*, 2012). The pathway of MCs destruction by photocatalysis can be summarized as shown in Figure 1-3.

For the application of photocatalysis, photocatalyst is the other essential element including two kinds of catalyst, only UV and UV-Vis absorbing materials. Although titania has been employed as a typical photocatalyst to remove MCs owing to its excellent stability and high photoactivity under ultraviolet (UV) light (Lawton *et al.*, 1999; Shephard *et al.*, 2002), the majority of studies tend to exploit visible-sensitive material to remove MCs due to visible light accounts for about 42% of solar light (Chong *et al.*, 2010; Graham *et al.*, 2010; Liou *et al.*, 2012; Triantis *et al.*, 2012).

Recently, Silver phosphate (Ag_3PO_4), a novel visible light sensitive photocatalyst, has been reported to be highly efficient in splitting water and removing organic pollutants compared with traditional catalysts such as WO_3, $TiO_{2-x}N_x$, $BiVO_4$ (Yi *et al.*, 2010). However, it's a pity that this material has a character of self-photocorrosion due to excessive electrons existing on the conductive band resulting from impossible conversion of hydrogen ion into hydrogen on the surface of the catalyst owing to the lower electrode potential of Ag/Ag_3PO_4 than the reduction potential of H^+ (Ag/Ag_3PO_4 = +0.42 V) (Yi *et al.*, 2010), which would lead to less photocatalytic oxidation capacity without employing $AgNO_3$ as electron trapper. Thereby, some appropriate

material serving as the site for hydrogen formation should be combined with Ag_3PO_4 in order to enhance the photocatalytic efficiency of Ag_3PO_4 or even prevent the photo-corrosion of it.

1.3. Aims and objectives

On the base of previous studies, I aim to alleviate the photo-corrosion of Ag_3PO_4 and achieve a highly efficient and relatively stable photocatalyst under simulated solar light irradiation through a series of modification experiments. Furthermore, the achieving photocatalyst is used to degrade MCs under simulated solar light irradiation. Besides, the influences of environmental factors (e.g. pH, cations, anions and humic acid) on the photocatalytic activity of the achieving photocatalyst will be also investigated to evaluate its value for future application in real MCs polluted sites.

1.4. Research contents

In order to achieve a highly efficient and low cost photocatalyst, a series of experiments have been conducted in this study. The contents for this thesis are summarized as follows:

Chapter 1: Introduction of research background, previous studies and objectives.

Chapter 2: Preparation of Ag/Ag_3PO_4 heterojunction and investigation of its photocatalytic activity firstly using methyl orange (MO) as targeted pollutant. Then apply this heterojunction to degrade MCs (MC-LR, -YR, -RR). And the role of morphology and the amount of Ag nanoparticles (NPs) in the photocatalytic efficiency of Ag/Ag_3PO_4 was fully elucidated.

Chapter 3: Another hybrid $AgBr/Ag_3PO_4$ was prepared by producing a low solubility film of AgBr surrounding Ag_3PO_4 since the continual dissolved Ag_3PO_4 was thought to be the main reason for the unstable state of Ag/Ag_3PO_4. Degradation of MCs (MC-LR, -YR, -RR) by this hybrid was investigated.

Chapter 4: In order to achieve a low cost photocatalyst basing on $AgBr/Ag_3PO_4$, a novel catalyst, $AgBr/Ag_3PO_4/TiO_2$ was prepared by by *in situ* deposition method. The photocatalytic

activity of this hybrid was measured using methyl orange. The role of the ratio of Ag to Ti in the photocatalytic activity of $AgBr/Ag_3PO_4/TiO_2$ was fully elucidated. The mechanism of MO degradation over BrPTi during photocatalytic process was also revealed.

Chapter 5: Application of highly efficient and relatively stable hybrids, $AgBr/Ag_3PO_4/TiO_2$, in degrading MCs (MC-LR, -YR, -RR). The influences of environmental factors (pH, cations, anions, humic acid) on the photocatalytic activity of this hybrid in degrading MC-LR were fully investigated.

Chapter 6: Conclusions and outlook.

Lake Dianchi, China; 2008

Lake Kasumigaura, Japan; 2011

Lake Little Rock, USA; 2007

Figure 1-1 Cyanobacteria bloom all over the world

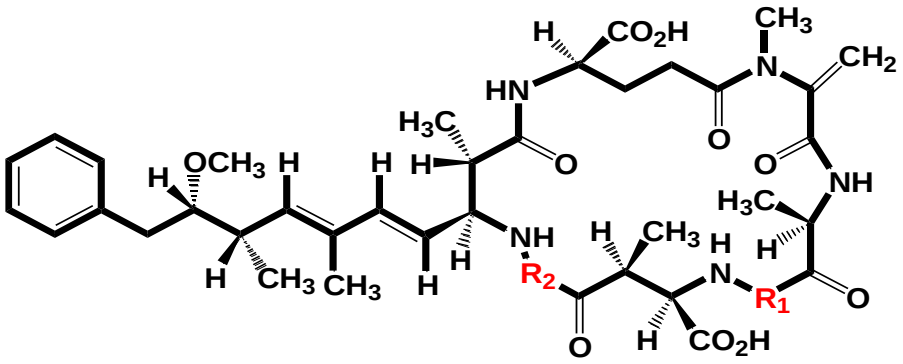

	R_1	R_2
microcystin-RR	arginine	arginine
microcystin-YR	tyrosine	arginine
microcystin-LR	leucine	arginine

Figure 1-2 Structure of microcystin and isoforms

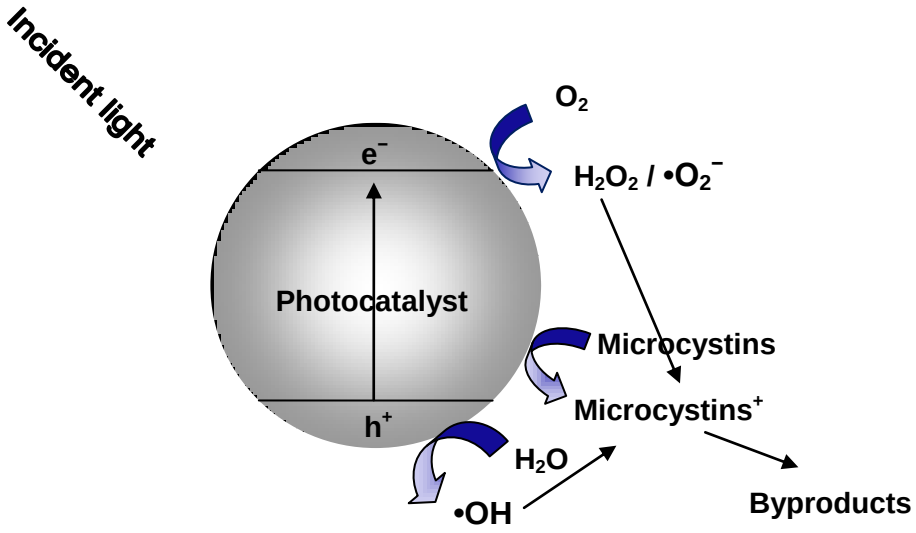

Figure 1-3 The scheme of microcytions pathway in photocatalylsis process

Chapter 2 Removal of microcystins (MC-LR, -YR, -RR) by highly efficient photocatalyst Ag/Ag_3PO_4 under simulated solar light condition

2.1. Introduction

Algal bloom mainly resulting from eutrophication, has caused the generation of microcystins. Microcystins (MCs), which is of increasing concern all over the world. Hence, more and more attention has been attracted by the issue of MCs removal worldwide. Photocatalysis has been proved to be an suitable method for the abatement of MCs since it offers possibilities of being applied as an immediate approach for target pollutants removal and being installed at remote locations.

The roles of some transition metals (Pt, Pd, Cu, Ag etc.) doped in catalyst support (TiO_2, WO_3 etc.) as electron trappers and sites for H_2 formation have been reported by many researchers (Abdulla-Al-Mamun *et al.*, 2011; Liu *et al.*, 2006; Liu *et al.*, 2010; Yu *et al.*, 2010). In terms of silver salt photocatalyst, it has been revealed that photo-deposition of Ag on the surface of AgCl/AgBr in the early stage greatly enhanced the photocatalytic efficiency and prevented the photo-corrosion of AgCl/AgBr itself (Wang *et al.*, 2008; Wang *et al.*, 2009). However, little information regarding the role of Ag as a doped element in enhancing the photocatalytic activity or preventing the photo-corrosion of Ag_3PO_4 has been reported.

On the base of previous studies, I aims to explore a novel visible light sensitive photocatalyst, Ag/Ag_3PO_4, for the removal of MCs under simulated solar light irradiation. In this chapter, attention has been given to the role of Ag content in photocatalytic activity of this combined catalyst and also to various factors influencing photocatalytic efficiency such as catalyst dosage and irradiation intensity which have received attention in the cases of photocatalytic oxidation

reactions. Besides, the performances of three MCs variants (-LR, -YR, -RR) under photocatalytic treatment using this combined catalyst were also investigated.

2.2. Materials and methods

2.2.1. Catalyst preparation

All chemicals were analytical grade without further purification. The Ag/Ag_3PO_4 heterojunction catalysts were synthesized using a simple irradiation method. In typical procedure, The Ag_3PO_4 powder was put into a solution of methyl orange (MO) of 10^{-3} mol L^{-1}, which was then irradiated with a 100 W filament lamp. Then the resulting precipitate, which consists of silver nanoparticles (NPs) deposited and Ag_3PO_4 particles, was washed with distilled water and dried at 60 ℃ overnight. To change the amount of Ag deposited on the surface of Ag_3PO_4 powder, the Ag_3PO_4 powder was irradiated according to the above described method for various time (5, 30, 70, 120 min, respectively). These Ag/Ag_3PO_4 composites with various Ag loadings were synthesized, labeled by Ag_3PO_4, 5 Ag/Ag_3PO_4, 30 Ag/Ag_3PO_4, 70 Ag/Ag_3PO_4, and 120 Ag/Ag_3PO_4, respectively. Ag_3PO_4 powder sample was prepared by the ion-exchange method: Appropriate amounts of raw powders of $Na_3PO_4 \cdot 12\ H_2O$ and $AgNO_3$ were thoroughly mixed in dark until the initial white color changed to yellow. The mixture was kept stirring for 3 hours in dark under ambient air, then washed with distilled water to dissolve any unreacted raw material. Finally, the vivid yellow powders obtained were dried at 60 ℃ in air overnight.

2.2.2. Catalyst characterization

The crystalline phases of the samples were determined by powder X-ray diffraction (XRD) (Rigaku RINT2200, Japan). The morphology of the samples was obtained by scanning electron microscopy (SEM) (JEOL, JSM-5600, Japan). UV–vis diffuse reflectance spectra (DRS) of

different samples were recorded in the range of 200 - 800 nm on a Shimadzu UV-3100PC Scan UV–vis-NIR spectrometer with $BaSO_4$ as the background.

2.2.3. Photocatalytic removal of MCs

2.2.3.1. Influence of irradiation time applied in preparation process on the photocatalytic removal of MC-LR by Ag/Ag_3PO_4

MCs (-LR, -YR and -RR) used for this study were purchased (Wako Pure Chemical Industries, Ltd., Japan) and stored at −20 ºC as stock solution prepared with a concentration of 50 mg L^{-1}. The measurement of photocatalytic oxidation of MC-LR by Ag/Ag_3PO_4 was performed in a 100 mL beaker placed on a magnetic stirrer. A simulated solar lamp (XC-100B, SERIC Ltd., Japan) positioned axially at the centre as a simulated solar light source was employed. The photocatalytic degradation experiments were carried out by adding the stock solution of MC-LR (50 mg L^{-1}) and catalyst (0.05 g) in distilled water at the desired MC-LR concentration of 200 μg L^{-1}. The total volume of the solution for reaction was adjusted to 30 mL and the light intensity was set to 4 W m^{-2}. Before irradiation, the suspension was magnetically stirred for 60 min in the dark to achieve adsorption equilibration. Then the lamp was switched on to initiate the photocatalytic reaction which was kept for 120 min. During irradiation, samples were taken and centrifuged at a constant time interval. The catalyst of Ag/Ag_3PO_4 with the highest photocatalytic activity in removing MC-LR was selected as catalyst for the follow-up impact factors investigation.

2.2.3.2. Ag/Ag_3PO_4 photocatalytic efficiencies in degrading MCs under various factors

The evaluation of various factors in Ag/Ag_3PO_4 photocatalytic efficiency was performed using MC-LR as target pollutant. Catalyst dosage (0.025, 0.050, 0.075, 0.100 g, respectively), light intensity (2, 4, 8 W m^{-2}, respectively) were selected as the influence factors for investigation.

Whilst a majority of photocatalytic studies have focused on MC-LR, as it is one of the most toxic variants in MCs, attention should also be attracted to other variants as most microcystin-producing blooms generally yield others, and in many cases MC-LR is not always the most abundant (Falconer, 2005). Therefore, as well as MC-LR, the other two common microcystin variants, MC-YR and MC-RR, were selected as pollutant targets being oxidized in this study for the investigation of the performances of MCs variants under photocatalytic treatment using this combined catalyst.

2.2.3.3. Detection of reactive oxygen species

A series of tests were conducted to probe the mechanism responsible for this simulated solar light-induced photocatalysis in degrading MC-LR. Some sacrificial agents, such as ammonium oxalate (AO) (10 mmol L^{-1}), *tert*butanol (TBA), benzoquinone (BQ), were added to the degradation system in order to ascertain the active species, h^+, •OH and $•O_2^-$, respectively in degradation process. The dosages of these scavengers were referred to the previous studies (Bandara and kiwi, 1999; Kim *et al.*, 2010 a; Yin *et al.*, 2009; Zhang *et al.*, 2011).

2.2.4. Analysis

2.2.4.1. Measurement of MCs

The concentration of MCs were measured by high performance liquid chromatographic (HPLC) (Shimadzu 10A series, Shimadzu, Japan) equipped with a photodiode array detector (PDA) set at 235 nm. A Waters SunFire™ C18 column (3.0 × 250 mm, 5 μm, Ireland) was utilized as a

stationary phase, while the mobile phase was a mixture of methanol and 0.05 M phosphate buffer (pH 2.5) in a 50:50 ratio. The analysis was performed under isocratic conditions at a flow rate of 0.58 mL min^{-1}, with an injection volume of 50 μL and an oven temperature of 37 ℃. The MCs concentrations were measured by calibrating the peak areas (at wavelength of 235 nm) with external standards. The HPLC system had a detection limit of 0.1 μg L^{-1}. Before MCs analysis, the sample was filtered (pore size: 0.22 μm, PTFE Hydrophilic, Millipore, USA), then mixed with methanol in a 2:1 (v/v) ratio.

2.2.4.2. Calculation of removal rate and removal activity

Removal rate (%) was calculated as the average decrease rate of MCs over 120 min. While removal activity (μg min^{-1} g^{-1}) was measured as the average reaction rate over a 30 min period commencing after dark adsorption period had passed as follows:

$$\text{Removal activity} = (C_0 - C_i) \times V/\Delta t/\text{m} \quad (1)$$

where C_0 and C_i are the initial MCs concentration and the MCsconcentration at 30 min of photocatalytic reaction process, respectively, V is reaction volume, Δt is photocatalytic reaction time (Δt = 30 min), and m is catalyst dosage.

2.2.4.3. Kinetic analysis

The photocatalytic oxidation kinetics of many organic compounds have often been modeled with the Langmuir-Hinshelwood equation expressed as Eq. (2):

$$r = \mathrm{d}C/\mathrm{d}t = kKC/(1+KC) \quad (2)$$

since KC is very small compared with 1, by neglecting KC in the denominator and integrating with respect to time t, Eq. (2) can be simplified to a pseudo first order kinetic equation (Eq. (3)):

$$\ln(C_0/C) = kKt = k_{app}t \qquad (3)$$

where r is the reaction rate (μg L^{-1} min^{-1}), C_0 is the initial concentration of the MC-LR (μg L^{-1}); C is the concentration of the MC-LR at time t (μg L^{-1}), t is the irradiation time (min), k is the reaction rate constant (min^{-1}), K is the adsorption coefficient of MC-LR on a photocatalyst particle (L μg $^{-1}$). The apparent reaction rate constants (k_{app}) for the photocatalytic degradation of MC-LR under various factors were evaluated from experimental data using a linear regression.

2.3. Results and discussion

2.3.1. Catalyst characterization

2.3.1.1. XRD analysis

The XRD diffraction patterns for the Ag/Ag_3PO_4 samples are showed in Figure 2-1. For comparison, the XRD pattern for the pure Ag_3PO_4 is also given. It can be seen that the prepared Ag_3PO_4 powder was in good agreement with the monoclinic phase of Ag_3PO_4 (JCPDS NO. 06-0505). The peaks corresponding to monoclinic Ag_3PO_4 were observed in the diffraction peaks of all the prepared Ag/Ag_3PO_4 catalysts, while the peak corresponding to Ag appeared in the case of 70 Ag/Ag_3PO_4 and 120 Ag/Ag_3PO_4 with the much more obvious peak appearing in the case of 120 Ag/Ag_3PO_4. These results indicated that Ag was gradually generated as the irradiation time increased from 5 to 120 min.

2.3.1.2. Morphology measurement

Figure 2-2 shows the SEM images of Ag_3PO_4, Ag/Ag_3PO_4 catalysts. As Fig 2-2 (a) shown, Ag_3PO_4 particles exhibited irregular spherical morphology and non-uniform diameters, which was similar to the results of a study conducted by Liu et al. (2012b). The size of Ag_3PO_4 particles is estimated to be 0.1 - 1.5 μm. As the photo-deposition progressed, the size distribution of

particles gradually changed from non-uniform diameters to medium and large size (1 - 1.5 μm) dominance (Fig 2-2 (b) - (e)). It is well known that Ag_3PO_4 is slightly soluble in aqueous solution, which greatly reduces its structural stability during the photocatalytic process (Bi *et al.*, 2011). Therefore, during the photo-deposition and washing process in preparation period, the tiny particles of Ag_3PO_4 would gradually disappear as Ag_3PO_4 slightly dissolved, which resulted in the distribution of particle size of Ag_3PO_4 becoming large particles dominance. Unlike the results showed in previous studies of making Ag/X heterojunction catalyst, the doped Ag cannot be clearly distinguished from Ag_3PO_4 in these Ag/Ag_3PO_4 samples by the SEM images, since the Ag_3PO_4 particles made in this study was non-uniform diameters.

2.3.1.3. Optical properties

The UV-vis diffuse reflectance spectra of the prepared samples are showed in Figure 2-3. The pattern for UV-vis diffuse reflectance spectra of Ag_3PO_4 prepared in this study was similar to the results which were reported by Liu et al. (2012b) and Cao et al. (2012a). Furthermore, the absorbance in 307 - 800 nm range which responds to solar light emission spectrum by all the Ag/Ag_3PO_4 samples were remarkably higher than that by Ag_3PO_4 alone, though Ag_3PO_4 possessed higher absorbance in the range below 300 nm. It is surprising that this remarkable increase of spectrum absorbance also happened in the cases of 5 Ag/Ag_3PO_4 and 30 Ag/Ag_3PO_4 even though Ag NPs was not detected for these two samples (Figure 2-1). It has been revealed that size distribution and morphology is one of the factors in affecting the diffusive reflectance spectra of particles, which may influence the photocatalytic activity of catalyst (Chandrappa and Venkatesha, 2012; Kumar *et al.*, 2012; Lin *et al.*, 2006; Wei *et al.*, 2012). The smaller particles may absorb less incoming light of a certain wavelength range compared with larger particles owing to scattering effect of light by smaller particles. As clearly shown in Figure 2-2, the

particle size distribution of all the Ag/Ag_3PO_4 samples became larger particle dominance compared with Ag_3PO_4. Therefore, it was inferred that the increase of spectrum absorbance in the case of 5 Ag/Ag_3PO_4 and 30 Ag/Ag_3PO_4 was mainly owing to larger particles dominance in these two samples compared with Ag_3PO_4. The similar results were achieved in the studies relating to TiO_2 and ZnO (Chandrappa and Venkatesha, 2012; Kumar *et al.*, 2012). As the irradiation time increased, the absorption in the visible region of Ag/Ag_3PO_4 samples gradually became stronger, which may result from the strong SPR effect of Ag NPs gradually deposited on the Ag_3PO_4 particles (Figure 2-1). Hence, the differences occurred among Ag_3PO_4 and Ag/Ag_3PO_4 samples were induced by the variation of particle size distribution of Ag_3PO_4 and deposition of Ag NPs.

2.3.2. Photocatalytic removal of MC-LR

2.3.2.1. Influence of irradiation time applied in preparation process on the photocatalytic removal of MC-LR by Ag/Ag_3PO_4

As shown in Figure 2-4, MC-LR concentration in the case of no catalyst exhibited no obvious change after being irradiated for 120 min, which indicated that MC-LR exhibited a stable characteristic under simulated solar light irradiation. Meanwhile, in the cases of photocatalysis, significant differences were observed in removal of MC-LR over various catalysts. Specifically, the concentration of MC-LR showed a very slight change with about 5% removal rate during dark absorption period, while dramatically decreased as photocatalytic reaction started with 100% removal rate after 120 min irradiation treatment in the cases of Ag/Ag_3PO_4 and 93% in the case of Ag_3PO_4. However, the prepared samples (Ag_3PO_4, 5 Ag/Ag_3PO_4, 30 Ag/Ag_3PO_4, 70 Ag/Ag_3PO_4 and 120 Ag/Ag_3PO_4) exhibited differently in removing MC-LR over initial 30 min irradiation, with the removal activities of 1.54, 2.29, 2.31, 2.74, and 2.45 $\mu g\ min^{-1}\ g^{-1}$,

respectively (Figure 2-5). These results indicated that the photocatalytic activity of Ag_3PO_4 dramatically increased after a relatively short time irradiation treatment (≤ 30 min) even though no obvious Ag NPs deposited on it, which was owing to the remarkably increase of spectrum absorbance in a range of 307 - 530 nm by 5 Ag/Ag_3PO_4, 30 Ag/Ag_3PO_4. As the irradiation treatment was kept being conducted for 70 min, the photocatalytic activity of the prepared sample in degrading MC-LR showed a significant increase compared with 5 Ag/Ag_3PO_4 and 30 Ag/Ag_3PO_4 samples both of which possessed almost the same photocatalytic activity, which was owing to an obvious amount of Ag NPs deposited (Figure 2-1 (d)).

For the catalyst of M/X model (M: metal, X: homogeneous photocatalyst), metal mainly served as a trapper for electrons excited from the valence band of the catalyst, which prolonged the recombination time of photo-generated hole-electron pairs and facilitated the generation of super oxide ions (O_2^-) and other reactive radicals (Abdulla-Al-Mamun *et al.*, 2011; Liu *et al.*, 2006; Yu *et al.*, 2010). Similarly, for the prepared 70 Ag/Ag_3PO_4 samples in this study, the dopant metal of silver was expected to serve as a trapper for electrons separated from light-active Ag_3PO_4 and make the generation of some reactive radicals happen on its surface. It has also been revealed that the localized surface plasmon resonance (LSPR) produced by the collective oscillations of electrons on the surface of Ag NPs could induce enhancement of the local inner electromagnetic field (Abdulla-Al-Mamun *et al.*, 2011; Wang *et al.*, 2008). The electrons and holes generated by Ag_3PO_4 were accordingly separated efficiently with the help of this local electromagnetic field.

As the irradiation treatment was kept being conducted for 120 min, however, the photocatalytic activity of the prepared sample with much more amount of Ag NPs deposited decreased. It has been revealed that there was an optimal metal content for the dispersion morphology of metal clusters with high activity for M/X heterojunction catalyst (Liu *et al.*, 2010; Shibuya and

Miyauchi, 2009). Excessive amount of metal dispersing on the surface of X in M/X model catalyst would make the photocatalytic activity decrease by absorbing part of visible light for its plasmon state (Liu *et al.*, 2012 b; Shibuya and Miyauchi, 2009). Consequently, the lower MC-LR removal efficiency of 120 Ag/Ag_3PO_4 than that of 70 Ag/Ag_3PO_4 was attributed to visible light absorbed partly by Ag instead of Ag_3PO_4 for the plasmon state of Ag. In other words, the utilization of visible light by Ag_3O_4 decreased when too much Ag deposited on its surface, resulting in less of the holes photo-generated by Ag_3PO_4 which played critical roles in oxidizing organics. Accordingly, the content of Ag was a critical factor for the photocatalytic activity of Ag/Ag_3O_4 in removing MC-LR.

2.3.2.2. Kinetic analysis in a range of catalyst dosages and light intensities

The kinetic curves for the degradation of MC-LR by 70 Ag/Ag_3PO_4 under various catalyst dosages and light intensities conditions were shown in Figure 2-6 and 2-7, respectively. The R^2 (correlation coefficient) values in all the cases are higher than 0.96, which confirms the kinetics for MC-LR degradation by Ag/Ag_3PO_4 in these photocatalytic processes followed a pseudo-first-order mechanism. This was in agreement with previous studies which revealed a pseudo-first-order mechanism for the degradation of microcystin by photocatalysis (Feng *et al.*, 2006; Shephard *et al.*, 2002).

As shown in Figure 2-6, the highest photocatalystic rate in degrading MC-LR occurred in the case of 0.05 g catalyst. The apparent reaction rate constants (k_{app}) for the photocatalytic degradation of MC-LR was 0.022, 0.057, 0.046 and 0.043 min^{-1} in the cases of 0.025, 0.050, 0.075 and 0.100 g, respectively. These results suggested that the photocatalytic rate increased up to maxima as a function of catalyst loading and tended to decrease upon further loading, which was in agreement with a number of previous studies (Farooq *et al.*, 2009; Ismail, 2008; Liu *et al.*,

2010). More active sites on the surface of catalyst at which MC-LR can be adsorbed and hole-electron pairs which are responsible for the degradation of MC-LR were generated as the increase of catalyst loading. However, turbidity was created as the catalyst loading kept increasing, which was capable of reducing the penetration intensity of light by scattering effect**.** In the report of Liu et al., too much catalyst applied also induced another phenomenon of catalyst aggregation resulting in a decrease in total active surface area available for adsorbing organics and absorbing light radiation (Liu *et al.*, 2010), which was not expected to happen in this study since the dark absorption of MC-LR increased gradually with the catalyst dosage applied. Therefore, the decrease of photocatalytic efficiency in degrading MC-LR in the case of high dosage applied was mainly attributed to the generated turbidity. Since the maximum MC-LR degradation was observed with 0.05 g of catalyst 70 Ag/Ag_3PO_4, the other experiments were performed at this dosage.

It is also observed that the removal rate of MC-LR increased with the light intensity (Figure 2-7). The apparent reaction rate constants (k_{app}) for the photocatalytic degradation of MC-LR was 0.023, 0.057, and 0.086 min^{-1} in the cases of 2, 4 and 8 W m^{-2}, respectively. At higher radiation intensity, more electron-hole pairs were expected to generate in the catalyst, which are available for the degradation of MC-LR.

2.3.2.3. The mechanism of MC-LR degradation by 70 Ag/Ag_3PO_4

In order to figure out the mechanism of degradation of MC-LR by 70 Ag/Ag_3PO_4, the roles of reactive oxygen species were investigated. The kinetics analysis for MC-LR degradation by 70 Ag/Ag_3PO_4 with additional scavengers are shown in Figure 2-8. The k_{app} are calculated to be 0.062 ± 0.005, 0.032 ± 0.003, 0.061 ± 0.009, 0.003 ± 0.001 corresponding to no scavenger, TBA, BQ and AO conditions, respectively. These results suggest that the photocatalytic activity of 70 Ag/Ag_3PO_4 in degrading MC-LR is inhibited when TBA and AO are introduced. This fact

implies the most important role of h^+ and secondary important role of •OH for MC-LR degradation by 70 Ag/Ag_3PO_4 but the little influence of $•O_2^-$.

Consequently, the possible mechanism for photocatalytic degradation of MC-LR by 70 Ag/Ag_3PO_4 can be summarized to four steps as follows:

70 Ag/Ag_3PO_4 + *hv* (simulated solar light) → $h^+ + e^-$ (4)

MC-LR + h^+ → MC-LR^+

$H_2O + h^+ → O_2 + 2H^+$

$OH^- + h^+ → •OH$ (5)

$O_2 + 2H^+ + 2e^- → H_2O_2$

$H_2O_2 + e^- → OH^- + •OH$ (6)

MC-LR^+ + •OH → Products (7)

2.3.3. The comparison of photocatalytic performance of catalysts on removing different microcystins (MC-LR, -YR, -RR)

The dark adsorption rates of MC-LR, MC-RR and MC-YR by 70 Ag/Ag_3PO_4 were 5.5%, 7.3% and 41.4%, respectively (Figure 2-9). Subsequently, MC-YR was observed clearly to be the easiest to be removed with 100% destruction rate after 15 min photocatalytic reaction. In comparison, the destruction rate of MC-LR and MC-RR were 26.4% and 80.0%, respectively. These results suggested that the adsorption capacity of a definite catalyst to various microcystins was substantially distinct. Furthermore, the photocatalytic degradation rates of various

microcystin analogues with nearly the same adsorption rate over catalyst were also greatly different.

For the adsorption characteristics of microcystins over catalyst, previous studies have also shown that the percent dark adsorption of microcystin at equilibrium for a given catalyst dose relied on microcystin variants (Lawton *et al.*, 2003; Pelaez *et al.*, 2012a). The microcystin used for this study was a cyclic heptapeptide containing the amino acid 3-amino-9-methoxy-2, 6, 8-trimethyl-10-phenyldeca-4, 6-dienoic acid (Adda), with arginine in one variable position and leucine, arginine and tyrosine in the other variable position corresponding to MC-LR, MC-YR and MC-RR respectively. Compounds bearing more hydrophobic amino acid side chains were reported to more preferentially move to the surface of catalyst from aqueous solvents when the force of bilateral electrical charge could be ignored (Hoffman *et al.*, 1995). In this study, the order of the hydrophobicity of tyrosine, leucine and arginine consisting respectively in MC-YR, MC-LR and MC-RR followed the trend: tyrosine > leucine > arginine. Accordingly, the greater hydrophobicity of tyrosine than that of the other two amino acid side chains was expected to mainly contribute to the higher dark adsorption rate of MC-YR compared with that of MC-LR and MC-RR. However, the hydrophobicity of amino acid side chains was not always the key factor to determine the adsorption efficiency of microcystin by catalyst when the forces of bilateral electrical charge were taken into account.

Three microcystin variants applied in this study, MC-LR, MC-YR and MC-RR, have been revealed to be negatively charged, negatively charged and charge-neutral respectively at pH 6-10 (Ho *et al.*, 2011; Pelaez *et al.*, 2012a). As a result of different net charge held in MC-LR and MC-RR respectively, the adsorption of MC-LR over 70 Ag/Ag_3PO_4 sample was less than that of MC-RR although the hydrophobicity of leucine consisting in MC-LR was greater than that of

arginine consisting in MC-RR. Meanwhile, the adsorption of MC-LR on 70 Ag/Ag_3PO_4 sample was much less than that of MC-YR despite they held the same net charge, suggesting that hydrophobicity played a more dominated role in affecting the adsorption characteristic of MC-YR than its net charge. Besides, it was reported that MC-RR was much more easily adsorbed onto particle active carbon than MC-LR due to the smaller molecular size and conformation of the MC-RR than that of MC-LR which favoring adsorption (Ho *et al.*, 2011). Consequently, we concluded that the absorption characteristic of microcystin on the surface of catalyst was determined by the combined effects of its hydrophobicity property, charge forces and other factors such as molecular size and conformation rather than sole effect of these factors.

One more aspect worth to be discussed was that the extent of being susceptible to photocatalytic attack varied among microcystin variants. Only one study conducted by Lawton et al. revealed the similar result that MC-RR was much more susceptible to TiO_2 photocatalytic attack than MC-LR in the case of pH 12 where MC-LR and MC-RR exhibited the same dark absorption rate over TiO_2 (Lawton *et al.*, 2003), however, with no further discussion about it. Still, the removal efficiencies of three microcystin analogues by chlorine and permanganate oxidization were revealed to follow a trend of MC-YR>MC-RR>MC-LR (Ho *et al.*, 2006; Rodr ǵuez *et al.*, 2008; Rodr ǵuez *et al.*, 2007), which were in agreement with the results obtained in this study. Literature reports of chlorination of peptides and proteins generally indicated that the peptide bonds between individual amino acids react slowly, and that the terminal, or side amino groups are more reactive, determining the overall reactivity of the compounds (Hureiki *et al.*, 1994; Reckhow *et al.*, 2001). For the amino acid group of MCs attacked by photocatalysis, the conjugated double bond of the Adda group contained as a side chain in microcystins has been reported to be susceptible to photocatalytic attack (Antoniou *et al.*,

2008; Chen *et al.*, 2012; Liu *et al.*, 2003). However, there are also other amino side chains present in the microcystin molecules which may be reactive with photocatalyst. Tran et al. (2006) found a wide range of reactivity between photocatalyst and the free amino acids, with aliphatic acids such as leucine and alanine the least reactive, compounds with a terminal amine group, for example arginine, more reactive, and tyrosine the most reactive due to its activated terminal hydroxy group. Similar trend has also been found in reactivity between chlorine and the free amino acids (Hureiki *et al.*, 1994). Therefore, it can be inferred that the discrepancies of the photocatalytic destruction of MCs were partly related to the reactivities between distinct amino side chains they held respectively and 70 Ag/Ag_3PO_4 during photocatalysis process.

2.3.4. The stability of Ag/Ag_3PO_4 under repeated applications

As shown in Figure 2-10, for the first cycling run, the photocatalytic activity of $70Ag/Ag_3PO_4$ sample in removing MC-LR was much higher than that of 120 Ag/Ag_3PO_4, which was consistent with the result revealed above (Figure 2-4). Subsequently, for the second cycling run, both of these two Ag/Ag_3PO_4 catalysts showed lower capacity in removing MC-LR compared with that in the first run. However, it was worth noticing that the removal rate of MC-LR over the resulting catalysts tended to be stable in the subsequent third and forth cycling runs but was slightly lower than that over Ag_3PO_4 (Table 2-1). Similarly, a kind of Ag/Ag_3PO_4 which showed lower photocatalytic activity than Ag_3PO_4 but was stable was reported by Liu et al. (2012b). These results indicated that the amount of Ag NPs doped in 70 Ag/Ag_3PO_4 and 120 Ag/Ag_3PO_4 were enough to make the photocatalytic activity of Ag_3PO_4 increase but not enough to make this Ag/Ag_3PO_4 heterojunction stable for cycling use under simulated solar light irradiation. As shown in the results of XRD analysis (Figure 2-1), the ratio of Ag NPs in 70 Ag/Ag_3PO_4 and 120 Ag/Ag_3PO_4 samples were both much less than that of Ag_3PO_4. Therefore, Ag_3PO_4 was expected

to occupy most of the sites in the surface of these Ag/Ag_3PO_4 catalysts. It is well known that Ag_3PO_4 is very slightly soluble in aqueous solution (Ksp (Ag_3PO_4) = 1.4×10^{-16}). However, since the free Ag^+ may be transformed to metal Ag via $Ag^+ + e \rightarrow Ag$ during photocatalysis, the solubility of Ag_3PO_4 in the surface of 70 Ag/Ag_3PO_4 and 120 Ag/Ag_3PO_4 in water may be continuously promoted by this process, which might be responsible for the instability of 70 Ag/Ag_3PO_4 and 120 Ag/Ag_3PO_4 during the photocatalytic processes. As the photocatalystic process kept being conducted, more and more Ag deposited on the surface of Ag_3PO_4, a film consisting of Ag NPs was expected to form surrounding the Ag_3PO_4. And this film could be likely to separate the inner Ag_3PO_4 from water and therefore preventing Ag_3PO_4 from being continuously soluble in water and making the resulting Ag/Ag_3PO_4 stable. On the other hand, more Ag NPs doped in Ag_3PO_4 might prevent more electrons from combining with interstitial silver ions of Ag_3PO_4 to generate silver atoms by generating more LSPR which can effectively separate the hole-electron pairs.

2.4. Conclusion

A novel wide spectral responsive Ag/Ag_3PO_4 has been successfully synthesized by a simple irradiation method. The result that Ag/Ag_3PO_4 possessed much higher photocatalytic activity than Ag_3PO_4 towards the removal of MCs confirms the combined role of particle morphology and metal in accelerating the photocatalytic efficiency of homogeneous catalyst. Besides, as MC-LR showed very slight adsorption over Ag/Ag_3PO_4 although it can be efficiently degraded, some materials possessing high adsorption capacity to MC-LR can be combined to Ag/Ag_3PO_4 to achieve a much better removal efficiency of MC-LR. Doping a small amount of Ag on the surface of Ag_3PO_4 would greatly accelerate the oxide activity of Ag_3PO_4 but cannot effectively prevent photo-corrosion characteristic of it unless increasing the amount of Ag doped which

would adversely decrease the photocatalytic activity of Ag/Ag_3PO_4. Therefore, it needs to pursue a way to keep this highly efficient catalyst, Ag/Ag_3PO_4, stable for its application in the future. As the character of Ag_3PO_4 being slightly soluble in aqueous solution was inferred as the main reason for the unstable state of Ag/Ag_3PO_4 during photocatalysis process, the way aiming at preventing Ag_3PO_4 from being soluble in aqueous solution might be a good way to keep Ag/Ag_3PO_4 stable. Some stable catalyst of which the photocatalytic activity can be accelerated by Ag^0 can also be combined with this Ag/Ag_3PO_4 to counteract the loss of Ag_3PO_4 photocatalytic capacity.

Table 2-1 Removal rates of MC-LR over Ag_3PO_4, 70 Ag/Ag_3PO_4 and 120 Ag/Ag_3PO_4 under simulated solar light for recycling runs.

Recycling time	Removal rate of MC-LR (%)		
	Ag_3PO_4	70 Ag/Ag_3PO_4	120 Ag/Ag_3PO_4
1^{st}	39.4%	100%	74.2%
2^{nd}	—	41.5%	41.1%
3^{rd}	—	35.1%	31.7%
4^{th}	—	37.1%	32.3%

The symbol of "—" represents the experiment which was not conducted.

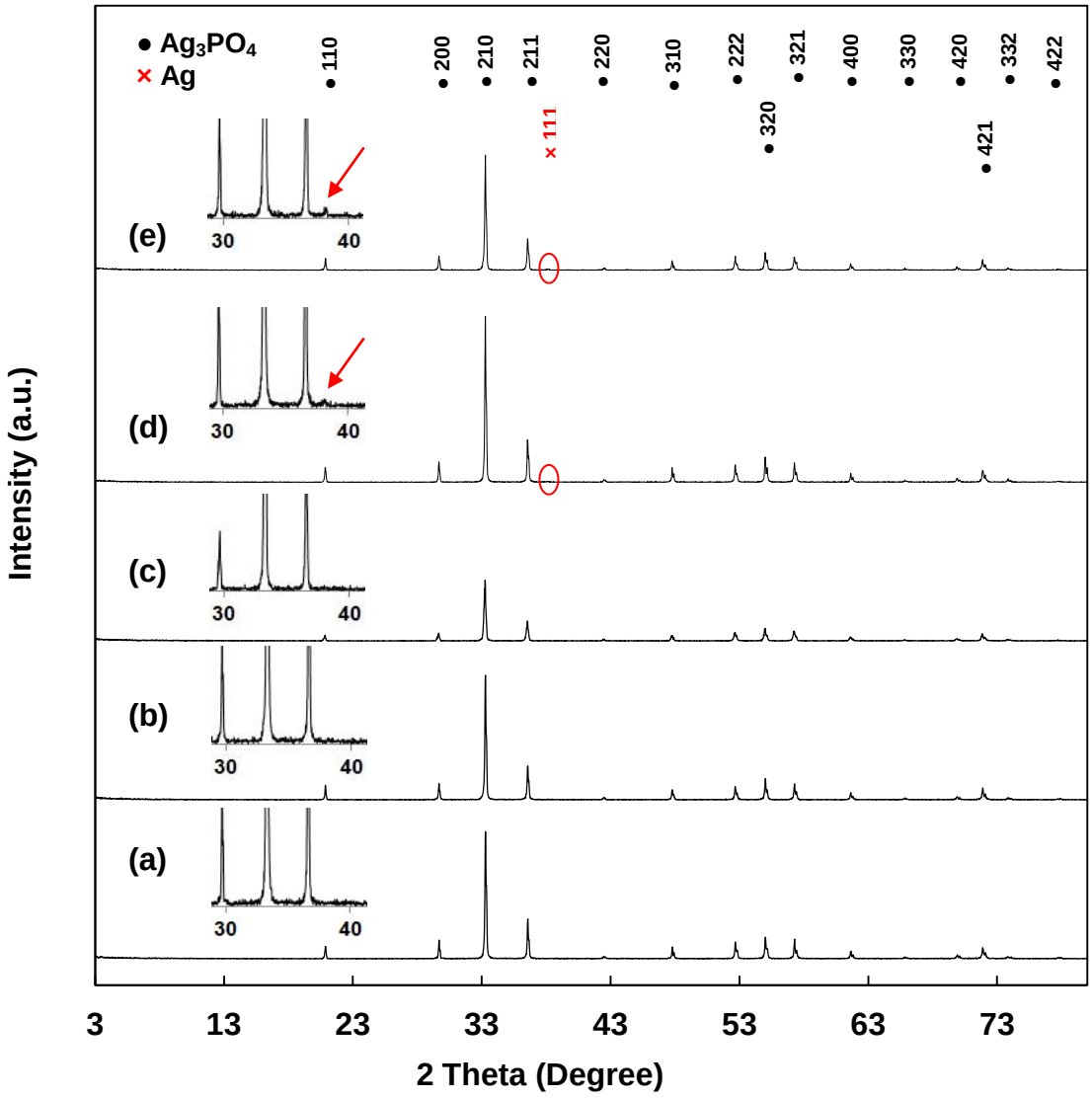

Figure 2-1 XRD patterns of the (a) Ag_3PO_4 powders prepared by the ion-exchange method, (b) 5 Ag/Ag_3PO_4, (c) 30 Ag/Ag_3PO_4, (d) 70 Ag/Ag_3PO_4 (e) 120 Ag/Ag_3PO_4 prepared by photodeposition method.

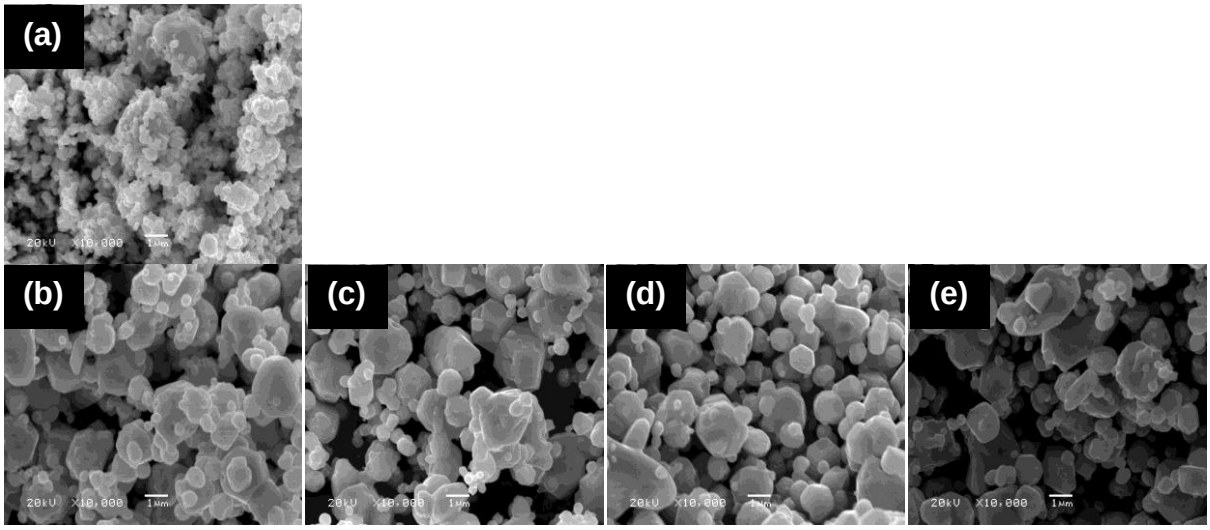

Figure 2-2 SEM images of (a) Ag_3PO_4, (b) 5 Ag/Ag_3PO_4, (c) 30 Ag/Ag_3PO_4, (d) 70 Ag/Ag_3PO_4 and (e) 120 Ag/Ag_3PO_4 powder samples.

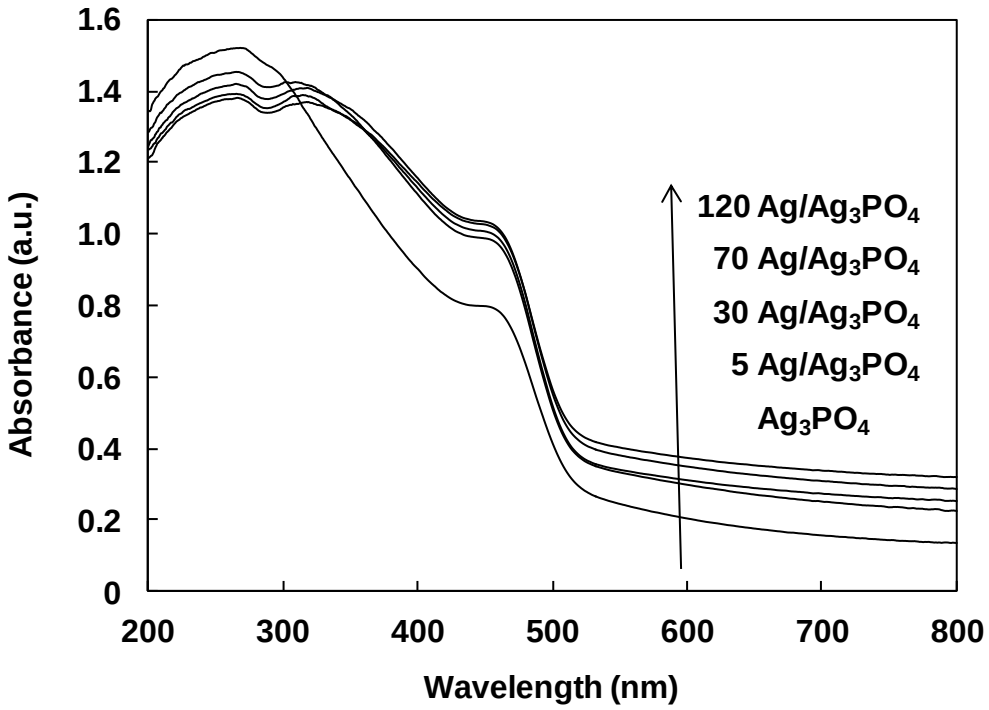

Figure 2-3 Ultraviolet–visible diffusive reflectance spectrum of the Ag_3PO_4 and Ag/Ag_3PO_4 samples (5 Ag/Ag_3PO_4, 30 Ag/Ag_3PO_4, 70 Ag/Ag_3PO_4, 120 Ag/Ag_3PO_4, respectively).

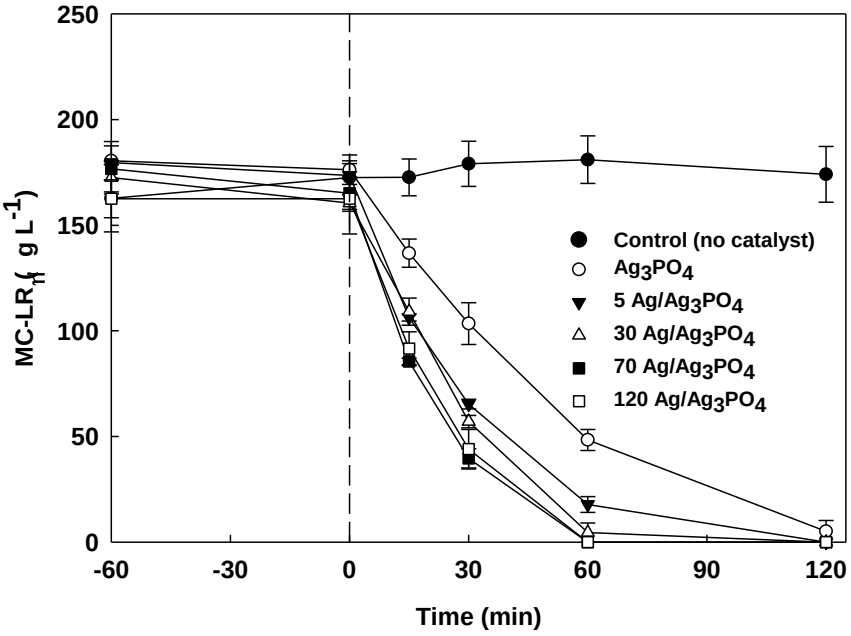

Figure 2-4 Variation of MC-LR concentration as a function of illumination time (with the time of light on set as 0) under simulated solar light with Ag_3PO_4 and Ag/Ag_3PO_4 powder samples (5 Ag/Ag_3PO_4, 30 Ag/Ag_3PO_4, 70 Ag/Ag_3PO_4, 120 Ag/Ag_3PO_4, respectively). Error bars indicate the ranges of duplicate measurements.

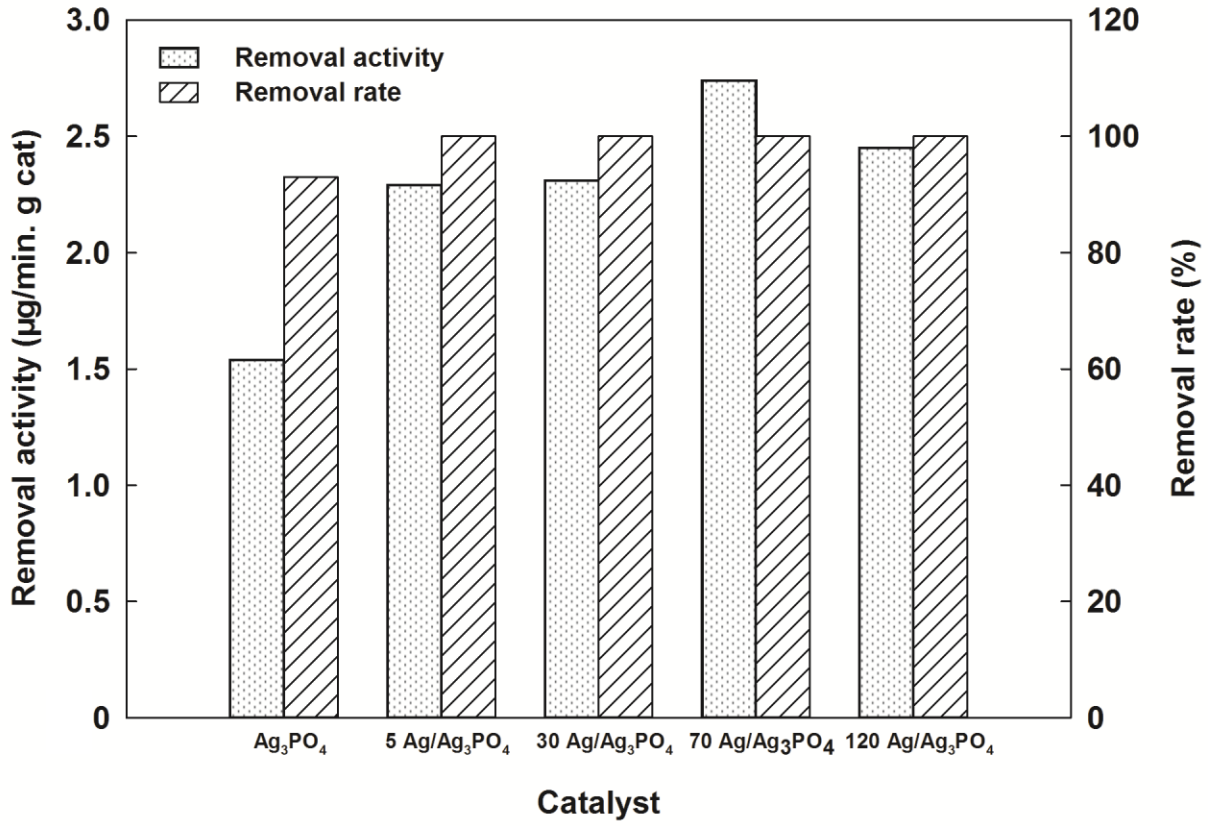

Figure 2-5 Removal rate of various catalysts over 120 min photocatalysis period, and removal activity of various catalysts measured as the average reaction rate over a 30 min period commencing after dark adsorption period had passed.

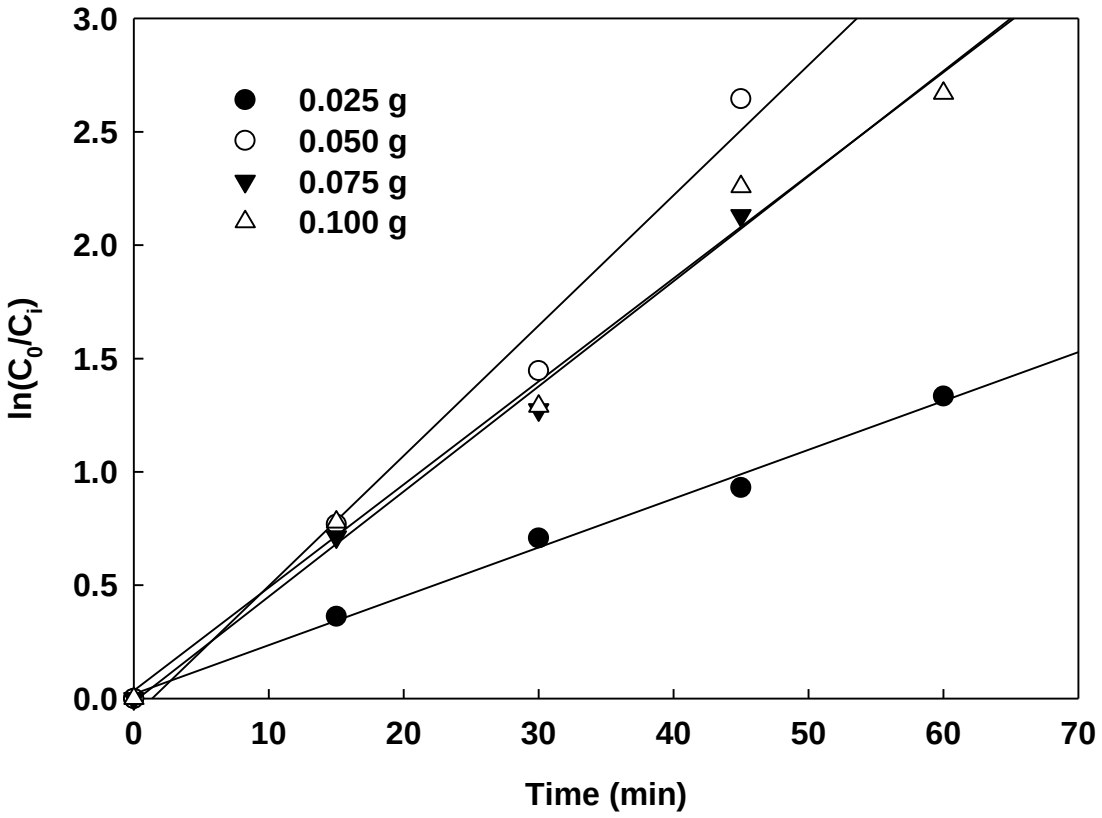

Figure 2-6 The pseudo-first-order kinetics for photocatalytic destruction of MC-LR under simulated solar light at a range of 70 Ag/Ag_3PO_4 catalyst dosages. Irradiation intensity: 4 W m^{-2}.

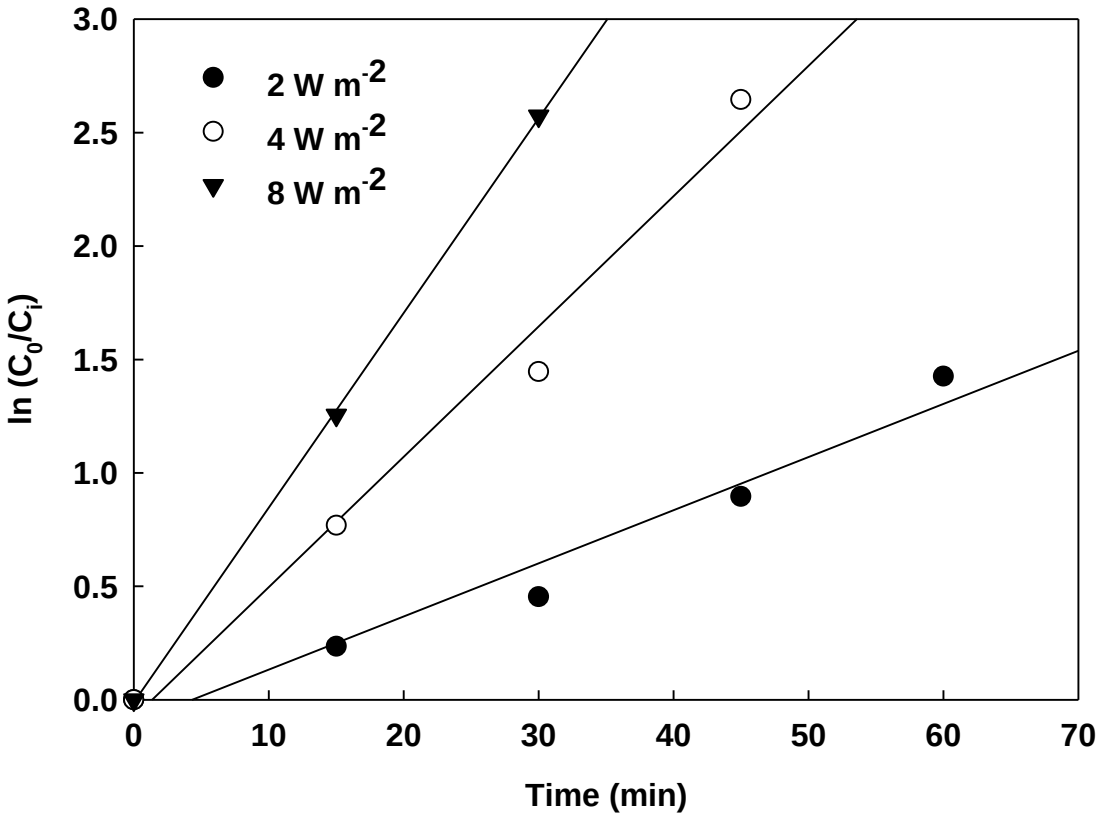

Figure 2-7 The pseudo-first-order kinetics for photocatalytic destruction of MC-LR under simulated solar light with 70 Ag/Ag_3PO_4 sample in a range of light intensities. Catalyst dosage: 0.05 g.

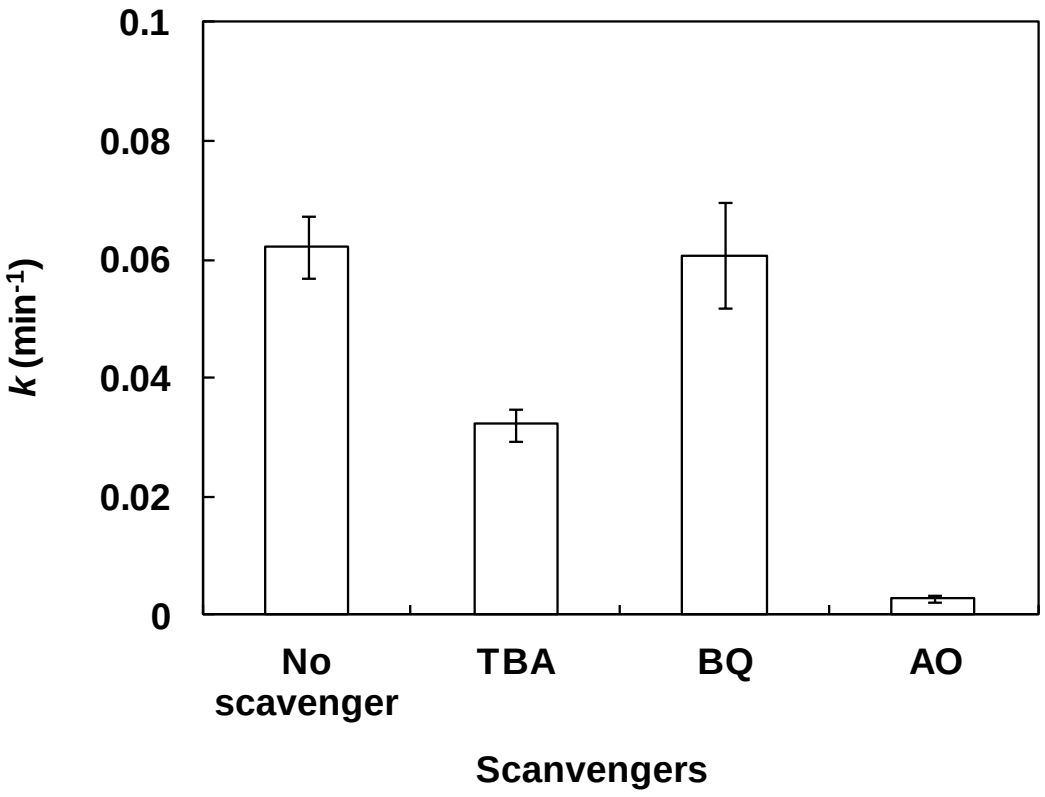

Figure 2-8 The apparent rate constant *k* for MC-LR degradation under various scavengers. Error bars indicate the ranges of duplicate measurements.

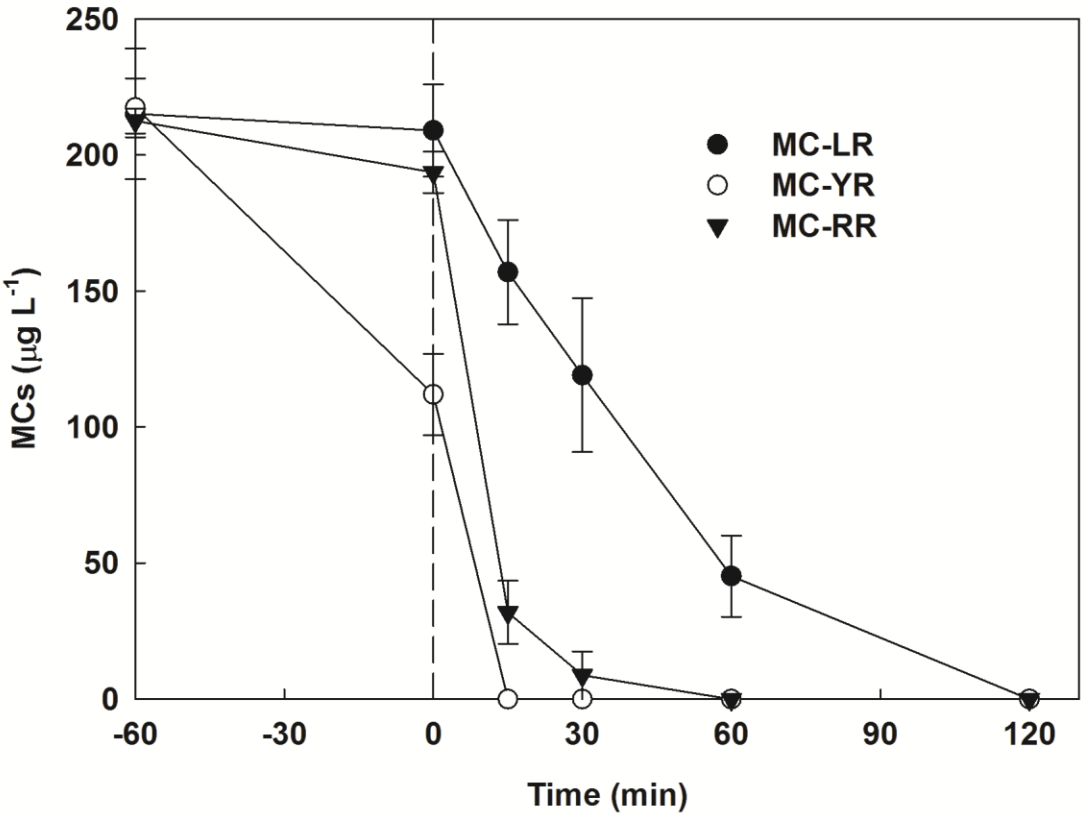

Figure 2-9 Variations of microcystin (MC-LR, MC-YR and MC-RR, respectively) concentration as a function of illumination time (with the time of light on set as 0) under simulated solar light with 70 Ag/Ag_3PO_4 sample. Error bars indicate the ranges of duplicate measurements.

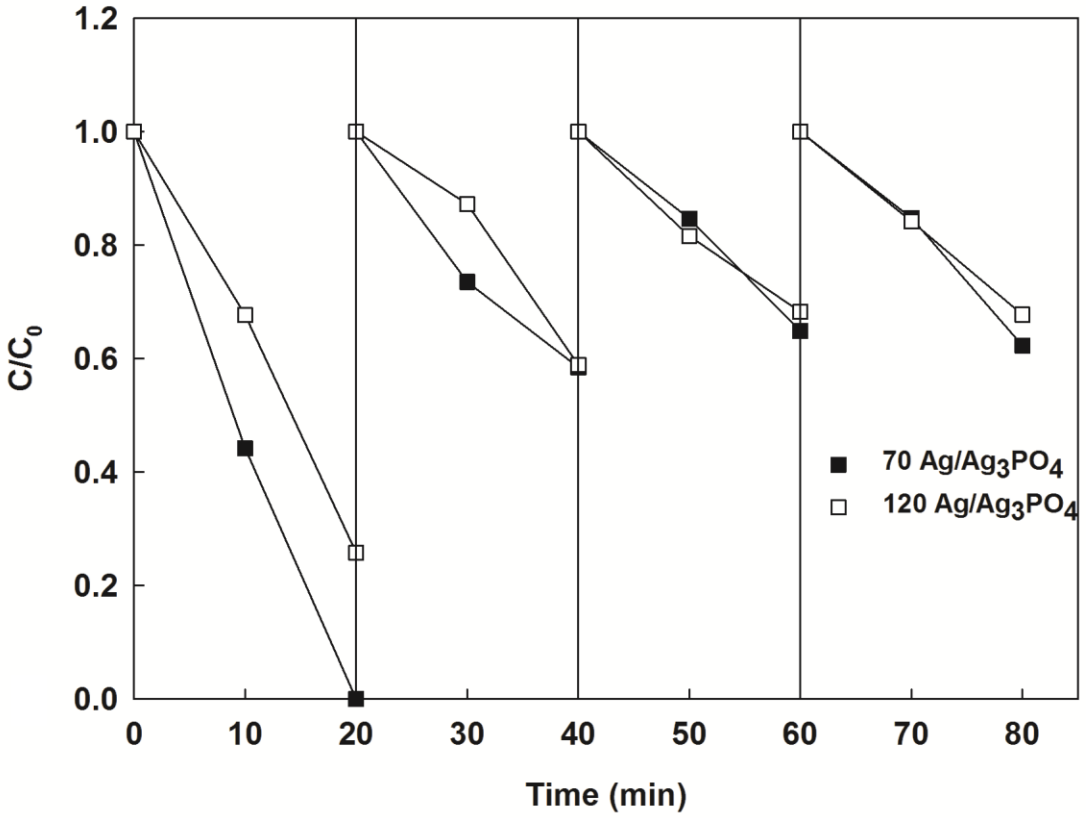

Figure 2-10 Photocatalytic degradation of MC-LR under simulated solar light for four cycling runs with 70 Ag/Ag_3PO_4 and 120 Ag/Ag_3PO_4, respectively.

Chapter 3 Degradation of MCs by highly efficient $AgBr/Ag_3PO_4/TiO_2$ heterojunction photocatalyst under simulated solar light condition

3.1. Introduction

For other silver salts such as AgCl or AgBr, it has been reported that the photocatalytic activity and stability of it can be greatly enhanced by doping an appropriate amount of Ag NPs on it (Wang *et al.*, 2008; Wang *et al.*, 2009). Based on these studies, I previously revealed the role of Ag NPs on the photocatalytic activity and stability of Ag_3PO_4 under simulated solar light condition. And the results indicated that doping a small amount of Ag on the surface of Ag_3PO_4 would greatly accelerate the oxide activity of Ag_3PO_4 but cannot effectively prevent photo-corrosion characteristic of it unless increasing the amount of Ag doped which would adversely decrease the photocatalytic activity of Ag/Ag_3PO_4. Similarly, a heterojunction Ag/Ag_3PO_4 prepared in the study of Liu et al. (2012b) was found relatively stable for successive photocatalysis but less efficient than Ag_3PO_4 under visible light condition, suggesting the photocatalitic activity and stability of Ag_3PO_4 cannot be simultaneously enhanced by introducing Ag NPs (Liu *et al.*, 2012). Meanwhile, as the character of Ag_3PO_4 being slightly soluble in aqueous solution was inferred as a main reason for the unstable state of Ag_3PO_4 during photocatalysis process ($K_{sp}=1.4\times10^{-16}$, 0.02 g L^{-1} 25 ℃), Bi et al. (2011) and Cao et al. (2012a) reported a successful method of preventing Ag_3PO_4 from dissolving and achieving much more photoctalytically efficient catalyst, $AgBr/Ag_3PO_4$, by doping an insoluble AgBr nanoshell around Ag_3PO_4 particle. However, the photo-corrosion phenomenon cannot be avoided after several cycling photocatalytic runs as AgBr was also a type of photo-corrosive silver salt, although Ag_3PO_4 was relatively stable in this heterojunction (Cao *et al.*, 2012a). Therefore, some stable catalyst of which the photocatalytic activity can be accelerated by Ag^0 can be combined with this

$AgBr/Ag_3PO_4$ to counteract the decrease of photocatalytic capacity caused by the loss of AgBr during photocatalytic process. Furthermore, as silver is noble metal, in order to decrease the cost of catalyst, priority should be given to the lower cost materials serving as dopant.

TiO_2, which is the most traditional and stable photocatalyst, has been proved to be able to react with Ag^0 to achieve a more efficient photocatalytic activity under UV-Vis light (Abdulla-Al-Mamun *et al.*, 2011; Cheng *et al.*, 2012; Yun *et al.*, 2009). Therefore, in this chapter, TiO_2 serving as a dopant was combined with the $AgBr/Ag_3PO_4$ to achieve a novel catalyst, $AgBr/Ag_3PO_4/TiO_2$ (BrPTi) and the influence of TiO_2 ratio on the photocatalytic activity of BrPTi was also investigated. Furthermore, the mechanism of MO degradation by BrPTi under simulated solar light condition was fully illustrated by analyzing the role reactive oxygen species generated during photocatalysis period. To evaluate the prospective application of this heterojunction in photocatalytic field, the stability of it for successive photocatalysis under simulated solar light condition was also investigated.

3.2. Materials and methods

3.2.1. Preparation of catalyst

All chemicals were analytical grade without further purification. The BrPTi heterojunction catalysts were synthesized by *in situ* depositing AgBr/ Ag_3PO_4 onto TiO_2 (P25) surface. In typical procedure, TiO_2 (P25) powder was dissolved in distilled water and sonicated for 10 min to form homogenous TiO_2 suspension. And appropriate dosage of $AgNO_3$ was then added into the TiO_2 dispersed water (pH=7). After magnetically stirring for 20 min, appropriate dosage of $Na_3PO_4 \cdot 12H_2O$, which was previously dissolved in 25 mL distilled water, was added dropwise into the solution. The theoretical molar rate of added Ag/original Ti was controlled to be 0.3, 0.9, 1.5 and 2.4, respectively. After the resulting Ag_3PO_4/TiO_2 solution was magnetically stirred for 3

hours, NaBr solution was subsequently added slowly into above suspension with the theoretical molar percentages of added Br/P being controlled to be 60%. The mixture was vigorously stirring for 3 h. Finally, the precipitates were collected, washed with distilled water for 4 times, and dried at 60 ℃ for 24 h.

3.2.2. Catalyst characterization

The crystalline phases of the samples were determined by powder X-ray diffraction (XRD) (Rigaku RINT2200, Japan). The morphology of the samples was obtained by scanning electron microscopy (SEM) (JEOL, JSM-5600, Japan). UV-vis diffuse reflectance spectra (DRS) of different samples were recorded on a Shimadzu UV-3100PC Scan UV-vis-NIR spectrometer with $BaSO_4$ as the background and in the range 200-800 nm. The specific surface area of the developed samples were determined using Brunauer – Emmett – Teller (BET) specific surface analysis device (Coulter SA3100, US).

3.2.3. Photocatalytic activity of $AgBr/Ag_3PO_4/TiO_2$ in degrading methyl orange

The photocatalytic activity of BrPTi heterojunction was measured using methyl orange (MO) as targeted pollutant. The measurement was carried out by adding the stock solution of MO and catalyst in distilled water at the MO concentration of 8.2 mg L^{-1}. The total volume of the solution for the reaction was adjusted to 60 mL. Before irradiation, the suspension (60 mL) was magnetically stirred for 30 min in the dark to achieve equilibration. Then the lamp was switched on to initiate the photocatalytic reaction which was kept for 50 min. During irradiation, samples were taken at intervals of 10 min, 2 mL of the suspension was collected, then centrifuged to remove the photocatalyst particles. The catalyst-free MO solultion was analyzed with a UV-VIS spectrophotometer (Shimadzu, UV-MINI-1240-100V, Japan). The concentration of MO was

determined from its maximum absorption at a wavelength of 464 nm with deionized water as a reference sample.

3.2.4. Detection of reactive oxygen species

A series of tests were conducted to probe the mechanism responsible for this simulated solar light-induced photocatalysis in degrading methyl orange. Some sacrificial agents, such as ammonium oxalate (AO) (10 mmol L^{-1}), *tert*butanol (TBA), benzoquinone (BQ), were added to the degradation system in order to ascertain the active species, h^+, •OH and $•O_2^-$, respectively in degradation process. The dosages of these scavengers were referred to the previous studies (Bandara and kiwi, 1999; Kim *et al.*, 2010a; Yin *et al.*, 2009; Zhang *et al.*, 2011).

In addition, the formed hydroxyl radicals (•OH) was detected by photoluminescence (PL) technique (Cao *et al.*, 2012b). Terephthalic acid, which reacts readily with •OH to produce a highly fluorescent product, 2-hydroxyterephthalic acid, was employed as a probe molecule to detect •OH. The fluorescence intensity around 425 nm, which can be ascribed to the characteristic of 2-hydroxyterephthalic acid, is proportional to the amount of hydroxyl radicals formed in solution. The detection experiment process was similar to the photodegradation experiment, with the exception of a basic terephthalic acid solution instead of MO suspension. The concentration of terephthalic acid was set at 5×10^{-4} mol L^{-1} in a dilute NaOH solution (2×10^{-3} mol L^{-1}). The sampling was carried out at intervals, and the withdrawn solution was centrifuged and filtered (pore size: 0.22 μm, PTFE Hydrophilic, Millipore, USA), then measured on a Hitachi F-4500 fluorescence spectrophotometer. The excitation wavelength was 315 nm.

3.2.5. The stability of $AgBr/Ag_3PO_4/TiO_2$ under repeated application

To evaluate the prospective application of $AgBr/Ag_3PO_4/TiO_2$, the stability of it was determined using MO as target pollutant. Three reaction dishes were set for once, two times and

3 times photocatalysis runs, respectively. For each run, the total volume of the solution for the reaction was adjusted to 6 mL in the glass dish of 5 cm diameter with MO initial concentration of 8.2 mg L^{-1}. For each dish, the catalyst dosage was set to be 0.001 g at the beginning. And the resulting suspensions from last run was washed with distilled water and centrifuged to remove the remaining organics in previous run and retrieve the catalyst for the next run. During photocatalysis period, samples were taken at intervals, and measured by spectrophotometer at 464 nm.

3.2.6. Removal of MCs by $AgBr/Ag_3PO_4/TiO_2$

3.2.6.1. Comparison of photocatalytic activities of BrPTi and other traditional photocatalyst in degrading MC-LR

The BrPTi with the best photocatalytic activity (1.5 BrPTi) was applied to degrade MC-LR. The measurement was performed in a 100 mL beaker placed on a magnetic stirrer. A simulated solar lamp (XC-100B, SERIC Ltd., Japan) positioned axially at the centre as a simulated solar light source was employed. The photocatalytic degradation experiments were carried out by adding the stock solution of MC-LR (50 mg L^{-1}) and catalyst (0.01 g) in distilled water at the desired MC-LR concentration of 200 μg L^{-1}. The total volume of the solution for reaction was adjusted to 30 mL and the light intensity was set to 4 W m^{-2}. Before irradiation, the suspension was magnetically stirred for 60 min in the dark to achieve adsorption equilibration. Then the lamp was switched on to initiate the photocatalytic reaction which was kept for 25 min. During irradiation, samples were taken and centrifuged at a constant time interval.

As well as MC-LR, the other two common microcystin variants, MC-YR and MC-RR, were selected as pollutant targets being oxidized in this study for the investigation of the performances of MCs variants under photocatalytic treatment using this combined catalyst. Besides, the effects

of catalylst dosage and light intensity on the photocatalytic activity of 1.5 BrPTi in degrading MC-LR were also investigated.

3.2.6.2. Byproducts of MC-LR degraded by 1.5 BrPTi

The MC-LR solution (200 μg L^{-1}, 20 ml) having been treated with 1.5 BrPTi catalyst (0.004 g) for 25 min under simulated solar light irradiation (4 W m^{-2}) was used for MC-LR degradation products analysis. The treated MC-LR solution was purified by centrifugation and filtration (0.2 μm filter) before analysis. For comparison, the MC-LR solution before being treated was also analyzed. The purified samples were analyzed by high performance liquid chromatography (Waters Acquity) and mass spectrometry (Waters Quattro micro API). The mobile phase was a combination of CH_3OH and 0.1% HCOOH (50:50).The flow rate was set at 0.1 mL min^{-1}. The ionization mode was set to be ESI+ and ESI−. And the spray voltage and cone voltage were set to be 3.1 kV and 25 V.

3.3. Results and discussion

3.3.1. Synthesis process of $AgBr/Ag_3PO_4/TiO_2$ photocatalysts

TiO_2 is an amphoteric oxide. When it is suspended in a solution with pH greater than 6 the surface of TiO_2 particles is negatively charged with O^- anions which are the main surface species (Fu *et al.*, 2005; Zanella *et al.*, 2002). In this case, positively charged silver ions (Ag^+) can be adsorbed onto the TiO_2 surface due to the existence of O^- anions. When Ag^+ ion was adsorbed, the reaction of Ag^+ (ad) and PO_4^{3-} takes place on the surface of TiO_2 forming an Ag_3PO_4/TiO_2 heterostructure. The Br anion (Br^-) was then introduced into the above resulting solution in order to form a thin AgBr film on Ag_3PO_4. The synthetic process of the $AgBr/Ag_3PO_4/TiO_2$ composite photocatalyst can be summarized as follows:

TiO_2 (s) + Ag^+ (aq) → TiO_2–Ag^+ (ad) pH = 7 (8)

TiO_2–Ag^+ (ad) + PO_4^{3-} (aq) → Ag_3PO_4/TiO_2 (9)

Ag_3PO_4/TiO_2 + Br^- → $AgBr/Ag_3PO_4/TiO_2$ (10)

3.3.2. Catalyst characterization

3.3.2.1. XRD analysis

The XRD diffraction patterns for the BrPTi samples are shown in Figure 3-1. For comparison, the XRD pattern for the pure $AgBr/Ag_3PO_4$ is also given, which shows the same pattern as that Cao et al. reported (Cao *et al.*, 2012a). The peaks corresponding to monoclinic Ag_3PO_4, AgBr and TiO_2 are all observed in the diffraction peaks of the prepared BrPTi catalysts, suggesting these prepared BrPTi heterojunctions all consist of AgBr, Ag_3PO_4 and TiO_2. Still, differences are observed among them that the XRD peaks for the commercial TiO_2 (P25) can be more clearly distinguished from the XRD patterns of the BrPTi catalyst with more TiO_2 being doped in it. This result suggests different ratio of $AgBr/Ag_3PO_4$ to TiO_2 among these BrPTi catalysts.

3.3.2.2. Morphology measurement

Figure 3-2 shows the SEM images of TiO_2, $AgBr/Ag_3PO_4$ and BrPTi catalysts. It can be seen clearly that P25 nanoparticles show a great spherical morphology and uniform diameters of about 25 nm. Meanwhile, $AgBr/Ag_3PO_4$ particles exhibits irregular spherical morphology and non-uniform diameters ranging from 0.2 μm - 1 μm, which is similar to the result of a study conducted by Cao et al. (2012a). For the prepared BrPTi samples, the size of all the prepared BrPTi samples are much smaller than that of $AgBr/Ag_3PO_4$ particles while a little larger than that of P25. Furthermore, as the ratio of P25 decreases, the size distribution of particles of BrPTi changed gradually from homogeneously small size to non-uniform size in which larger size took

account for a certain proportion. Besides, the result of BET surface area analysis shows the surface area of BrPTi gradually declines as the ratio of Ag to Ti increases, which further confirms the variations of particle size distribution among the prepared BrPTi samples with different ratio of Ag to Ti (Table 3-1). Therefore, a novel catalyst of nanoscale, $AgBr/Ag_3PO_4/TiO_2$, was successfully prepared by a simple ion exchange method in this study.

3.3.2.3. Optical properties

Figure 3-3 shows the UV-vis diffusive reflectance spectra of pure TiO_2, $AgBr/Ag_3PO_4$ and BrPTi (Ag/Ti = 1.5), respectively. It can be clearly seen that the pure TiO_2 (P25) absorbs solar energy with a wavelength shorter than 400 nm. Meanwhile, the $AgBr/Ag_3PO_4$ hybrid exhibits visible light sensitive characteristic with the absorption edge of around 550, which is in agreement with the results previously reported (Bi *et al.*, 2011). Upon the epitaxial growth of $AgBr/Ag_3PO_4$ on the surfaces of TiO_2, the absorption edge of the heterocrystal drastically extends to around 570 nm. However, the absorption intensity in the wavelength range from 380 to 500 nm is much lower than that of $AgBr/Ag_3PO_4$ which might be partly due to much smaller particle size of BrPTi (Figure 3-2). These results demonstrate that the absorption spectrum of TiO_2 can be readily adjusted to visible light region by the heteroepitaxial growth of $AgBr/Ag_3PO_4$ on it.

3.3.3. Degradation of MO using $AgBr/Ag_3PO_4/TiO_2$

3.3.3.1. Effects of the ratio of Ag to Ti on the degradation activity of BrPTi

As shown in Figure 3-4, pure TiO_2 (P25) exhibits an extremely low photocatalytic activity in degrading MO under simulated solar light condition, which confirms the weak visible light

absorption by TiO_2. As $AgBr/Ag_3PO_4$ was doped on it, the resulting heterojunction BrPTi showed high activity in degrading MO.

The photocatalytic activity of this BrPTi catalyst in degrading MO is observed to increase up to maxima as a function of the ratio of Ag to Ti and tend to decrease upon further higher value (Figure 3-5). The highest value of 0.397 mg min^{-1} g^{-1} is found in the case with the molar ratio of Ag to Ti being 1.5. The results clearly indicate that the photoatalytic activity of this BrPTi heterojunction is closely relevant to the molar ratio of Ag and Ti. This variation tendency occurred over the prepared BrPTi in this study is similar to the patterns reported previously over some heterojunctions (e.g., $AgBr/WO_3$, Ag_3PO_4/TiO_2, $AgBr/TiO_2$, $AgBr/Ag_3PO_4$) (Cao *et al.*, 2011b; Cao *et al.*, 2012a; Yao *et al.*, 2012; Zang *et al.*, 2008).

3.3.3.2. Comparison of photocatalytic activities of BrPTi and other traditional photocatalyst

Although the optimum ratio of Ag to Ti for the best photocatalytic activity of BrPTi has been figured out, comparison of the photocatalytic activity between the BrPTi with the best photocatalytic activity (1.5 BrPTi) and other traditional photocatalysts (P25, Ag_3PO_4 and $AgBr/Ag_3PO_4$) needs to be conducted to evaluate its value for future application.

It can be clearly seen from Figure 3-6 that MO is most easily degraded by $AgBr/Ag_3PO_4$, and the photocatalytic activities among these various catalylsts follow the trend as: $AgBr/Ag_3PO_4$ > 1.5 BrPTi > Ag_3PO_4 > TiO_2 (P25). The results of apparent rate constant k_{app} analysis also reveal the same trend among these catalysts (Table 3-2). These suggest that the photocatalytic activity of Ag_3PO_4 can be promoted by doping AgBr on it, which coincides with the results reported in some studies (Bi *et al.*, 2011; Cao *et al.*, 2012a). Meanwhile, 1.5 BrPTi is found to possess much higher photocatalytic activity than Ag_3PO_4 and TiO_2 while a little lower than $AgBr/Ag_3PO_4$. Still,

the turbidity of BrPTi solution was observed much higher than that of $AgBr/Ag_3PO_4$ solution under the condition with catalyst dosage of 0.025 g, which was due to about three fold higher surface area of BrPTi than $AgBr/Ag_3PO_4$ (Table 3-1). The penetration ratio of incident light to solution of high turbidity would be reduced by scattering effect. Consequently, the advantage one between BrPTi and $AgBr/Ag_3PO_4$ cannot be identified in terms of photocatalytic activity under this catalyst loading. Comparison of photocatalytic activities in degrading MO among these catalysts should be conducted under further low catalyst loading condition in order to alleviate the effects of turbidity.

Under the condition with the catalyst loading of 0.01 g when the differences in turbidity among these catalysts solution was narrowed, a slight difference was found comparing with the case of 0.025 g catalyst loading that the MO degradation efficiency followed the trend as: 1.5 BrPTi > $AgBr/Ag_3PO_4$ > Ag_3PO_4 > TiO_2 (P25) (Figure 3-7). This result reveals the always higher photocatalytic activity of 1.5 BrPTi than Ag_3PO_4 and TiO_2 (P25) without affecting by the differences in turbidity. Additionally, it is interesting to find that 1.5 BrPTi is more efficient in degrading MO than $AgBr/Ag_3PO_4$ although its solution still seemed more turbid than $AgBr/Ag_3PO_4$ solution. In other words, 1.5 BrPTi possesses higher photocatalytic activity than $AgBr/Ag_3PO_4$ when the negative impact of turbidity is alleviated. Therefore, in comparison with Ag_3PO_4 and $AgBr/Ag_3PO_4$ which have been proved to possess highly photocatalytic efficiency, this novel catalyst, $AgBr/Ag_3PO_4/TiO_2$ consisting of much less Ag, exhibits a much more efficient photocatalytic performance instead (Table 3-2).

The much larger surface area of the 1.5 BrPTi heterojunction than that of the $AgBr/Ag_3PO_4$ photocatalyst is responsible for the improvement of photocatalytic activity of the heterostructured photocatalyst (Table 3-1). Generally, the activity of a photocatalyst increases

with the increase of catalyst surface area. A large surface area can promote photocatalytic reaction because (I) more active sites on the surface are involved in the photocatalytic reaction, and (II) the efficiency of electron–hole separation is enhanced (Zang *et al.*, 2008).

3.3.4. The mechanism of degradation of methyl orange by $AgBr/Ag_3PO_4/TiO_2$

In order to figure out the mechanism of degradation of MO by BrPTi, the role of reactive oxygen species were investigated. As Figure 3-8 shows, under the conditions with addition of AO and BQ, 1.5 BrPTi exhibits little capacity in degrading MO. While the photocatalytic activity of it in degrading MO under the condition with addition of TBA is a little higher than that in no TBA introduced case. These results suggest the critically important roles of h^+ and $\bullet O_2^-$ for 1.5 BrPTi in degrading MO under simulated solar light condition but the little influence of •OH.

As previous study revealed, O_2 was unlikely to converse directly to into $\bullet O_2^-$ on the surface of $AgBr/Ag_3PO_4$ consisting in the BrPTi owing to the lower E_{CB} values of AgBr and Ag_3PO_4 than the reduction potential of O_2 (O_2 / $\bullet O_2^-$ = −0.33 V/NHE) (Cao *et al.*, 2012a). Consequently, it can be inferred that O_2 combined with electrons trapped by Ag NPs which generated on 1.5 BrPTi and therefore forming $\bullet O_2^-$. Besides, since there is no evidence revealing the involvement of TBA in degrading organics during photocatalysis process, the promoted efficiency of MO degradation by 1.5 BrPTi in the case with the addition of TBA might be attributed to the role of TBA as a dispersed agent in preventing the aggregation of BrPTi nanoparticles.

On the other hand, in the study of Zhang et al. (2011), P25 was proved to possess high capability of generating •OH using PL technique even though •OH showed little contribution to the degradation of RhB by P25. This suggests that the contribution of •OH to the degradation of targeted pollutant do not always coincide with the yield of it during photocatalysis period and

partly related to the reaction rate between •OH and targeted pollutants. Consequently, although •OH has been proved to contribute little to the degradation of MO by 1.5 BrPTi in this study, the •OH generation capacity of 1.5 BrPTi is still not clear. The PL technique was therefore employed to detect the •OH formed on the surfaces of 1.5 BrPTi. For comparison, P25 was also tested as a reference. Figure 3-9 shows the fluorescence spectral changes observed during light irradiation of P25 and 1.5 BrPTi in a basic terephthalic acid solution (excitation wavelength at 315 nm). As shown, the PL intensity around 425 nm corresponding to 2-hydroxyterephtalic acid which is formed by the reaction between •OH and terephthalic acid are proportional to the light irradiation time for P25, which demonstrates the production of the hydroxyl radicals. In comparison, for the case of 1.5 BrPTi sample, the photofluorescence around 425 nm is very weak although the PL intensity is also observed to gradually increase with the irradiation time, confirming the very little generation of •OH during the photocatalysis process.

The mechanism for photocatalytic degradation of MO varied with the catalysts (Gomathi Devi and Mohan Reddy, 2010; Han *et al.*, 2009; Meng *et al.*, 2011). For 1.5 BrPTi heterostructure in this study, therefore, the possible mechanism for MO degradation can be summarized to four steps as follows:

$$\text{BrPTi} + h\nu \text{ (simulated solar light)} \rightarrow \text{Ag}^0/\text{BrPTi}$$

$$\text{Ag}^0/\text{BrPTi} + h\nu \text{ (simulated solar light)} \rightarrow h^+ + e^- \qquad (11)$$

$$\text{MO} + h^+ \rightarrow \text{MO}^+$$

$$H_2O + h^+ \rightarrow O_2 + 2H^+ \qquad (12)$$

$$O_2 + e^- \rightarrow \bullet O_2^-$$

$O_2 + 2H^+ + 2e^- \rightarrow H_2O_2$ (13)

$MO^+ + \bullet O_2^- \rightarrow$ Products

$MO^+ + H_2O_2 \rightarrow$ Products (14)

In addition, the role of H_2O_2 which is vital in degrading organics during some photocatalysis processes has also been investigated using catalase as scavenge (Li *et al.*, 2009a). In this study, however, the catalase became floccose sediment from homogeneous solution after 30 min dark reaction, which suggested the denaturation of catalase before photocatalytic reaction. This might be attributed to toxic effect of silver compound on catalase (Zhang *et al.*, 1998). Therefore, the role of H_2O_2 cannot be properly evaluated for 1.5 BrPTi sample in this study. Still, it is reasonable for O_2 to be able to reduce to H_2O_2 on the surface of 1.5 BrPTi as the higher E_{CB} values of AgBr and Ag_3PO_4 than the reduction potential of O_2 (O_2 / H_2O_2= + 0.69 V/NHE) (Cao *et al*., 2012a; Liu *et al.*, 2010).

3.3.5. The stability of $AgBr/Ag_3PO_4/TiO_2$

The stability of photocatalyst is an important parameter for its prospective application. As shown in Figure 3-10, for the first cycling run, the degradation of MO is observed to be degraded more easily in the case of 1.5 BrPTi comparing with $AgBr/Ag_3PO_4$ with the removal efficiencies of 97.8% and 94.2%, respectively. This result reconfirms the higher photocatalytic activity of 1.5 BrPTi. Subsequently, for the second cycling run, both $AgBr/Ag_3PO_4$ and 1.5 BrPTi show slightly lower photocatalytic activities compared with that in the first run, but still exhibits high capacities in degrading MO with removal efficiencies of 85.2% and 73.5%, respectively. As the recycling runs progresses, the removal efficiencies of MO keep decreasing to 52.8% and 31.2% corresponding to $AgBr/Ag_3PO_4$ and 1.5 BrPTi, respectively.

These results indicate $AgBr/Ag_3PO_4$ is not stable for successive use to degrade MO under simulated solar light condition (300-800 nm). The similar result was observed in the study of degradation MO by $AgBr/Ag_3PO_4$ under visible light condition (>420 nm) although the decomposing extent was a little different which might be caused by the differences in light source, light intensity and the concentration of sacrificial reagent between each other (Cao *et al.*, 2012a). Meanwhile, a gradual downtrend is also observed in three successive experimental runs using 1.5 BrPTi, suggesting that it is still difficult to keep the photocatalytic activity of $AgBr/Ag_3PO_4$ after introducing TiO_2. However, it can be clearly seen from Figure 3-10 that the degradation efficiency of MO keeps constantly being higher in the case of 1.5 BrPTi than $AgBr/Ag_3PO_4$ for each recycle run. Moreover, the difference in MO degradation efficiency between these two catalysts gradually increases as the recycle runs progresses, which reveals that the rate of MO degradation over $AgBr/Ag_3PO_4$ particles decreases more significantly than 1.5 BrPTi after three cycles under the same conditions. These results indicate the introduction of TiO_2 to $AgBr/Ag_3PO_4$ not only enhance the photocatalytic activity of $AgBr/Ag_3PO_4$ but also alleviate the elapse of its photocatalytic capacity under successive use. Similar result was reported in the study on introducing TiO_2 to Ag_3PO_4 (Yao *et al.*, 2012).

After three recycle runs, the color of 1.5 BrPTi heterojunction changed to brown even a slightly dark. Since silver salt or its heterojunctions have been fully proved to decompose in photocatalysis process (Cao *et al.*, 2012a; Liu *et al.*, 2012b; Wang *et al.*, 2008; Wang *et al.*, 2009), it can be inferred that Ag in metallic state was generated on this BrPTi heterojunction, leading to the slightly dark of catalyst after photocatalytic reaction. Therefore, the improved stability of BrPTi photocatalyst under simulated solar light irradiation might result from Ag NPs that are produced from the decomposition of AgBr and Ag_3PO_4 and deposited on BrPTi. This

sandwiched Ag/AgBr/Ag_3PO_4/TiO_2 structure can promote charge separation and catalyze the photooxidation of the MO solution. The further reduction of AgBr and Ag_3PO_4 catalyst could be inhibited by injecting photo-generated electrons into the conduction band of TiO_2 through the Ag/TiO_2 interface similar to that found on the Ag_3PO_4/ TiO_2 and Ag/AgCl/TiO_2 system (Morimoto *et al.*, 2007; Yao *et al.*, 2012; Yu *et al.*, 2009). Moreover, since it has been fully proved that the photocatalytic activity of TiO_2 can be accelerated by Ag NPs (Abdulla-Al-Mamun *et al.*, 2011; Cheng *et al.*, 2010; Yun *et al.*, 2009), the Ag/TiO_2 composition in Ag/BrPTi can possibly counteract the decrease of photocatalytic capacity caused by the loss of AgBr/Ag_3PO_4 during photocatalytic process.

3.3.6. Comparison of photocatalytic activities of BrPTi and other traditional photocatalyst in degrading MC-LR

It can be clearly seen from Figure 3-11 that MC-LR was most easily degraded by 1.5 BrPTi, and the photocatalytic efficiency among these various catalylsts followed the trend as: 1.5 BrPTi > AgBr/Ag_3PO_4 > Ag_3PO_4. This result is similar to my previous study using methyl orange as targeted pollutant (3.3.3.2). The results of apparent rate constant k_{app} analysis also revealed the same trend among these catalysts (Figure 3-11(b)). These results suggested that the photocatalytic activity of Ag_3PO_4 can be promoted by doping AgBr on it, which coincided with the resultes reported in some studies (Bi *et al.*, 2011; Cao *et al.*, 2012a). Meanwhile, the highest photocatalytic activity of 1.5 BrPTi was attributed to its high surface area and the combined action among Ag nanoparticles (NPs), AgBr, Ag_3PO_4 and TiO_2 consisting in it.

3.3.7. Byproducts of MC-LR degraded by 1.5 BrPTi heterojunction

As the results shows (Figure 3-12), the peak corresponding to MC-LR (ESI+: m/z = 995.13; ESI−: m/z = 992.56) occurs in the sample, which suggesting the existence of MC-LR in the stock solution we used for this experiment. However, other relatively obvious peaks (e.g. ESI+: m/z= 424.44, 551.33, 663.08 and 860.96) are also observed in the results of MS spectrum. This indicates the existence of other organics in the sample before treatment. This is because the MC-LR powder sample we purchased from commercial company is made by extraction method from cyanobacteria. And the purity of this MC-LR powder was not 100% percent but about 90%. This result makes it difficult to recognize MC-LR byproducts under the attack of 1.5 BrPTi.

Still, from Figure 3-12, it can be seen clearly that the peak corresponding to MC-LR (ESI+: m/z = 995.13; ESI−: m/z = 992.56) disappeared after being treatment. Meanwhile, there are several new peaks with m/z smaller than 900 show up in the case of being treated by 70 Ag/Ag_3PO_4 (ESI+: m/z = 769.81, 662.72, 606.74, 518.98, 502.70 493.27, 428.37, 370.26, 354.42, 294.20, 264.32, 190.48, 136.30; ESI−: m/z = 513.62, 472.35, 389.18, 299.91, 283.50, 264.39, 180.15, 108.06), comparing with no treatment case. This indicates that MC-LR was degraded by 70 Ag/Ag_3PO_4 into some byproducts in a range of smaller molecule weight.

3.3.8. Degradation of MCs by 1.5 BrPTi heterojunction

As shown in Figure 3-13, MCs (MC-LR, -YR and -RR) are observed to be effectively removed by 1.5 BrPTi under two cases of different MCs loading (100 and 200 mg L^{-1}). For these two MCs loadings, the removal efficiency of different MC variety by this heterojunction catalyst under simulated solar light irradiation follows the same trend as: MC-YR > MC-RR > MC-LR. The same pattern was revealed in chapter 2. During dark adsorption period, the adsorption efficiency

of MC follows the tendency as: MC-YR > MC-RR > MC-LR. It has been proved that the adsorption efficiency of MC on particles depends on a combine effects of its hydrophobicity property, charge forces and other factors such as molecular size and conformation rather than sole effect of these factors. Consequently, this distinct difference is attributed to different characteristics among MC varieties.

3.3.9. Degradation efficiencies of MC-LR by 1.5 BrPTi in a range of catalyst dosages and light intensities

The degradation efficiencies of MC-LR over 1.5 BrPTi in a range of catalyst dosages and light intensities are shown in Figure 3-14 and Figure 3-15, respectively. It can be clearly seen in Figure 3-14 that the degradation efficiency of MC-LR is proportional to catalyst dosage of 1.5 BrPTi. And the highest photocatalystic efficiency in degrading MC-LR occurred in the case of 0.01 g catalyst. The apparent reaction rate constants (k_{app}) for the photocatalytic degradation of MC-LR also reveal the same tendency (Table 3-3). It is worth noting that there is only a slight difference in the rate constant between the cases of 0.008 g and 0.01 g. These results suggested that the photocatalytic rate increased up to maxima as a function of catalyst loading and tended to stable upon further loading, which was in agreement with a number of previous studies (Farooq *et al.*, 2009; Ismail, 2008; Liu *et al.*, 2010). More active sites on the surface of catalyst hole-electron pairs which are responsible for the degradation of MC-LR were generated as the increase of catalyst loading. However, turbidity was created as the catalyst loading kept increasing, which was capable of reducing the penetration intensity of light by scattering effect**.** In the report of Liu et al. (2010), too much catalyst applied also induced another phenomenon of catalyst aggregation resulting in a decrease in total active surface area available for adsorbing organics and absorbing light radiation. Therefore, it can be inferred that the photocatalytic

efficiency in degrading MC-LR in the case of 0.01g almost the same as that in the case of 0.008 g was attributed to the generated turbidity and aggregation of nano-scale 1.5 BrPTi particles.

It is also observed that the degradation efficiency of MC-LR increased with the light intensity (Figure 3-15). The apparent reaction rate constants (k_{app}) for the photocatalytic degradation of MC-LR was 0.062, 0.1167, and 0.142 min^{-1} in the cases of 2, 4 and 6 W m^{-2}, respectively (Table 3-3). At higher radiation intensity, more electron-hole pairs were expected to generate in the catalyst, which are available for the degradation of MC-LR.

3.4. Conclusion

I have demonstrated a facile method to improve the photocatalytic activity and stability of the $AgBr/Ag_3PO_4$ photocatalyst by deposition of $AgBr/Ag_3PO_4$ nanoparticles onto TiO_2 (P25). In comparison with Ag_3PO_4 and $AgBr/Ag_3PO_4$ which have been proved to possess great photocatalytic activities, this novel catalyst, $AgBr/Ag_3PO_4/TiO_2$ consisting of much less Ag, exhibits a much more efficient photocatalytic performance instead in degrading MO and MC-LR. Photocatalytic mechanism investigation demonstrates that the degradation of MO over the as-prepared $AgBr/Ag_3PO_4/TiO_2$ under simulated solar light condition was mainly via h^+ and $\bullet O_2^-$ oxidation pathway in which Ag NPs also involves. In addition to higher activity, $AgBr/Ag_3PO_4/TiO_2$ heterostructured photocatalyst shows more stable than $AgBr/Ag_3PO_4$ under simulated solar light condition. Therefore, this photocatalyst would be required, which is of importance to the potential application in the photocatalytic field.

Table 3-1 Estimated particle size and specific surface area for TiO_2, AgBr/ Ag_3PO_4 and BrPTi samples.

Catalysts	Estimated particle size (μm)	BET surface area (sq.m./g)
$AgBr/Ag_3PO_4$	0.2-1.0	7.322
TiO_2	0.025	50.0
0.3 BrPTi	0.03-0.05	37.136
0.9 BrPTi	0.03-0.1	23.671
1.5 BrPTi	0.03-0.1	21.406
2.4 BrPTi	0.03-0.15	16.604

Table 3-2 Nominal silver loading and apparent rate constant for TiO_2, Ag_3PO_4, $AgBr/Ag_3PO_4$ and 1.5 BrPTi samples.

Catalysts	Silver content (%)	Apparent rate constant k (min^{-1})	
		0.01 g	0.025 g
TiO_2	0	0.0011	0.0007
Ag_3PO_4	77	0.0073	0.033
$AgBr/Ag_3PO_4$	72	0.0143	0.0693
1.5 BrPTi	53	0.0156	0.0481

Table 3-3 Pseudo first order kinetics parameters of MC degradation by 1.5 BrPTi under various environmental conditions.

Catalyst dosage and light intensity		Apparent rate constant k (min^{-1})	R^2
Catalyst dosage	0.002 g	0.059	0.856
	0.004 g	0.137	0.979
	0.006 g	0.317	0.975
	0.008 g	0.421	1.00
	0.010 g	0.471	1.00
Light intensity	2 W m^{-2}	0.062	0.892
	4 W m^{-2}	0.117	0.989
	6 W m^{-2}	0.142	0.970

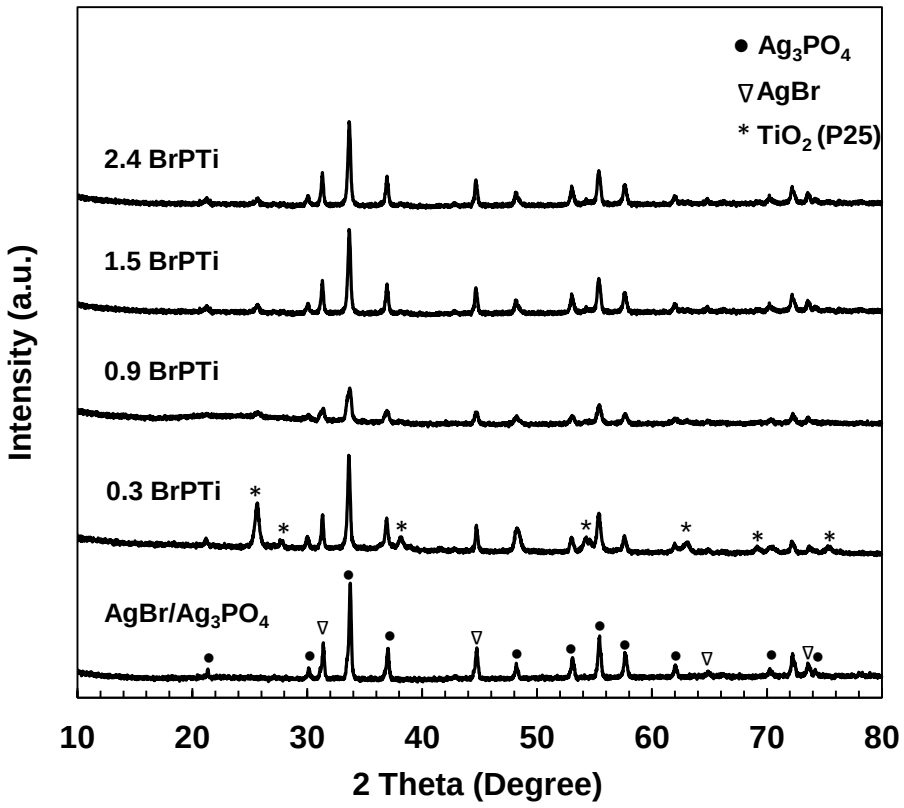

Figure 3-1 XRD patterns of the prepared $AgBr/Ag_3PO_4$ and various BrPTi powders.

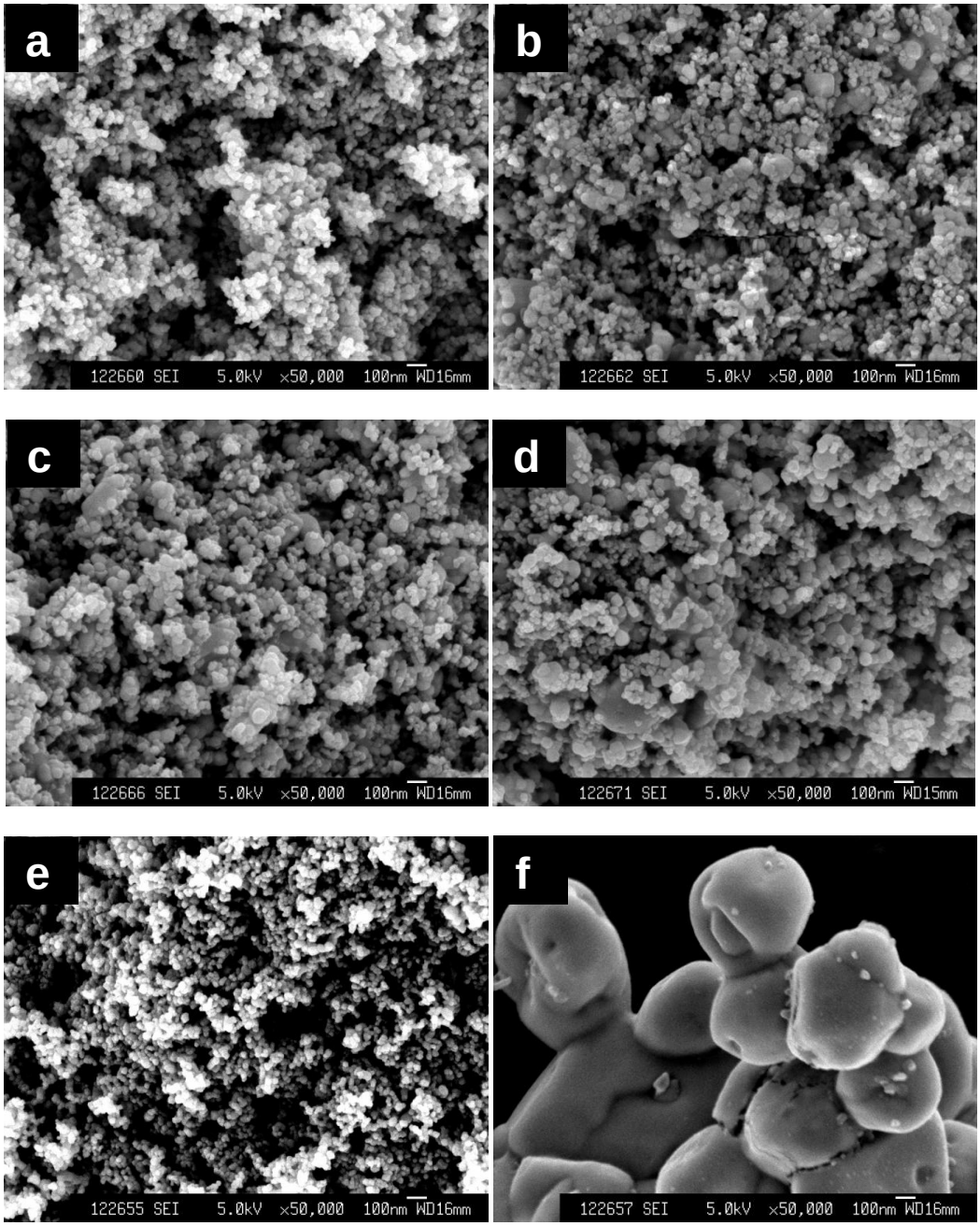

Figure 3-2 SEM images of (a) 0.3 BrPTi, (b) 0.9 BrPTi, (c) 1.5 BrPTi, (d) 2.4 BrPTi and (e) TiO_2 and (f) $AgBr/Ag_3PO_4$ powder samples.

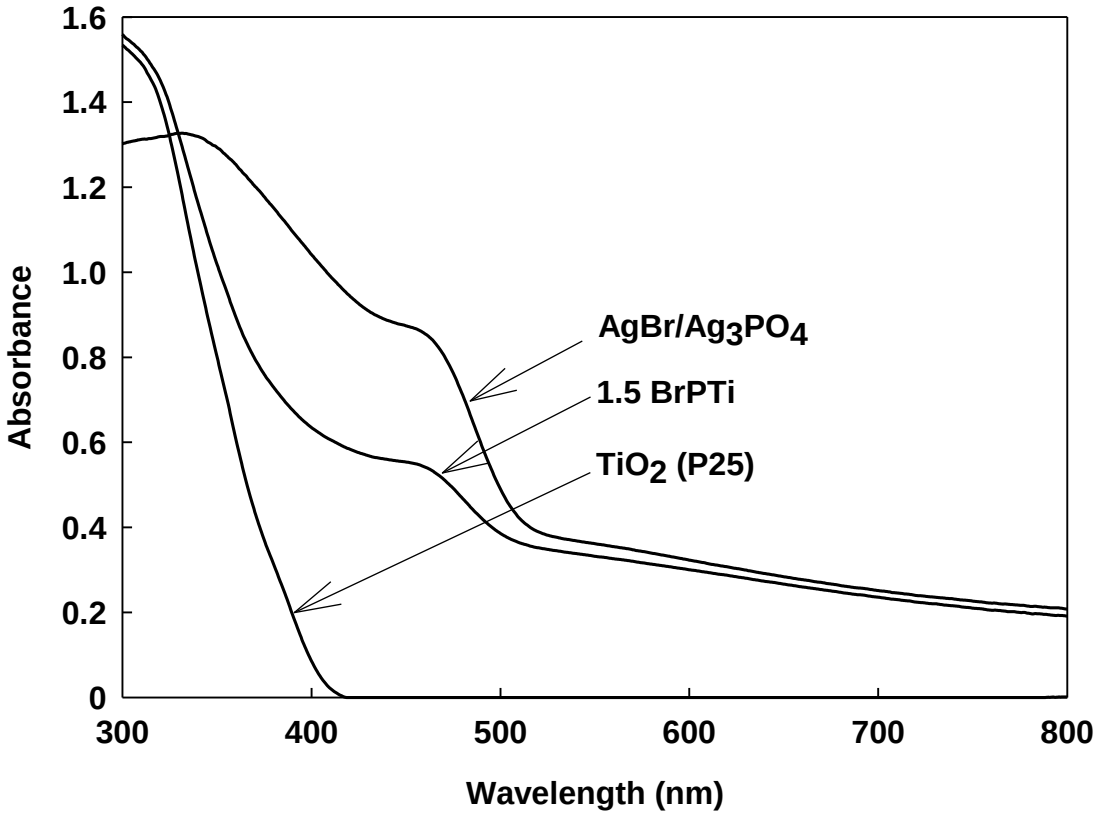

Figure 3-3 Ultraviolet–visible diffusive reflectance spectrum of the TiO_2 (P25), $AgBr/Ag_3PO_4$ and BrPTi (molar ratio $_{Ag:Ti}$ = 1.5) samples.

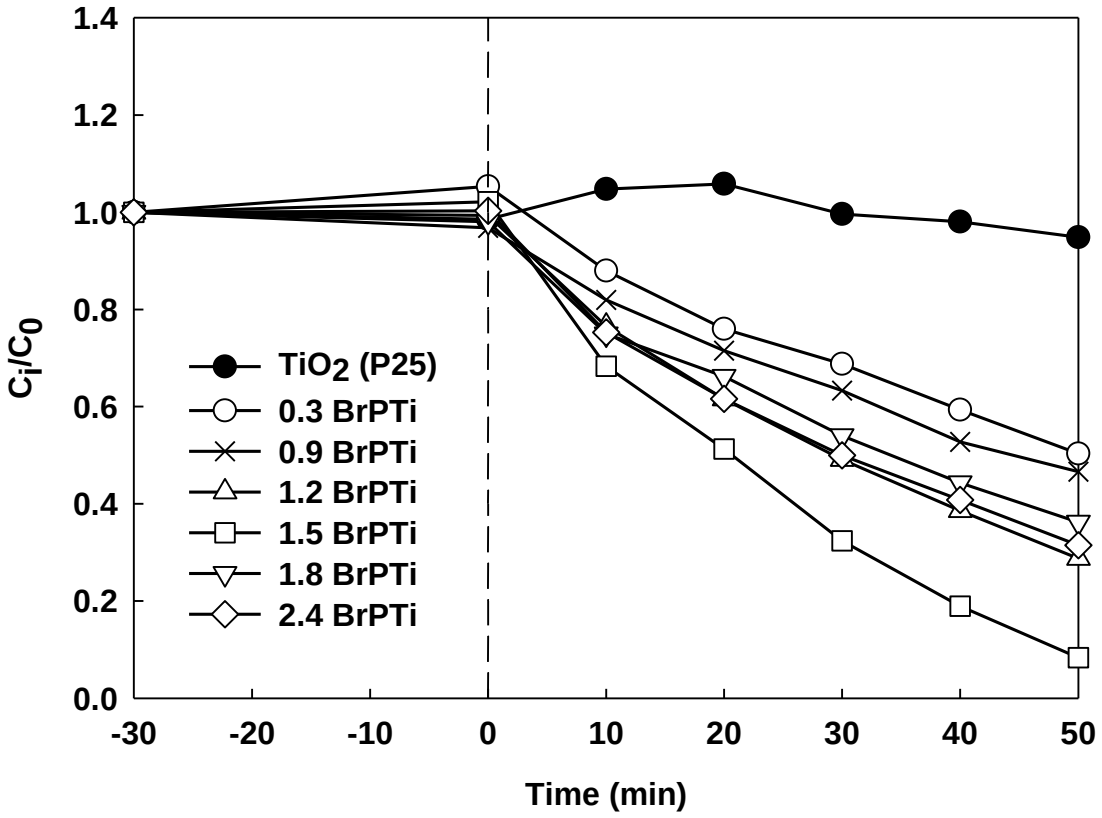

Figure 3-4 Photocatalytic activities of BrPTi heterojunctions on the degradation of MO under simulated solar light condition (with the time of light on set as 0).

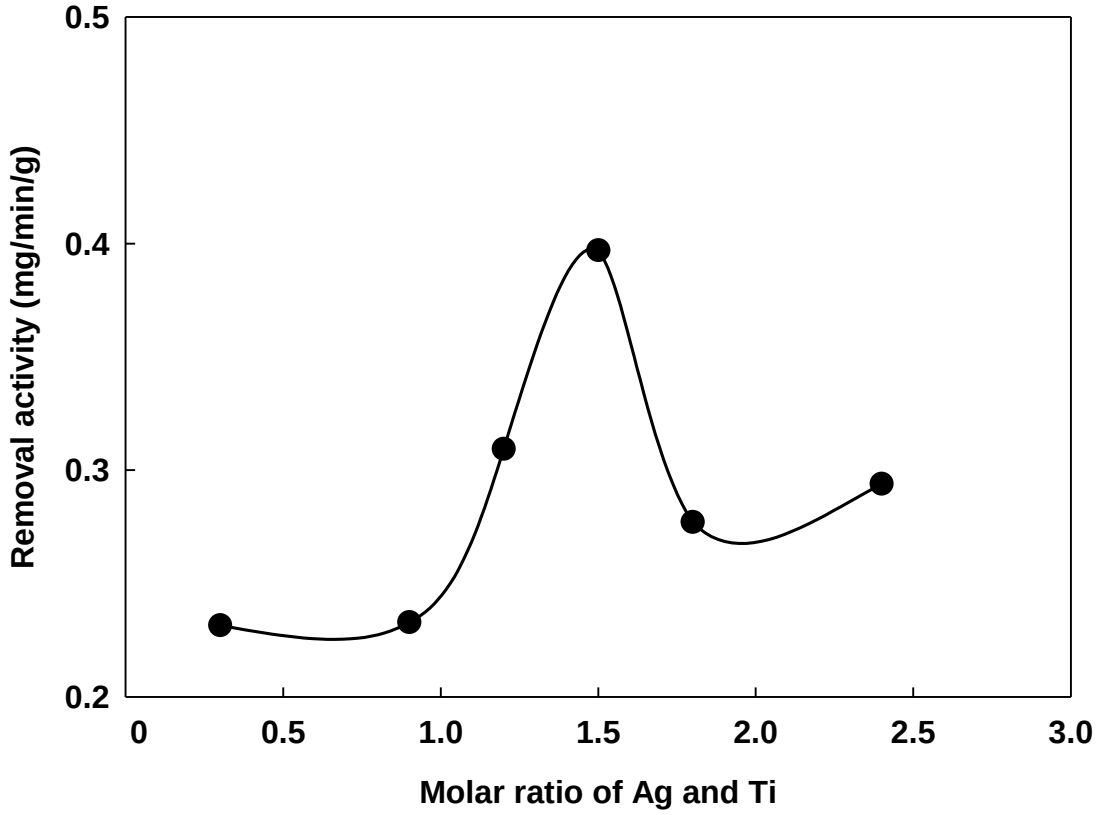

Figure 3-5 Effect of Ag/TiO_2 molar ratio on the photocatalyltic activity of BrPTi heterojunction in removing MO under simulated solar light condition.

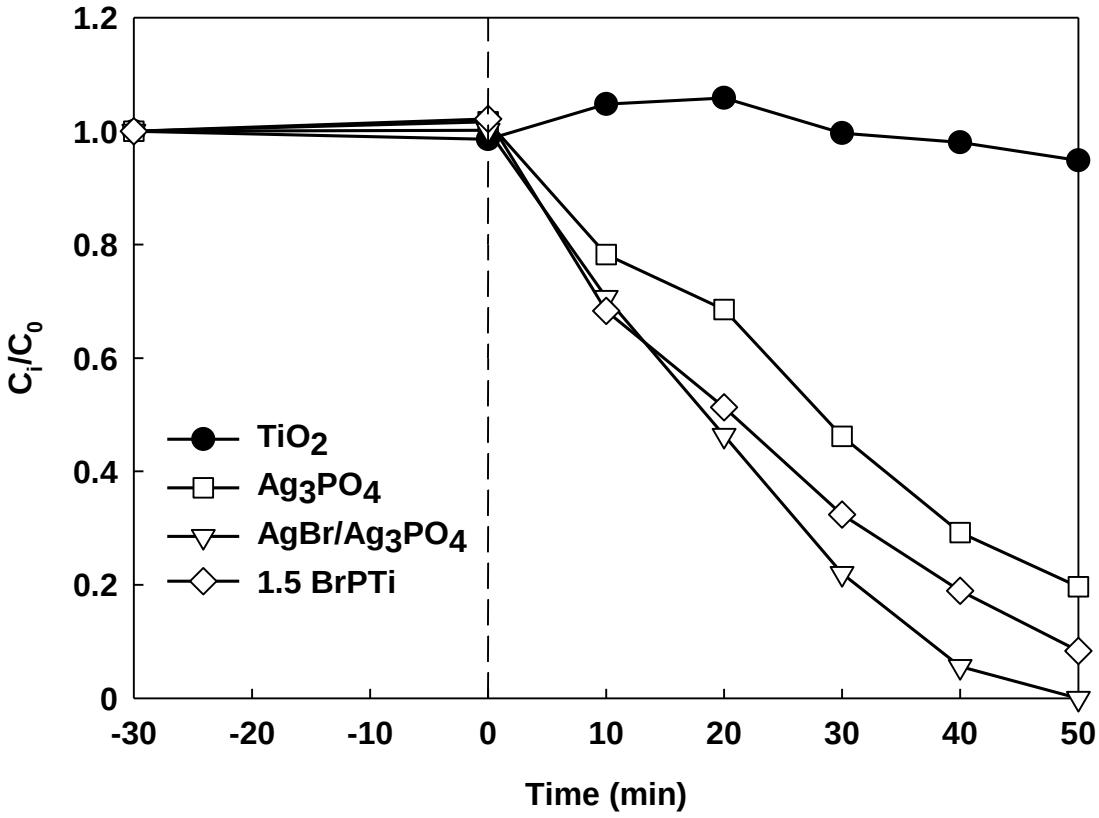

Figure 3-6 Comparision of photocatalytic activities of different photoatalysts (TiO_2, Ag_3PO_4, $AgBr/Ag_3PO_4$ and 1.5 BrPTi) in degrading MO under simulated solar light condition (catalyst dosage: 0.025 g).

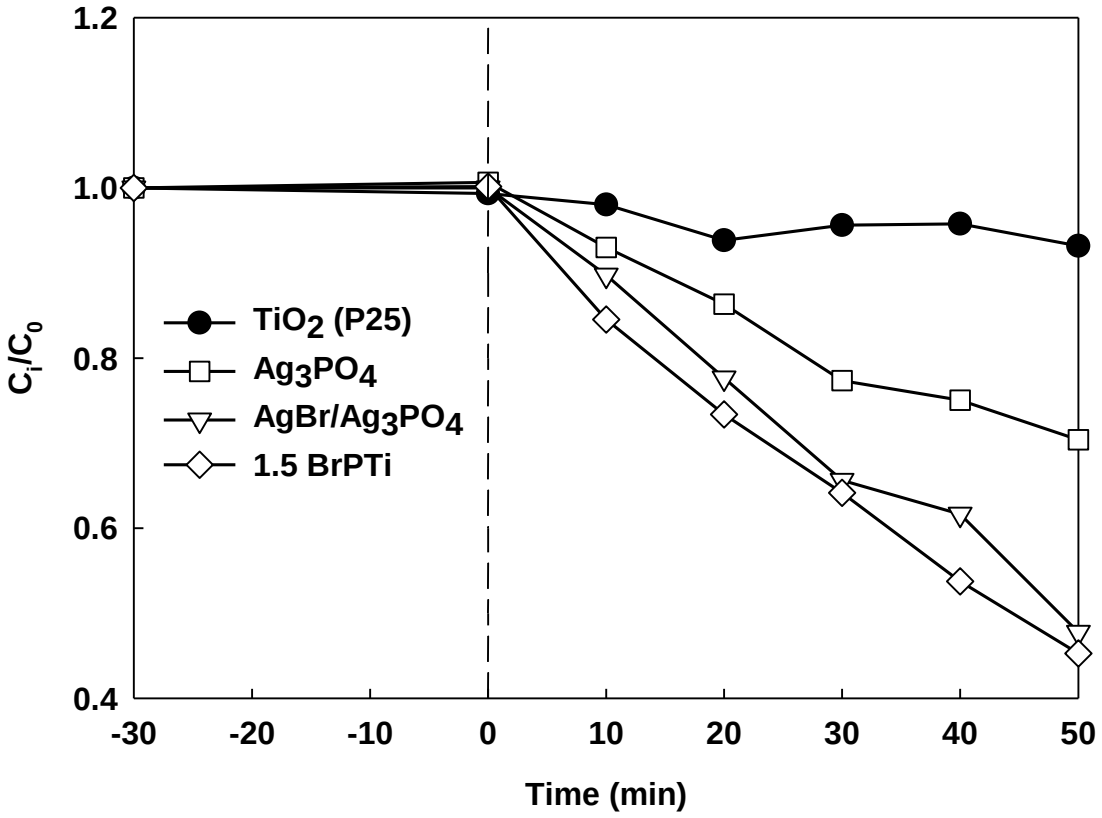

Figure 3-7 Comparision of photocatalytic activities of different photoatalysts (TiO_2, Ag_3PO_4, $AgBr/Ag_3PO_4$ and 1.5 BrPTi) in degrading MO under simulated solar light condition (catalyst dosage: 0.01 g).

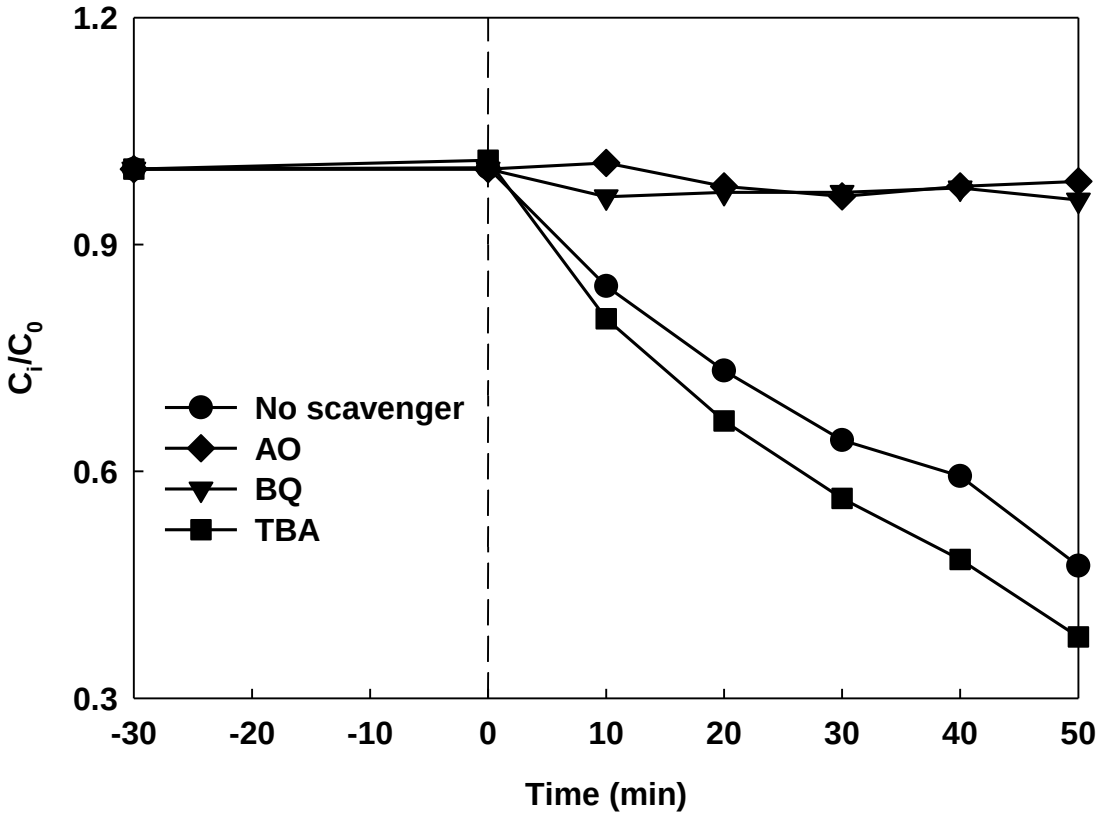

Figure 3-8 Effects of different scavengers on MO degradation with 1.5 BrPTi catalyst.

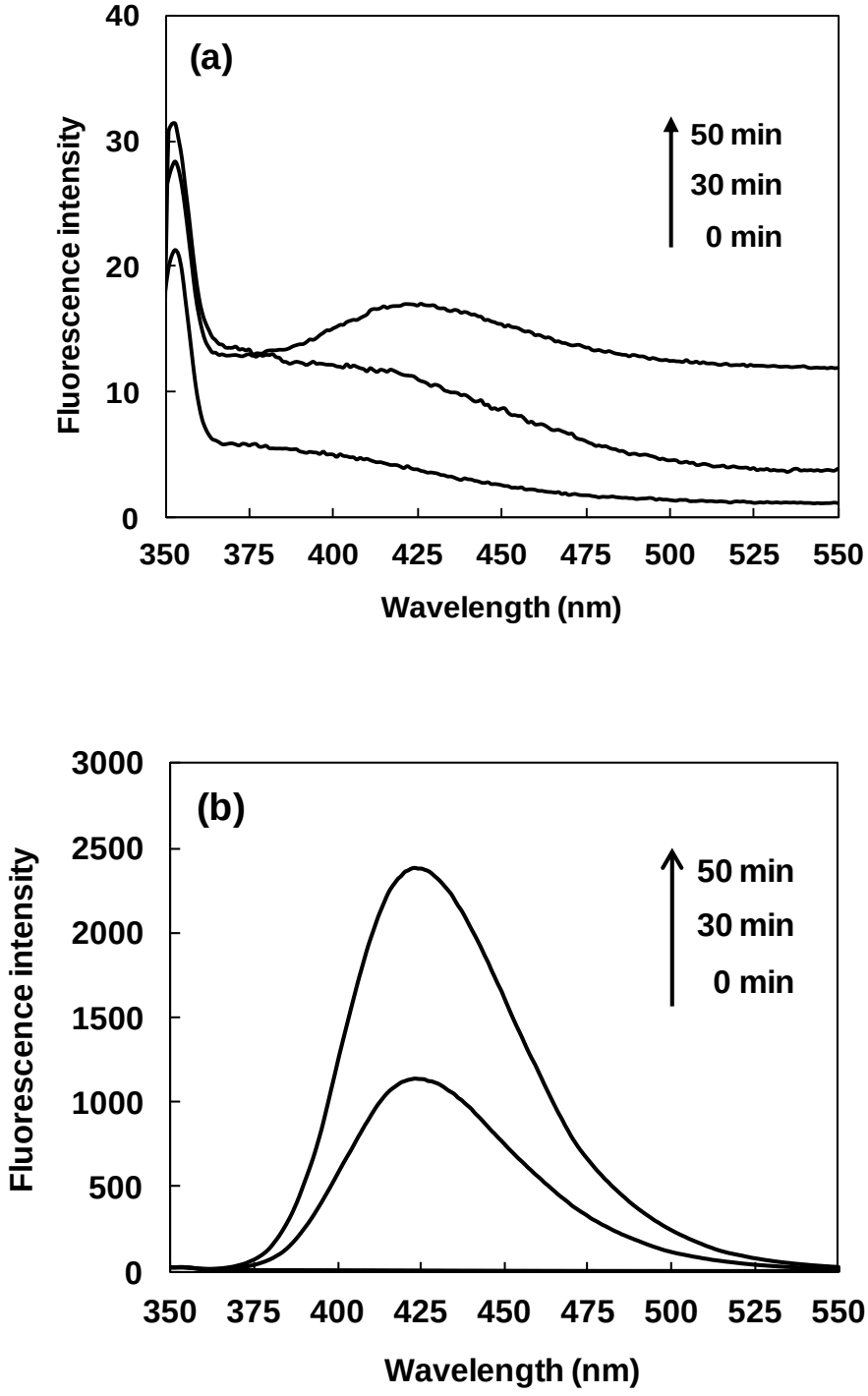

Figure 3-9 •OH trapping PL spectra of (a) 1.5 BrPTi and (b) TiO_2 in TA solution under simulated solar light irradiation.

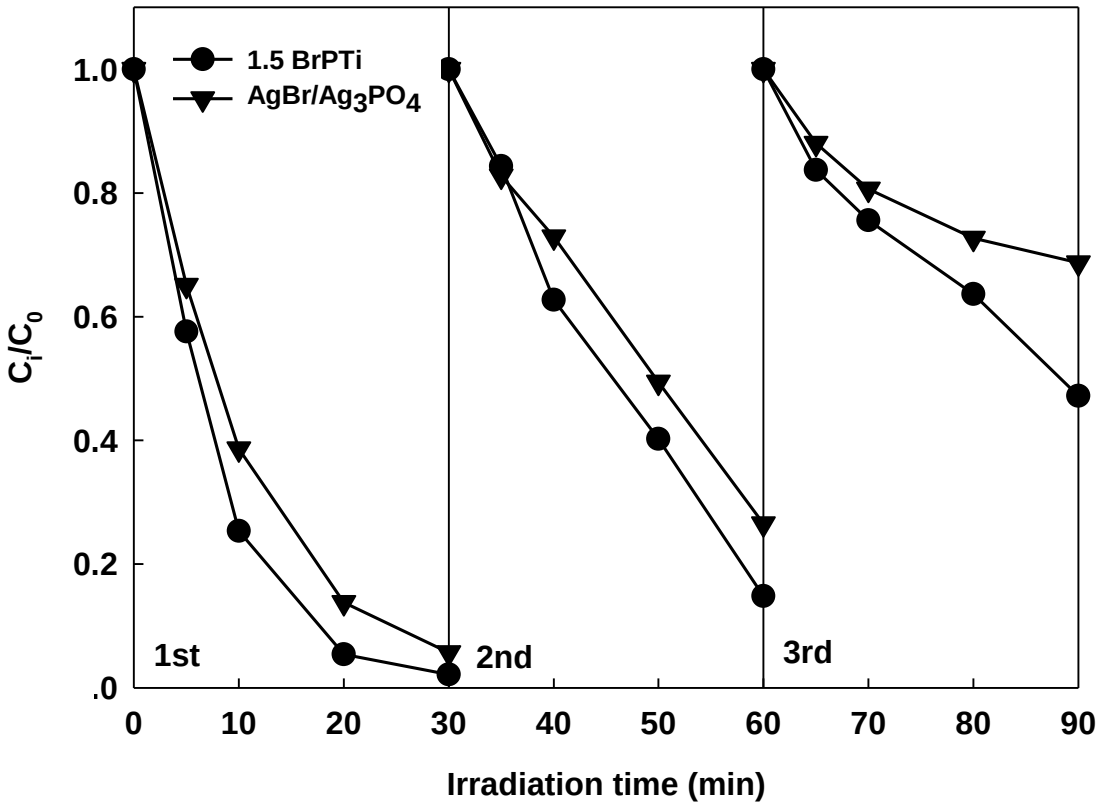

Figure 3-10 Photocatalytic degradation of MO under simulated solar light condition for three cycling runs with $AgBr/Ag_3PO_4$ and 1.5 BrPTi, respectively.

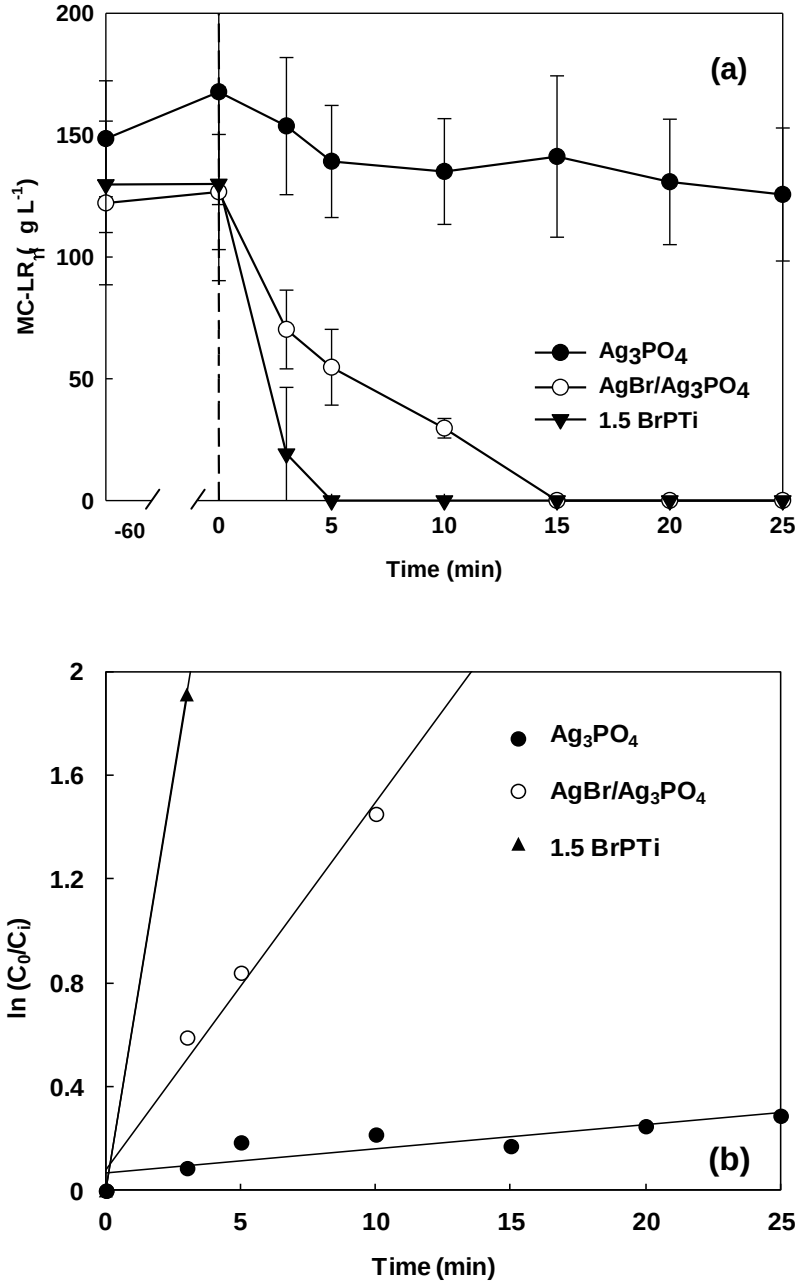

Figure 3-11 Degradation of MC-LR by Ag_3PO_4, $AgBr/Ag_3PO_4$ and 1.5 BrPTi catalysts under simulated solar light irradiation (catalyst dosage: 0.01g) (Error bars indicated the ranges of duplicated measurements) (a) and the pseudo-first-order kinetics for photocatalytic destruction of MC-LR (b).

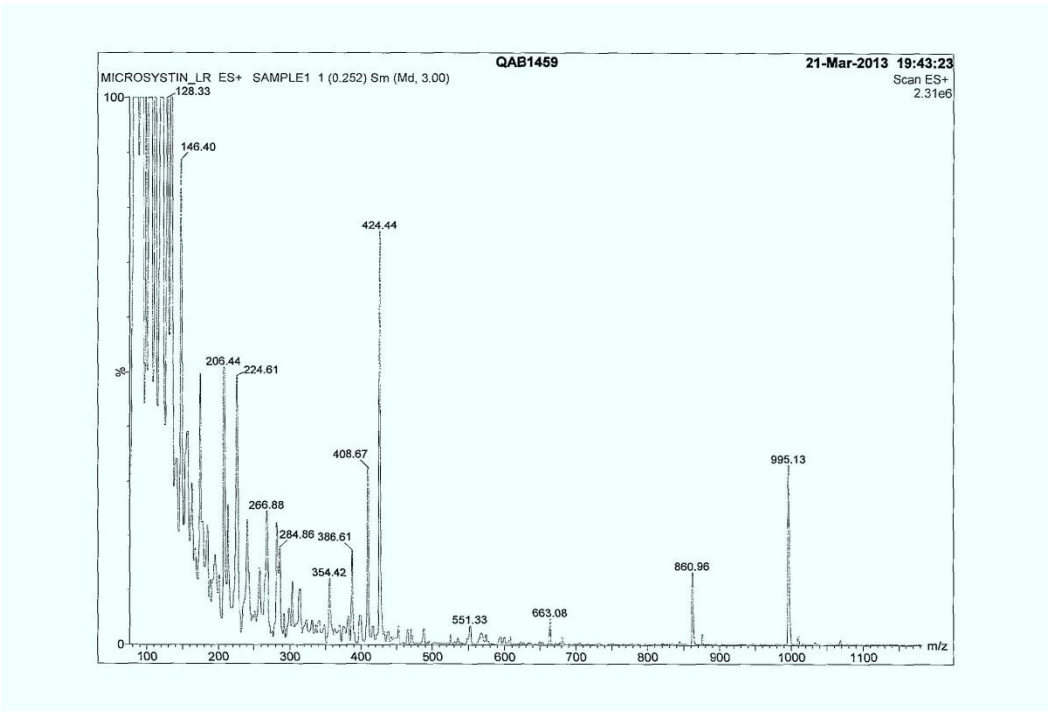

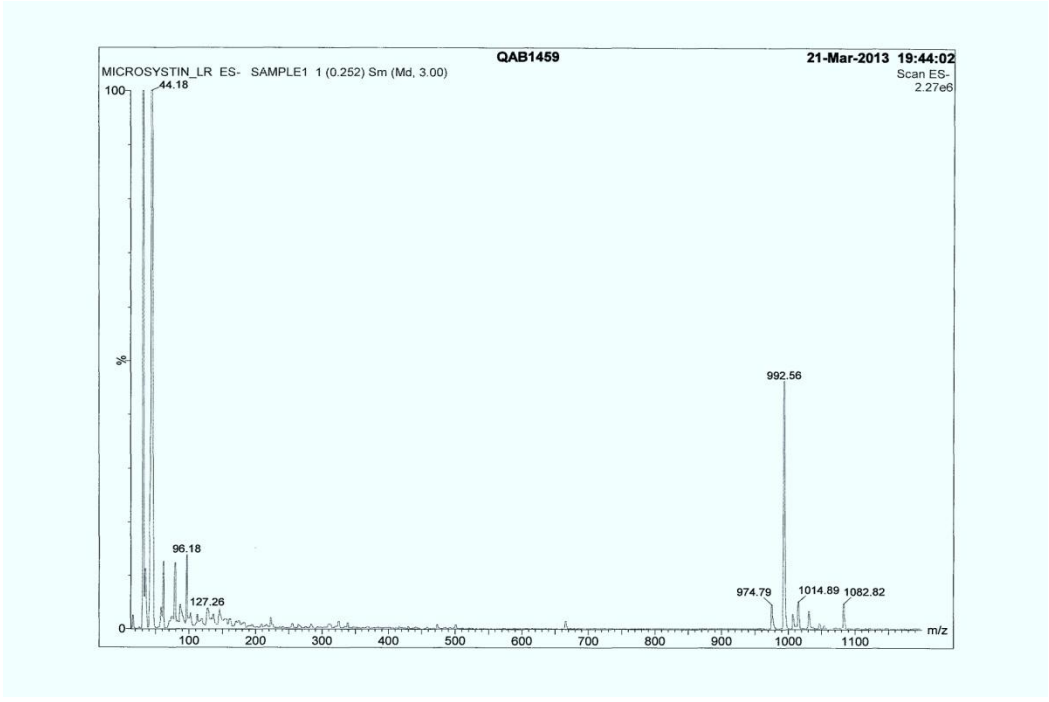

(a) The mass spectrum for the MC-LR solution before being treated by 1.5 BrPTi

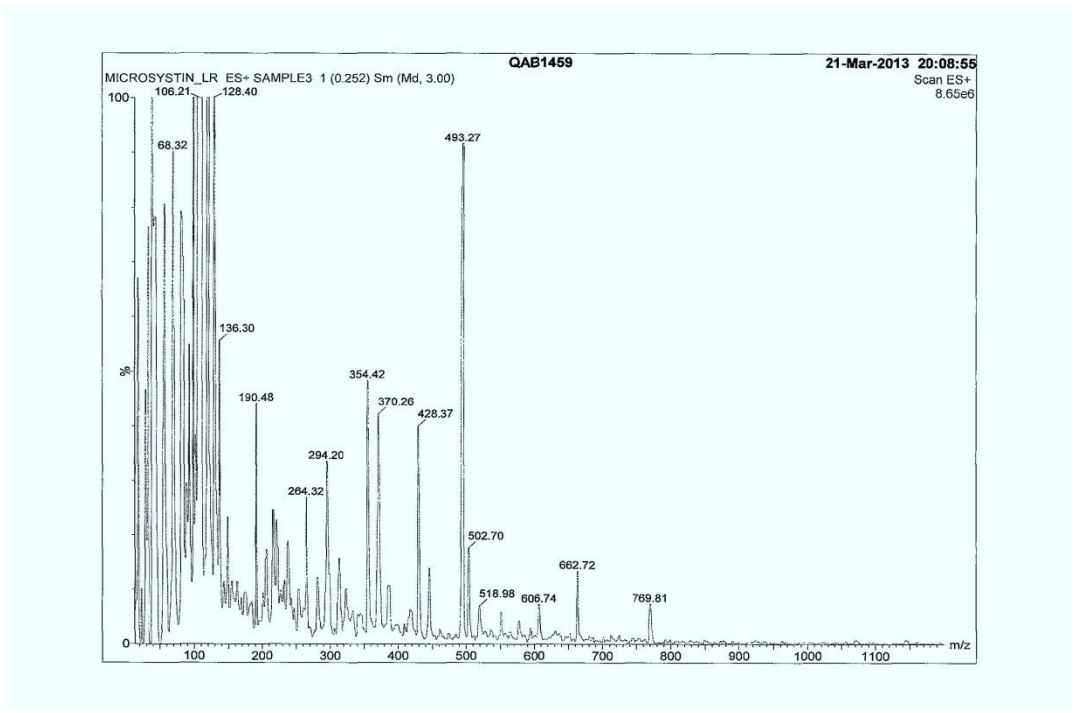

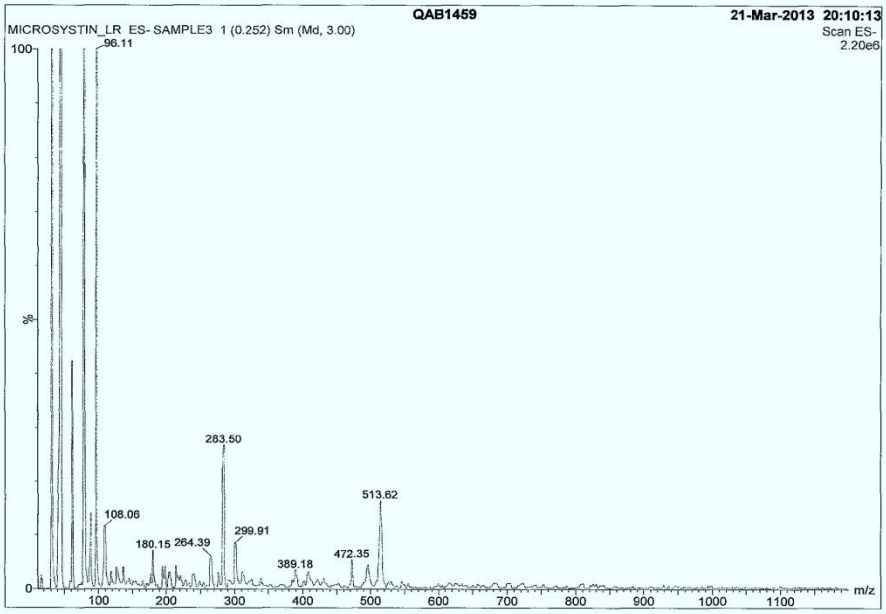

(b) The mass spectrum for the MC-LR solution after being treated for 25 min by 1.5 BrPTi

Figure 3-12 The mass spectrum for the MC-LR solution before being treated by 1.5 BrPTi (a) and after being treated for 25 min by 1.5 BrPTi (b).

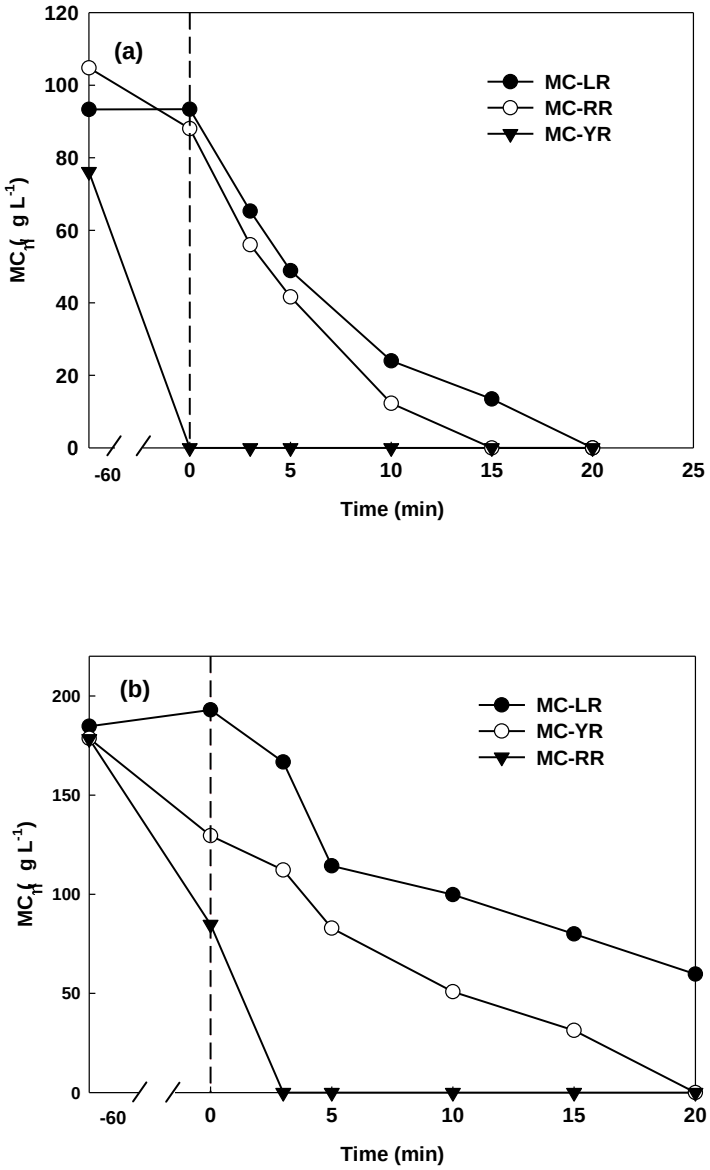

Figure 3-13 Degradation of MC-LR, -YR and RR with Initial concentration of (a) 100 mg L^{-1}, (b) 200 mg L^{-1} by 1.5 BrPTi catalysts under simulated solar light irradiation (catalyst dosage: 0.004 g).

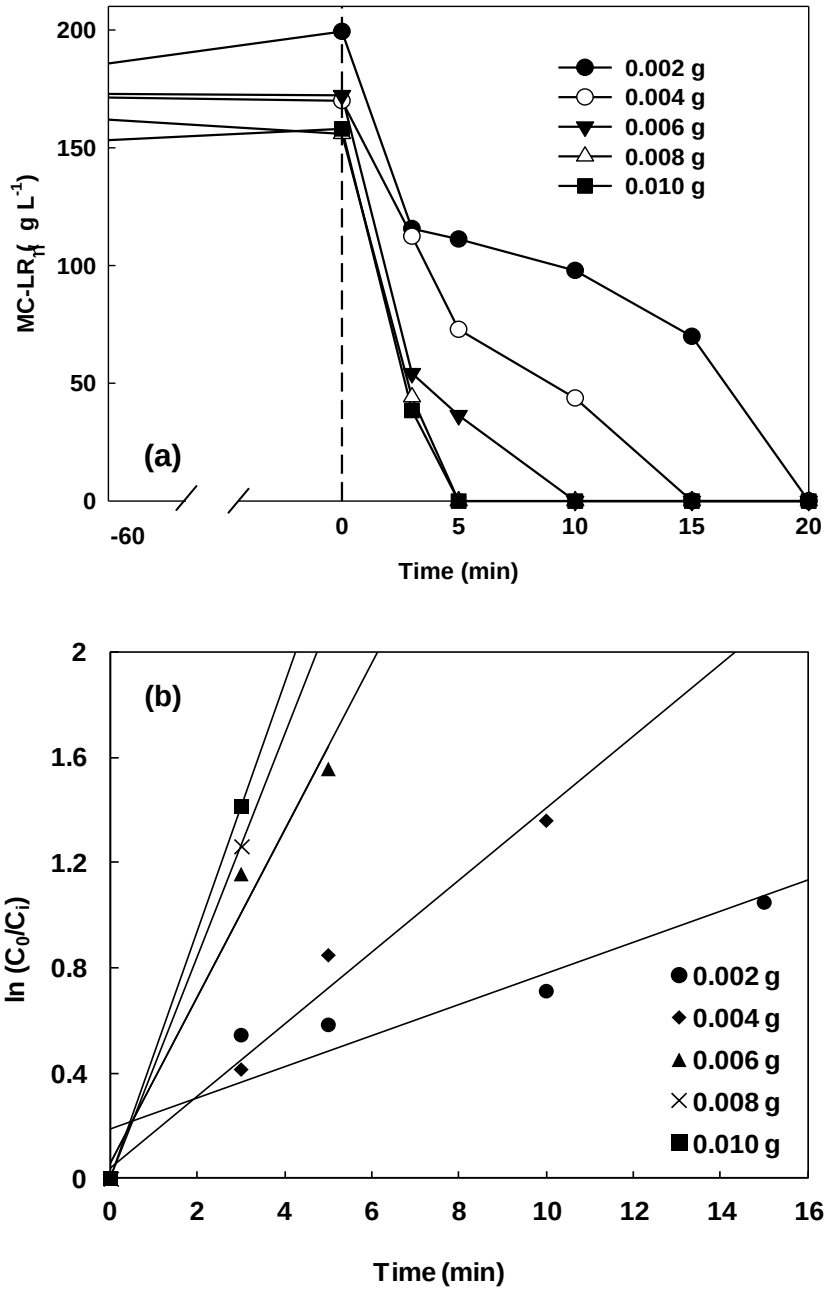

Figure 3-14 Degradation of MC-LR by 1.5 BrPTi (a) and the pseudo-first-order kinetics for photocatalytic destruction of MC-LR (b) under different catalyst dosage conditions.

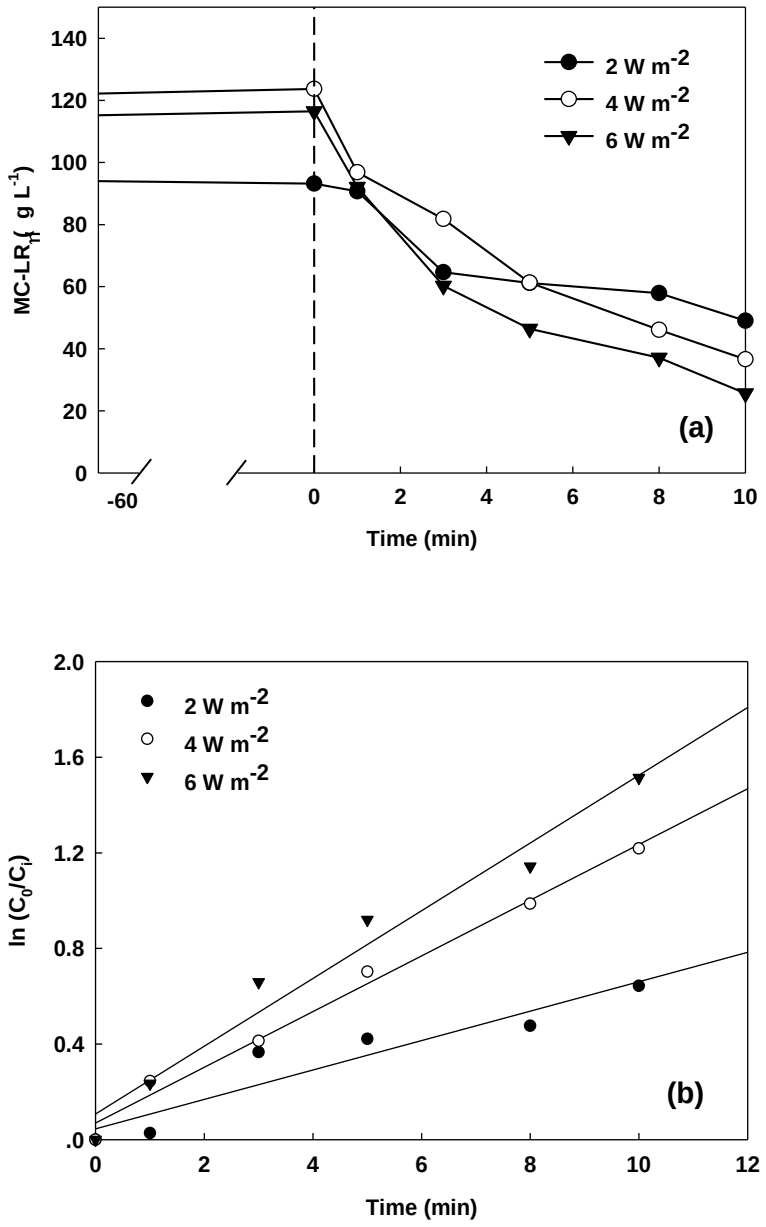

Figure 3-15 Degradation of MC-LR by 1.5 BrPTi (a) and the pseudo-first-order kinetics for photocatalytic destruction of MC-LR (b) under different light intensity conditions (catalyst dosage: 0.004 g).

Chapter 4 Influences of environmental factors on degradation of MCs by $AgBr/Ag_3PO_4/TiO_2$ heterojunction

4.1. Introduction

MCs have been found susceptible to photocatalytic degradation with the heterojunction, 1.5 BrPTi, under simulated solar light irradiation in my study. However, the photocatalytic reaction system was conducted with 'clean' synthetic water. Several matrices and conditions present in natural water can influence the photocatalytic reaction (Pelaez *et al.*, 2011; Piscopo *et al.*, 2001). The characteristics of the solution matrix (i.e., alkalinity, pH, natural organic matter) are critical to determine the photocatalytic degradation of organic contaminants in water with this technology (Antoniou *et al.*, 2005). Therefore, their roles on the photocatalytic process need to be evaluated and understood to develop effective solar-driven technologies for MCs polluted water purification.

A major factor influencing the rate of degradation of organic compounds in TiO_2-based photocatalytic processes is pH (Kim *et al.*, 2010b; Wang *et al.*, 2011a; Zhu *et al.*, 2005). Changes in pH could affect the surface charge of TiO_2 and the ionization of compounds present in solution is critical to the adsorption and interaction between catalyst and microcystins (Lawton *et al.*, 2003; Sharma *et al.*, 2012). MC-LR initial degradation rate increased in acidic pH when employing thin TiO_2 films compared to thick films (Antoniou *et al.*, 2009).

Natural organic matter (NOM), which consists mainly of fulvic and humic substances, is a normal constituent existing in natural water. The presence of natural organic matter (NOM) has been revealed to have a pronounced influence on the photocatalytic degradation of organic molecules via TiO_2 (Kull *et al.*, 2006; Welker and Steinberg, 2000). NOM can act as photosensitizers and mediate photodegradation. Feitz et al. (1999) suggested that high

concentrations of natural dyes secreted by cyanobacteria in natural water scavenged the surface-generated hydroxyl radicals or the organic radicals generated can react among the exudate and lose their oxidizing ability. It has also been reported that these NOM constituents retarded the photocatalytic degradation of carbamazepine, clofibric acid and iomeprol with TiO_2 materials by competition for active sites and surface deactivation of the catalyst by adsorption (Doll and Frimmel, 2005).

As well as NOM, inorganic anions, such as Cl^-, NO_3^-, SO_4^{2-}, and PO_4^{3-}, are basic components in natural water. Specific anions can influence the degradation process by affecting the concentration of reactive oxygen species formed during the photocatalytic process (Dionysiou *et al.*, 2000). Furthermore, anions can react with the hydroxyl radical to form the corresponding anion radical (Adbullah *et al.*, 1990). The effects of common inorganic anions (Cl^-, NO_3^-, SO_4^{2-}, and PO_4^{3-}) frequently present in industrial waste water are likely to retard the rates of oxidation of organic compounds by competing for the oxidizing radicals or by blocking the active sites of the TiO_2 catalyst (Piscopo *et al.*, 2001; Xia *et al.*, 2002).

Besides, the presence of dissolved metal ions is common in natural waters as well in industrial wastes, and they can sensibly affect the rate and efficiency of photocatalytic reactions (Litter, 1999). Such an effect has been found in the removal of brilliant blue dye, aromatic hydrocarbons, benzoic acids, phenols, aliphatic acids and other organic compounds in the presence of metallic ions (Mn^{2+}, Fe^{2+}, Co^{2+}), principally Cu^{2+}, Fe^{2+} and Ag^+ (Brezová *et al.*, 1995; Butler and Davis, 1993; Kumawat *et al.*, 2012; Litter, 1999). The increase in photooxidation rates by addition of metal ions has been attributed, in the first instance, to the ability of ions to scavenge electrons on the surface of catalyst. This would reduce the non-desired electron/hole recombination, resulting in an increased rate of $^{\bullet}HO$ formation (Litter, 1999).

Therefore, although 1.5 BrP has been proved to possess highly photocatalytic activity in degrading MCs, the photocatalytic activity of it in degrading MC under various environmental conditions needs to be further measured. In this chapter, the influences of pH, humic acid, cations and anions on the photocatalytic activity of 1.5 BrPTi nanoparticles in degrading MC-LR under s were investigated.

4.2. Materials and methods

4.2.1. Effects of pH

The degradation of MC-LR by 1.5 BrPTi was conducted under various pH conditions (pH=5, 7, 10). The measurement was performed in a 100 mL beaker placed on a magnetic stirrer. The photocatalytic degradation experiments were carried out by adding the stock solution of MC-LR (50 mg L^{-1}) and catalyst (0.004 g) in distilled water at the desired MC-LR concentration of 100 μg L^{-1}. The total volume of the solution for reaction was adjusted to 30 mL and the light intensity was set to 4 W m^{-2}. Before the measurement started, the pH of solution was adjusted with HNO_3 and NaOH solution (0.1 M, respectively).

4.2.2. Effects of anion

Various sodium salt (Cl^-, NO_3^- and SO_4^{2-}; initial concentration: 10 mg L^{-1}, respectively) was added to the photocatalytic system of 1.5 BrPTi and MC-LR to investigate the effect of anion. The measurement was performed in a 100 mL beaker placed on a magnetic stirrer. The photocatalytic degradation experiments were carried out by adding the stock solution of MC-LR (50 mg L^{-1}) and catalyst (0.004 g) in distilled water at the desired MC-LR concentration of 100 μg L^{-1}. The total volume of the solution for reaction was adjusted to 30 mL and the light intensity was set to 4 W m^{-2}.

4.2.3. Effects of cation

Various metal sulfate (Mg^{2+}, Cu^{2+} and Fe^{3+}; initial concentration: 10 mg L^{-1}, respectively) was added to the photocatalytic system of 1.5 BrPTi and MC-LR to investigate the effect of cation. The measurement was performed in a 100 mL beaker placed on a magnetic stirrer. The photocatalytic degradation experiments were carried out by adding the stock solution of MC-LR (50 mg L^{-1}) and catalyst (0.004 g) in distilled water at the desired MC-LR concentration of 100 μg L^{-1}. The total volume of the solution for reaction was adjusted to 30 mL and the light intensity was set to 4 W m^{-2}.

4.2.4. Effects of humic acid

The measurement was performed in a 100 mL beaker placed on a magnetic stirrer. The photocatalytic degradation experiments were carried out by adding the stock solution of MC-LR (50 mg L^{-1}), stock solution of Humic acid (100 mg L^{-1}, Wako Pure Chemical Industries, Ltd.) and catalyst (0.004 g) in distilled water at the desired MC-LR concentration of 100 μg L^{-1}. The total volume of the solution for reaction was adjusted to 30 mL and the light intensity was set to 4 W m^{-2}.

4.3. Results and discussion

4.3.1. The effects of pH on the degradation of MC-LR by $AgBr/Ag_3PO_4/TiO_2$

In order to investigate the effect of pH, the MC-LR degradation over 1.5 BrPTi catalyst was measured at different initial pH (pH 5, 7, and 10). The results are shown in Figure 4-1. Table 4-1 shows that MC-LR degradation is most effective at acidic pH 5, with k_{app} of 0.392, 0.236 and 0.213 min^{-1} corresponding to pH 5, 7 and 10 respectively. It has been reported that pH can affect the adsorption efficiency of targeted pollutants onto catalyst by changing the net charge of the surface of catalyst or the pollutants (Lawton *et al.*, 2003; Sushi *et al.*, 2009). However, in this

study, no obvious difference in the adsorption efficiency of MC-LR is found among various pH conditions during dark adsorption period, suggesting the interaction between the surface of catalyst and MC-LR is not affected by pH within the range of 5 to 10. The MC-LR has been revealed to be negatively charged at pH 4-12 (Ho *et al.*, 2011; Pelaez *et al.*, 2012a), which indicates MC-LR keeps negatively charged in a pH range from 5 to 10 set in this study. Consequently, it can be inferred that the net charge of the surface of 1.5 BrPTi catalyst was not obviously affected within this pH range.

Meanwhile, it is worth noting that the degradation efficiency of MC-LR by 1.5 BrPTi under various pH conditions showed distinctly as irradiation started. This result indicates that the photocatalytic activity of 1.5 BrPTi can be promoted by acidic condition, but shows no obvious change as the pH value increases from 7 to 10. It has been reported that the degradation of MC-LR by some catalysts (TiO_2 and NF-TiO_2) can be promoted by acidic condition owing to promoted attractive forces between the catalyst and the toxin (Lawton *et al.*, 2003). However, this scenario should not happen in this study since no obvious difference occurred in the adsorption of MC-LR by 1.5 BrPTi under these pH conditions. On the other hand, it has been revealed that the presence of large quantities of OH^- ions on the particle surface as well as in the reaction medium favors the formation of •OH radical, which is widely accepted as principal oxidizing species responsible for decolorization process at neutral or high pH levels, and results in enhancement of the efficiency of the process (Sushi *et al.*, 2009). However, this scenario was not expected to happen in this case as the degradation efficiency of MC-LR under alkaline condition (pH=10) is almost the same as that under neutral condition (pH=7). In my previous study, it has been reported that H_2O_2 is a main kind of oxygen reactive species generated during photocatalysis of 1.5 BrPTi following the reaction.

$O_2 + 2H^+ + 2e^- \rightarrow H_2O_2$ (15)

Consequently, it can be inferred that the higher degradation efficiency of MC-LR under acid condition might be attributed to promoted generation of H_2O_2 in the presence of large quantities of H^+.

4.3.2. The effects of normal anions on the degradation of MC-LR by $AgBr/Ag_3PO_4/TiO_2$

The degradation of MC-LR by 1.5 BrPTi with addition of various anions (Cl^-, NO_3^- and SO_4^{2-}) is shown in Figure 4-2. As shown, the degradation efficiencies of MC-LR over 1.5 BrPTi in the cases with addition of anion are all observed to be almost the same as that in the case not introducing anions. This result indicates that this species (Cl^-, NO_3^- and SO_4^{2-}) do not affect the rates of oxidation of MC-LR over 1.5 BrPTi. It has been reported that the anions (Cl^-, NO_3^- and SO_4^{2-}) are likely to retard the rates of oxidation of organic compounds by competing for the oxidizing radicals or by blocking the active sites of the TiO_2 catalyst (Abdullah *et al.*, 1990; Fan and Sun, 2001; Piscopo *et al.*, 2001; Xia *et al.*, 2002). However, this scenario is not expected to happen in this study as no inhibition phenomenon of MC-LR degradation occurred in anions addition cases. It is noting that the concentration of anions applied in previous study was higher than 100 mg L^{-1} (Abdullah *et al.*, 1990; Dionysiou *et al.*, 2000; Xia *et al.*, 2002), while 10 mg L^{-1} in this study. This fact might result in the little effect of anions on the photocatalytic activity of 1.5 BrPTi in degrading MC-LR.

4.3.3. The effects of normal metal cations on the degradation of MC-LR by $AgBr/Ag_3PO_4/TiO_2$

The removal efficiency of MC-LR by 1.5 BrPTi with addition of various anions (Cu^{2+}, Mg^{2+} and Fe^{3+}) is shown in Figure 4-3. As shown, differences are observed in absorption efficiency of MC-LR by 1.5 BrPTi during dark absorption period under various cations conditions. In the case

with no addition of anions, 1.5 BrPTi shows little capacity of adsorbing MC-LR during dark period. After introducing Mg^{2+}, no obvious change occurs in the adsorption of MC-LR by 1.5 BrPTi before irradiation starts. However, it is interesting that the concentration of MC-LR dramatically decreases to undetected level after 30 minutes dark stirring process in the cases of Cu^{2+} and Fe^{3+}. This result suggests that MC-LR can be efficiently adsorbed by 1.5 BrPTi and Fe^{3+} in the presence of Cu^{2+} and Fe^{3+}, which implies changes of the interaction between MC-LR and the surface of 1.5 BrPTi after introducing Cu^{2+} and Fe^{3+}. Similar result was reported by Fan and Sun (2001) that humic acid could be effectively adsorbed by TiO_2 after introducing Ca^{2+} and Mg^{2+} while showed no degradation in the case without Ca^{2+} and Mg^{2+}. This distinct change was expected to be attributed to the change of surface charge of catalyst induced by metal ions. The particles which are negatively charged would become positively charged after absorbing metal ions, and therefore promoting negatively charged organics to be adsorbed on the particles. MC-LR, as the targeted pollutant in this study, has been proved to be negatively charged in a pH range of 4-12 (Ho *et al.*, 2011; Pelaez *et al.*, 2012a). Thus, MC-LR is expected to be negatively charged as the pH of the photocatalysis reaction system in this study is about 6.5. As Cu^{2+} and Fe^{3+} were introduced into the system, the surface of 1.5 BrPTi was expected to become positively charged by absorbing these metal cations. The negatively charged MC-LR was therefore capable of adsorbing on the surface of 1.5 BrPTi particles, forming a complex of Cu^{2+}/Fe^{3+}, MC-LR and 1.5 BrPTi. That is, Cu^{2+}/Fe^{3+} can act as electrostatic bridges between 1.5 BrPTi particles and MC-LR. The hypothesis pathway of this interaction among Cu^{2+}/Fe^{3+}, MC-LR and 1.5 BrPTi can be described as follows:

$$1.5\ BrPTi + Cu^{2+}/Fe^{3+} \rightarrow (1.5\ BrPTi{-}Cu/Fe)^{+} \quad (16)$$

$$(1.5\ BrPTi{-}Cu/Fe)^{+} + MC\text{-}LR \rightarrow 1.5\ BrPTi{-}Cu/Fe{-}MC\text{-}LR \quad (17)$$

However, this scenario is unlikely to happen in the case of Mg^{2+} as no obvious promoted adsorption efficiency of MC-LR occurs during dark adsorption period. It has been reported that the adsorption efficiency of cations over a certain particle depend on cation varieties (Liang *et al.*, 2000; Rahman *et al.*, 2012; Xu *et al.*, 2010). Therefore, it can be inferred that the adsorption quantity of Mg^{2+} on 1.5 BrPTi might be not enough to make the surface of 1.5 BrPTi become positively charged and adsorb MC-LR.

On the other hand, it is interesting to note that the aggregation state of 1.5 BrPTi particles is affected by these introduced cations. As Figure 4-4 shown, 1.5 BrPTi solution is observed to be in suspension state in the case with no additional cations. After introducing Mg^{2+}, Fe^{3+} and Cu^{2+}, 1.5 BrPTi particles are observed to aggregate together and settle down to the bottom of beaker to different degrees. From the transparency of the solution shown in Figure 4-4, it can be clearly seen that the suspending1.5 BrPTi nano-scale particles most easily aggregate together to precipitate in the case of Mg^{2+}, then in the case of Cu^{2+}, and most difficultly in the case of Fe^{3+}. This phenomenon implies that the surface area of 1.5 BrPTi would decrease in the presence of Mg^{2+}, which is expected to contribute to the relatively lower degradation efficiency of MC-LR under Mg^{2+} condition compared with no introduced cation condition. As previous studies revealed, the zeta potential, which is an important indicator for evaluating the aggregation state of particles, could be changed by adding cations (French *et al.*, 2009). And the affecting extent depends on valence state of the cations and also the variety (Liu *et al.*, 2012a). Consequently, the different aggregation state of 1.5 BrPTi in the presence of Mg^{2+}, Fe^{3+} and Cu^{2+} is owing to different characteristic among them.

4.3.4. The effects of humic acid on the degradation of MC-LR by $AgBr/Ag_3PO_4/TiO_2$

Figure 4-5 shows the degradation of MC-LR over 1.5 BrPTi catalyst in the presence of humic acid with different concentration (1, 5 mg L^{-1}). As shown, the degradation efficiency of MC-LR decreases as humic acid is introduced into the reaction system, with the apparent rate (k_{app}) of 0.303, 0.178 and 0.168 min^{-1}corresponding to 0, 1, 5 mg L^{-1} humic acid, respectively (Table 4-1). This result indicated that the photocatalytic activity of 1.5 BrPTi in degrading MC-LR is inhibited by coexisting human acid and the inhibition extent is proportional to the concentration of humic acid. It has been widely reported that humic acid can be effectively degraded by photocatalysis (Patsios *et al.*, 2013; Xue *et al.*, 2011; Yang and Lee, 2006). Humic acid, therefore, is expected to compete with MC-LR to be degraded over 1.5 BrPTi, which contributes to the lower degradation efficiency of MC-LR in the presence of humic acid. Besides, humic acid of which the color is brown might decrease the intensity of incident light into the solution, therefore decreasing the photocatalytic activity of 1.5 BrPTi.

4.4. Conclusions

I have demonstrated a novel heterojunction photocatalyst, 1.5 BrPTi heterojunction, possessing much greater photocatalytic activity than Ag_3PO_4 and $AgBr/Ag_3PO_4$ in degrading MC-LR. Other two varieties of MCs, MC-YR and MC-RR, can also be effectively removed by 1.5 BrPTi. And the removal efficiency of the microcystins by this heterojunction catalyst is observed to exhibit rather differently with the removal efficiency following the trend: MC-YR>MC-RR>MC-LR. The roles of light intensity and catalyst dosage in photocatalytic activity of 1.5 BrPTi are also investigated. And the photocatalytic activity of 1.5 BrPTi in degrading MC-LR is proportional to light intensity and catalyst dosage

Degradation of MC-LR by1.5 BrPTi is affected by pH (pH=5, 7 and 10, respectively). MC-LR is more easily degraded under acidic condition, which is owing to the promoted generation of H_2O_2 by large quantities of hydrogen ions. For the effects of normal anions in natural water, the degradation efficiency of MC-LR over 1.5 BrPTi is not affected by the introduced anions (Cl^-, NO_3^- and SO_4^{2-}) of 10 mg L^{-1} level. On the other hand, removal of MC-LR by 1.5 BrPTi is observed to be greatly affected by coexisting cations in reaction system (Mg^{2+}, Fe^{2+} and Cu^{2+}). The adsorption of MC-LR on 1.5 BrPTi is greatly promoted by introducing Cu^{2+} and Fe^{3+}, while shows no obvious promoted efficiency in the case of Mg^{2+}.

These results can help provide a better understanding of the interactions and mechanisms of degradation of MC-LR in order to improve the viability of visible light-activated $AgBr/Ag_3PO_4/TiO_2$ for the development of solar-driven technologies for the remediation of contaminated water with cyanobacterial toxins or other emerging contaminants of concern.

Table 4-1 Pseudo first order kinetics parameters of MC degradation by 1.5 BrPTi under various environmental conditions.

Factors		Apparent rate constant k (min^{-1})	R^2
pH	5	0.375	0.990
	7	0.236	0.932
	10	0.203	0.954
Anions	None	0.117	0.989
	Cl-	0.127	0.983
	NO_3^-	0.118	0.994
	SO_4^{2-}	0.112	0.975
Humic acid	0 mg L^{-1}	0.303	0.950
	1 mg L^{-1}	0.178	0.961
	5 mg L^{-1}	0.168	0.927

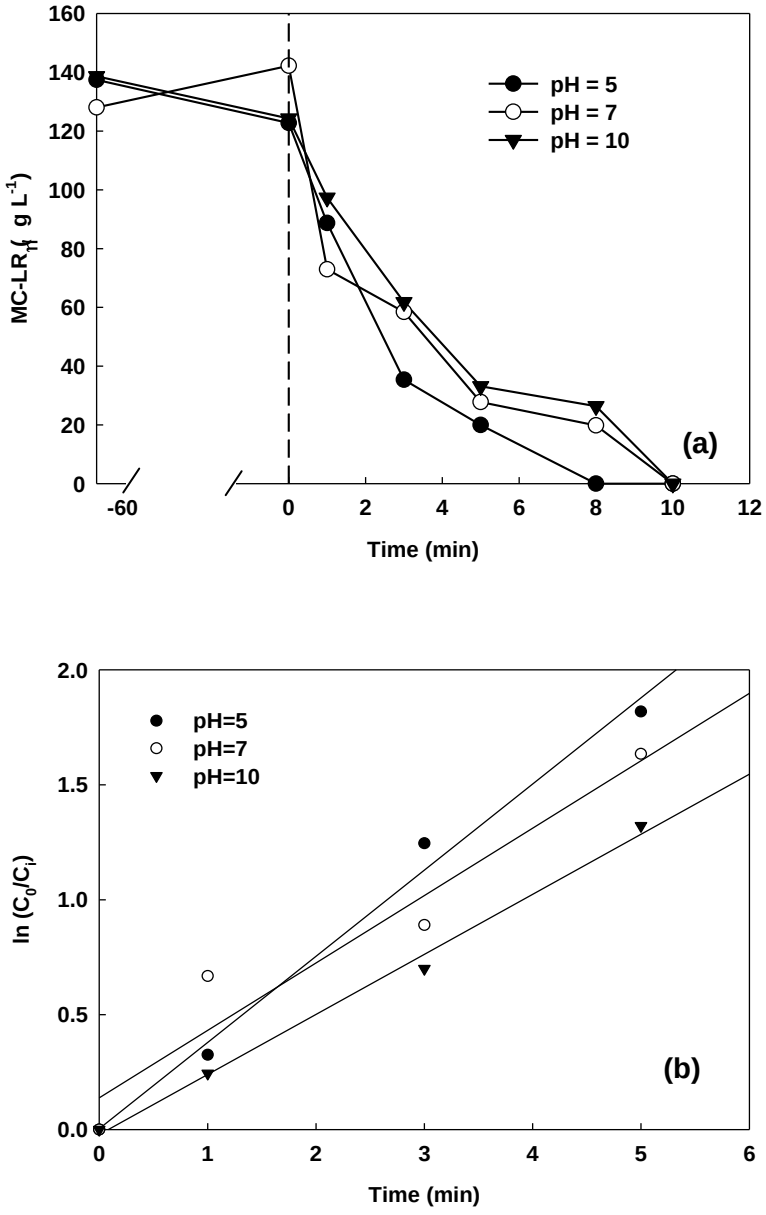

Figure 4-1 Degradation of MC-LR by 1.5 BrPTi (a) and the pseudo-first-order kinetics for photocatalytic destruction of MC-LR (b) under various pH conditions.

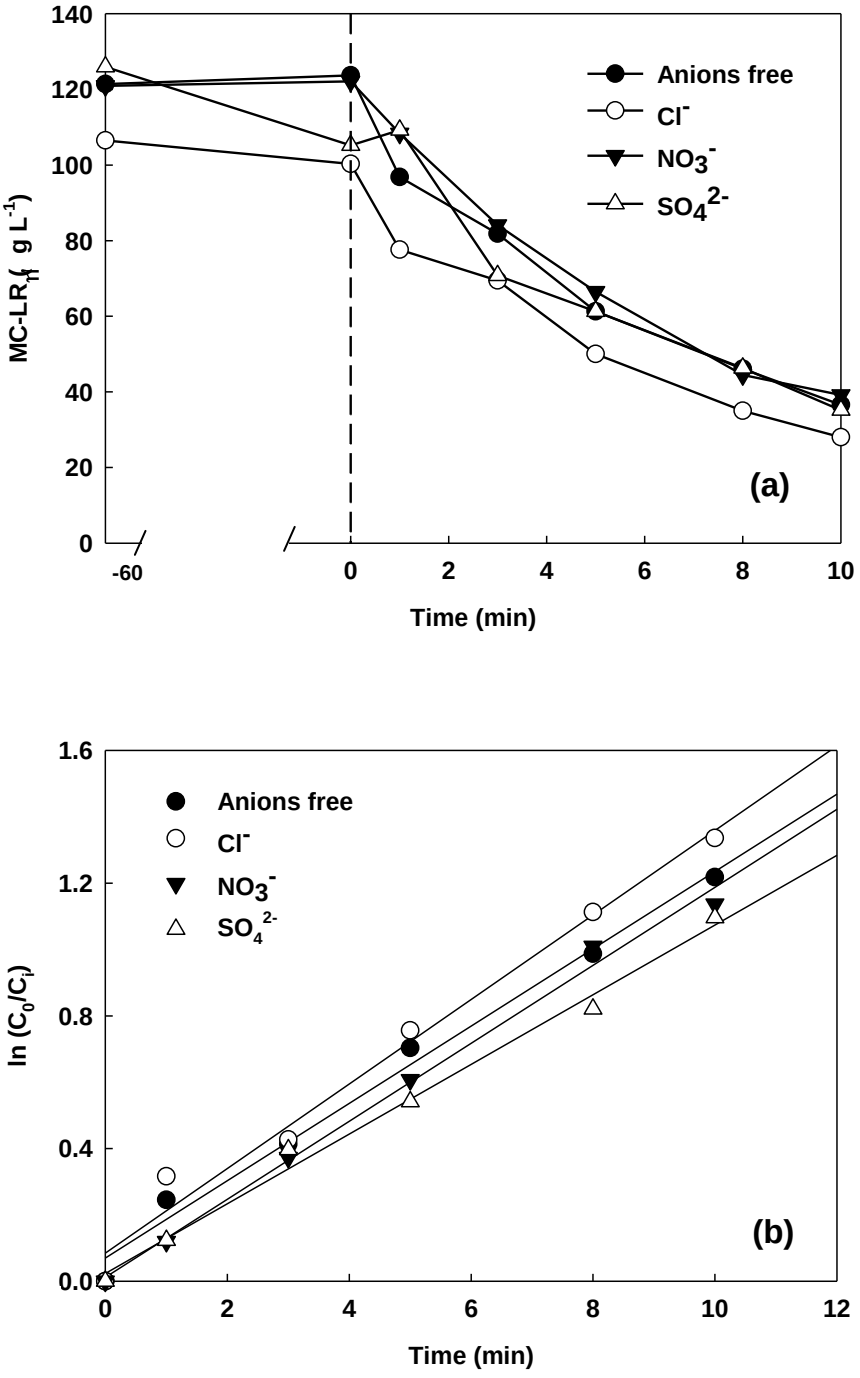

Figure 4-2 Degradation of MC-LR by 1.5 BrPTi (a) and the pseudo-first-order kinetics for photocatalytic destruction of MC-LR (b) under additional Anion conditions.

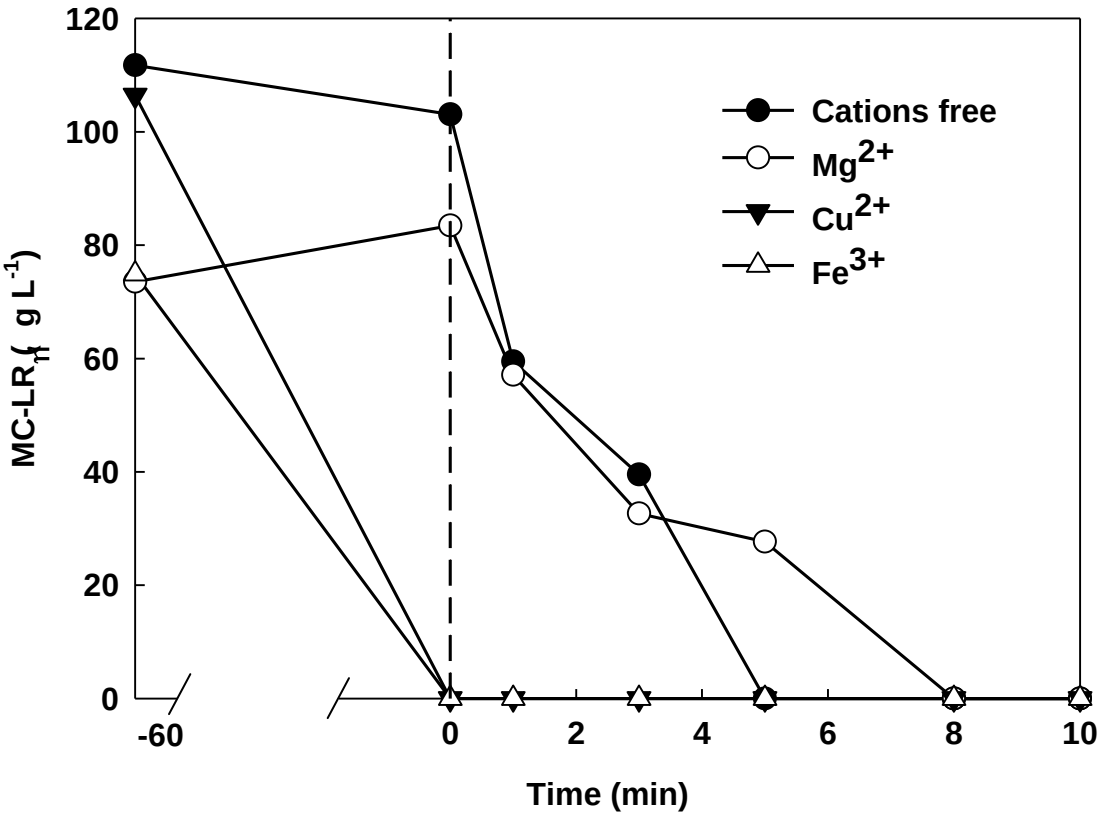

Figure 4-3 Degradation of MC-LR by 1.5 BrPTi under additional cation conditions (Mg^{2+}, Cu^{2+} and Fe^{3+}).

Mg^{2+}	Fe^{3+}	Cu^{2+}

No additional cation	Mg^{2+}	Fe^{3+}	Cu^{2+}

Figure 4-4 The aggregation state of 1.5 BrPTi catalyst in distilled water before adding metal cations (a), and after stirring 1h with additional metal cation (Mg^{2+}, Cu^{2+} and Fe^{3+}) (b).

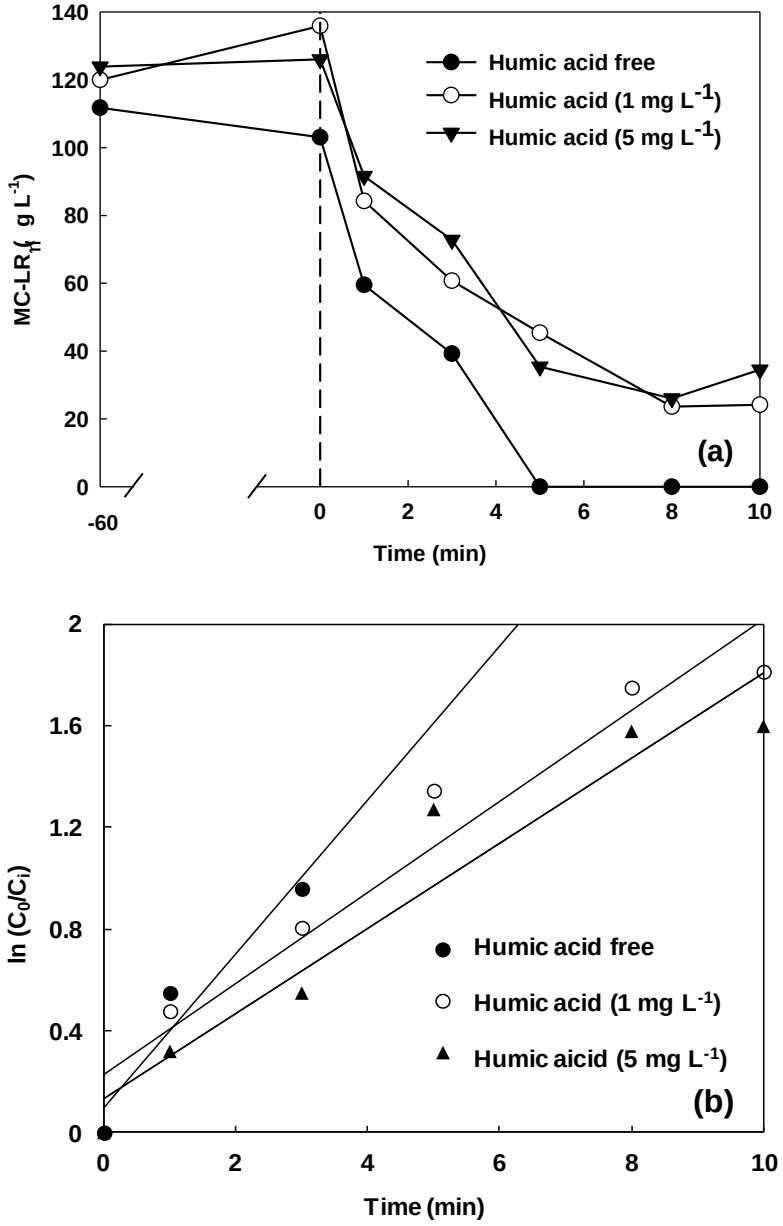

Figure 4-5 Degradation of MC-LR by 1.5 BrPTi (a) and the pseudo-first-order kinetics for photocatalytic destruction of MC-LR (b) under additional humic acid conditions.

Chapter 5 Conclusions and outlook

5.1. Conclusions

Microcystins (MCs), produced by various cyanobacteria such as *Microcystis*, *Anabaena*, *Oscillatoria* and *Nostoc* species, are a group of potent hepatotoxins for humans and wildlife. In this study, MCs (MC-LR, -YR and -RR) are proved to be effectively removed by photocatalysis. The aim of this study is to exploit a highly efficient and relatively stable photocatalyst based on Ag_3PO_4. Several attempts have been conducted to develop heterojunctions consisting of Ag_3PO_4.

Firstly, the role of Ag NPs on the photocatalytic activity and stability of Ag_3PO_4 was investigated. The results revealed that the photocatalytic activity of Ag_3PO_4 can be accelerated by Ag NPs doped on it. MC-LR was much more easily degraded by the Ag/Ag_3PO_4 catalysts than Ag_3PO_4 alone owing to the change of Ag_3PO_4 morphology and deposition of Ag nanoparticles (NPs) on Ag_3PO_4 after irradiation treatment. Besides, the oxidation of the microcystins over this heterojunction catalyst was observed to exhibit rather differently with the removal efficiency following the trend: MC-YR>MC-RR>MC-LR. However, the ratio of Ag NPs and Ag_3PO_4 for the best photocatalytic activity of the Ag/Ag_3PO_4 heterojunction in degrading MC-LR was not the one for the most stable state of it.

The AgBr was then introduced to make a further efficient and stable heterojunction $AgBr/Ag_3PO_4$, which was reported previously. However, the potential application of this heterojunction in water treatment might be not so exciting because of high cost as silver is a kind of noble metal. In this study, TiO_2 was introduced to make a novel heterojunction catalyst, $AgBr/Ag_3PO_4/TiO_2$. And the results indicated that $AgBr/Ag_3PO_4/TiO_2$ possessed higher photocatalytic capacity than $AgBr/Ag_3PO_4$ in degrading methyl orange (MO) under the simulated solar light condition, which was attributed to the increased surface area and the

combined action among Ag nanoparticles (NPs), AgBr, Ag_3PO_4 and TiO_2. Furthermore, the quenching effects of different scavengers proved that reactive h^+ and $\bullet O_2^-$ played the major role for MO degradation. In addition, $AgBr/Ag_3PO_4/TiO_2$ heterostructured photocatalyst was observed to be more stable than $AgBr/Ag_3PO_4$ in successive runs for MO removal under simulated solar light condition. On the other hand, this heterostructured $AgBr/Ag_3PO_4/TiO_2$ photocatalyst significantly decreases the loading of noble metal Ag from 72 wt% to 53 wt%, thereby significantly reducing the cost for the practical application of $AgBr/Ag_3PO_4$ photocatalyst.

This highly efficient and relatively low Ag content heterojunction was applied to degrade MCs. Similarly to methyl orange, MC-LR was observed to be more easily degraded by $AgBr/Ag_3PO_4/TiO_2$ than $AgBr/Ag_3PO_4$. And MC-YR and MC-RR could also be effectively removed by this heterojunction catalyst.

In order to evaluate the feasibility of this heterojunction catalyst applying in real MCs polluted sites. The photocatalytic activity of $AgBr/Ag_3PO_4/TiO_2$ in degrading MC-LR under various environmental conditions (pH, cations, anions and humic acid) was investigated. The results revealed that the photocatalytic activity kept high level during pH range of 5-7 although some differences were observed among these pH conditions with the highest level in the case of pH 5. Meanwhile, the photocatalytic activity of it was not affected by the introduced anions (Cl-, NO_3^- and SO_4^{2-}) of 10 mg L^{-1}. However, cations (Mg^{2+}, Fe^{3+} and Cu^{2+}) were observed to greatly affect the removal efficiency of MC-LR over this heterojunction. For Fe^{3+} and Cu^{2+}, the adsorption efficiency of MC-LR over $AgBr/Ag_3PO_4/TiO_2$ can be dramatically promoted by introducing these two cations. While Mg^{2+} was unlikely to obviously affect the adsorption capacity of MC-LR over the catalyst. Furthermore, Mg^{2+} could inhibit the degradation of MC-LR during

irradiation period, which was caused by the decrease in surface area of $AgBr/Ag_3PO_4/TiO_2$ under Mg^{2+} condition.

5.2. Outlook

A highly efficient and relatively low silver content catalyst ($AgBr/Ag_3PO_4/TiO_2$) in nano-scale has been successfully synthesized in this study. And MCs were observed to be effectively degraded by this heterojunction. As I aim to apply this heterojunction in cyanobacterial bloom sites in the future, the photocatalytic activity of it in removing other unfavorable pollutants existing in the bloom sites, such as musty odors (geosmin and 2-MIB), should be further investigated. On the other hand, photocatalysis is also an effective way to inactivate bacteria. Furthermore, the heterojunction of $AgBr/Ag_3PO_4/TiO_2$ prepared in this study is expected to release trace level of Ag^+ which possess high-performance bactericide. Therefore, it is also meaningful to investigate the activity of this heterojunction in inactivating blue-green algae in the future.

Although this nanoscale heterojunction has been proved to possess great photocatalytic activity in degrading refractory organics, a shortcoming of this nano-scale catalyst should be mentioned. That is, it cannot be directly applied to real MCs polluted sites (e.g., ponds or lakes) since nanoparticles are difficult to be separated and retrieved from water, which would raise another problem for water treatment. Therefore, for the application of this heterojunction in future, further studies should be carried out as follows:

(1) Making a photocatalytic film on solid plate using this nano-scale heterojunction by spray method, which might solve the problem of difficult separation for this catalyst.

(2) As some ions, such as Ag+ in trace concentration might release into the solution during photocatalysis, it needs to evaluate the effects of Ag+ on aquatic animals and plants.

References

Abdulla-Al-Mamun, M., Kusumoto, Y., Zannat, T., Islam M.S. (2011) Synergistic cell-killing by photocatalytic and plasmonic photothermal effects of Ag@TiO_2 core-shell composite nanoclusters against human epithelial carcinoma (HeLa) cells. *Appl Catal. A: Gen.* 398: 134-142.

Abdullah, M., Low, G.K.C., Matthews, R.W. (1990) Effects of common inorganic anions on rates of photocatalytic oxidation of organic carbon over illuminated titanium dioxide. *J. Phys. Chem.* 94: 6820-6825.

Anagnostidis, K., Komarek, J. (1985) Modern approach to the classification system of Cyanophytes 1 – Introduction. *Arch. Hydrobiol. Suppl.* 71: 291-302.

Antoniou, M.G., de la Cruz, A.A., Dionysiou, D.D. (2005) Cyanotoxins: New generation of water contaminants. *J. Environ. Eng.* 131: 1239-1243.

Antoniou, M.G., Shoemaker, J.A., de la Cruz, A.A., Dionysiou, D.D. (2008) LC/MS/MS structure elucidation of reaction intermediates formed during the TiO_2 photocatalysis of microcystin-LR. *Toxicon* 51: 1103-1118.

Antoniou, M.G., Nicolaou P.A., Shoemaker, J.A., dela Cruz, A.A., Dionysiou D.D. (2009) Impact of the morphological properties of thin TiO_2 photocatalytic films on the detoxification of water contaminated with the cyanotoxin, microcystin-LR. *Appl. Catal. B: Environ.* 91: 165-173.

Bandara, J., Kiwi, J. (1999) Fast kinetic spectroscopy, decoloration and production of H_2O_2 induced by visible light in oxygenated solutions of the azo dye Orange II. *New J. Chem.* 23: 717-724.

Bi, Y.P., Ouyang, S.X., Cao, J.Y., Ye, J.H. (2011) Facile synthesis of rhombic dodecahedral AgX/Ag_3PO_4 (X = Cl, Br, I) heterocrystals with enhanced photocatalytic properties and stabilities. *Phys. Chem. Chem. Phys.* 13: 10071-10075.

Bourne, D.G., Jones, G.J., Blakeley, R.L., Jones, A., Negri, A.P., Riddles, P. (1996) Enzymatic pathway for the bacterial degradation of the cyanobacterial cyclic peptide toxin microcystin LR. *Appl. Environ. Microbiol.* 62: 4086-4094.

Brezová, V., Borošová, A., Borošová, E., Čeppan, M., Fiala, R. (1995) The influence of dissolved metal ions on the photocatalytic degradation of phenol in aqueous TiO_2 suspensions. *J. Mol. Catal. A: Chem.* 98: 109-l 16.

Butler, E. C., Davis, A. P. (1993) Photocatalytic oxidation in aqueous titanium dioxide suspensions: The influence of dissolved transition metals. *J. Photochem. Photobiol. A: Chem*. 70: 273-283.

Cao, C.J., Zheng, B.H., Chen, Z.L. Huang, M.S. (2011a) Eutrophication and algal blooms in channel type reservoirs: A novel enclosure experiment by changing light intensity. *J. Environ. Sci. (China)* 23: 1660-1670.

Cao, J., Luo, B.D., Lin, H.L., Chen, S.F. (2011b) Photocatalytic activity of novel $AgBr/WO_3$ composite photocatalyst under visible light irradiation for methyl orange degradation. *J. Hazard. Mater*. 190: 700-706.

Cao, J., Luo, B.D., Lin, H.L., Xu, B.Y., Chen, S.F. (2012a) Visible light photocatalytic activity enhancement and mechanism of $AgBr/Ag_3PO_4$ hybrids for degradation of methyl orange. *J. Hazard. Mater*. 217-218: 107-115.

Cao, J., Luo, B.D., Lin, H.L., Xu, B.Y., Chen, S.F. (2012b) Thermodecomposition synthesis of WO_3/H_2WO_4 heterostructures with enhanced visible light photocatalytic properties. *Appl. Catal. B: Environ.* 111-112 288-296.

Chandrappa, K.G., Venkatesha, T.V. (2012) Electrochemical synthesis and photocatalytic property of zinc oxide nanoparticles, *Nano-Micro. Lett.* 4: 14-24.

Chen, P., Zhu, L.Y., Fang, S.H., Wang, C.Y., Shan, G.Q. (2012) Photocatalytic degradation efficiency and mechanism of Microcystin-RR by mesoporous Bi_2WO_6 under near ultraviolet light. *Environ. Sci. Technol.* 46: 2345-2351.

Cheng, B., Le, Y., Yu, J. G. (2010) Preparation and enhanced photocatalytic activity of Ag@TiO_2 core–shell nanocomposite nanowires. *J. Hazard. Mater.* 177: 971-977.

Chong, M.N., Jin, B., Chow, C.W.K., Saint, C. (2010) Recent developments in photocatalytic water treatment technology: A review. *Water Res.* 44: 2997-3027.

Chow, C.W.K., Drikas, M., House, J., Burch, M.D., Velzeboer, R. (1999) The impact of conventional water treatment processes on cells of the cyanobacterium *Microcystis Aeruginosa*, *Water Res.* 33: 3252-3262.

Damerval, T., Castets, A.M., Houmard, J., Tandeau de Marsac, N. (1991) Gas vesicle synthesis in the cyanobacterium Pseudanabaena sp: occurrence of a single photoregulated gene. *Mol Microbiol.* 5(3): 657-64.

Davidson, K., Gowen, R.J., Tett, P. (2012) Harmful algal blooms: How strong is the evidence that nutrient ratios and forms influence their occurrence? *Estuar. Coast. Shelf S.* 115: 399-413.

Dionysiou, D.D., Makram T.S., Evangelia B., Isabelle B., Jean-Michel L. (2000) Effect of ionic strength and hydrogen peroxide on the photocatalytic degradation of 4-chlorobenzoic acid in water. *Appl. Catal. B: Environ.* 26: 153-171.

Doll, T.E., Frimmel, F.H. (2005) Photocatalytic degradation of carbamazepine, clofibric acid and iomeprol with P25 and Hombikat UV100 in the presence of natural organic matter (NOM) and other organic water constituents. *Water Res.* 39: 403-411.

Dow, C.S., Swoboda, U.K. (2000) The Ecology of Cyanobacteria. In. Whitton, B.A., and Potts, M. (eds). *The Netherlands Kluwer Academic Publishers* pp. 613-632.

Eleuterio, L., Batista, J. R. (2010) Biodegradation studies and sequencing of microcystin-LR degrading bacteria isolated from a drinking water biofilter and a fresh water lake. *Toxicon* 55: 1434-1442.

Falconer, I.R. (2005) Cyanobacterial Toxins in Drinking Water Supplies: Cylindrospermopsins and microcystins. CRC Press, Boca Raton, Florida, USA.

Falkner, G., Strasser, P., Graffius, D. (1984) Phosphate uptake by blue green algae *in vitro* and in a lake during an algal bloom: Useful application of a force-flow relationship. *Hydrobiologia* 108: 265-271.

Fan, C.M., Sun, Y.P. (2001) Effect of calcium and magnesium on the photocatalytic oxidation of humic acid in water over TiO_2. *Chin. J. Process Eng.* 1: 427-431.

Farooq, M., Raja, I.A., Pervez, A. (2009) Photocatalytic degradation of TCE in water using TiO_2 catalyst. *Sol. Energy*. 83: 1527-1533.

Feitz, A.J., Waite, T.D., Jones, G.J., Boyden, B.H., Orr, P.T. (1999) Photocatalytic degradation of the blue green algal toxin microcystin-LR in a natural organic-aqueous matrix. *Environ. Sci. Technol.* 33: 243-249.

Feng, X.G., Rong, F., Fu, D.G., Yuan, C.W., Hu,,Y. (2006) Photocatalytic degradation of trace-level of Microcystin- LR by nano-film of titanium dioxide. *Chin. Sci. Bull.* 51: 1191-1198.

French, R.A., Jacobson, A.R., Kim, B., Isley, S.L., Lee Penn, R., Baveye, P.C. (2009) Influence of ionic strength, pH, and cation valence on aggregation kinetics of titanium dioxide nanoparticles. *Environ. Sci. Technol.* 43: 1354-1359.

Fu, G., Vary, P.S., Lin, C. J. (2005) Anatase TiO_2 nanocomposites for antimicrobial coatings. *Phys. Chem. B* 109: 8889-8898.

Gijsbertsen-Abrahamse, A.J., Schmidt, W., Chorus, I., Heijman, S.G.J. (2006) Removal of cyanotoxins by ultrafiltration and nanofiltration. *J. Membrane Sci.* 276: 252-259.

Gomathi Devi, L., Mohan Reddy, K. (2010) Enhanced photocatalytic activity of silver metallized TiO_2 particles in the degradation of an azo dye methyl orange: Characterization and activity at different pH values. *Appl. Surf. Sci.* 256: 3116-3121.

Graham, D., Kisch, H., Lawton, L.A., Robertson, P.K.J. (2010) The degradation of microcystin-LR using doped visible light absorbing photocatalysts. *Chemosphere* 78: 1182-1185.

Gupta, V., Ratha, S.K., Sood, A., Chaudhary, V., Prasanna, R. (2013) New insights into the biodiversity and applications of cyanobacteria (blue-green algae)-Prospects and challenges. *Algal Research* 2: 79-97.

Han, F., Kambala, V.S.R., Srinivasan, M., Rajarathnam, D., Naidu, R. (2009) Tailored titanium dioxide photocatalysts for the degradation of organic dyes in wastewater treatment: A review. *Appl. Catal. A: Gen.* 359: 25-40.

Harada, K., Tsuji, K., Watanabe, M.F., Kondo, F. (1996) Stability of microcystins from cyanobacteria—III.* Effect of pH and temperature. *Phycologia.* 35: 83-88.

Himberg, K., Keijola, A.M., Hiisvirta, L., Pyysalo, H., Sivonen, K. (1989) The effect of water treatment processes on the removal of hepatotoxins from *Microcystis* and *Oscillatoria* cyanobacteria; a laboratory study. *Water Res.* 23: 979-984.

Hiripi, L., Nagy, L., Kalmar, T., Kovacs, A., Voros, L. (1998) Insect (*Locusta migratoria migratorioides*) test monitoring the toxicity of cyanobacteria. *Neurotoxicology* 4-5: 605-608.

Ho, L., Onstad, G., von Guntern, U., Rinck-Pfeiffer, S., Craig, K., Newcombe, G. (2006) Differences in the chlorine reactivity of four microcystin analogues. *Water Res.* 40: 1200-1209.

Ho, L., Lambling, P., Bustamante, H., Duker, P., Newcombe, G. (2011) Application of powdered activated carbon for the adsorption of cylindrospermopsin and microcystin toxins from drinking water supplies. *Water Res.* 45: 2954-2964.

Hoffman, M.R., Martin, S.T., Choi, W., Bahnemann, D.W. (1995) Applications of Semiconductor Photocatalysis. *Chem. Rev.* 95: 69-96.

Hureiki, L., Croué, J.P., Legube, B. (1994) Chlorination studies of free and combined amino acids. *Water Res.* 28: 2521-2544.

Ismail, A.A. (2008) Single-step synthesis of a highly active photocatalyst for oxidation of trichloroethylene. *Appl. Catal. B: Environ.* 85: 33-39.

Iainliu, L., Lawton L.A., Robertson, P.J. (2003) Mechanistic studies of the photocatalytic oxidation of microcystin-LR: An investigation of byproducts of the decomposition process. *Environ. Sci. Technol.* 37: 3214-3219.

Jacinto Sá, Cristina Alcaraz Agüera, Silvia Gross, Anderson, J.A. (2009) Photocatalytic nitrate reduction over metal modified TiO_2. *Appl. Catal. B: Environ.* 85: 192-200.

Kim, J., Lee, C.W., Choi, W. (2010a) Platinized WO_3 as an environmental photocatalyst that generates OH radicals under visible light. *Environ. Sci. Technol.* 44: 6849-6854.

Kim, T.W., Lee, M.J. (2010b) Effect of pH and Temperature for Photocatalytic Degradation of Organic Compound on Carbon-coated TiO_2. *J.adv. Eng. Technol.* 3 (2): 193-198.

Kull, T.P.J., Backlund, P.H., Karlsson, K.M., Meriluoto, J.A.O. (2004) Oxidation of the cyanobacterial hepatotoxin microcystin-LR by chlorine dioxide: reaction kinetics, characterization and toxicity of reaction products. *Environ. Sci. Technol.* 38: 6025-6031.

Kull, T.P.J., Sjö vall, O.T., Tammenkoski, M.K., Backlund, P.H., Meriluoto, J.A.O. (2006) Oxidation of the cyanobacterial hepatotoxin microcystin-LR by chlorine dioxide: Influence of natural organic matter. *Environ. Sci. Technol.* 40: 1504-1510.

Kumar, S., Verma, N.K., Singla, M.L. (2012) Size dependent reflective properties of TiO_2 nanoparticles and reflectors thereof. *Dig. J. Nanomater. Bio. S.* 7: 607-619.

Kumawat, R., Bhati I., Ameta, R. (2012) Role of some metal ions enhancement of photocatalytic activity of zinc oxide. *Acta Chim. Pharm. Indica* 2: 46-53.

Lambert, T.W., Holmes, C.F.B., Hrudey, S.E. (1996) Adsorption of microcystin-LR by activated carbon and removal in full scale water treatment. *Water Res.* 30: 1411-1422.

Lawton, L.A., Robertson, P.K.J., Cornish, B.J.P.A., Jaspars, M. (1999) Detoxification of microcystins (cyanobacterial hepatotoxins) using TiO_2 photocatalytic oxidation. *Environ. Sci. Technol.* 33: 771-775.

Lawton, L.A., Robertson, P.K.J., Cornish, B.J.P.A., Marr, I.L., Jaspars, M. (2003) Processes influencing surface interaction and photocatalytic destruction of microcystins on titanium dioxide photocatalysts. *J. Catal.* 213: 109-113.

Li, G.T., Wong, K.H., Zhang, X.W. (2009a) Degradation of acid orange 7 using magnetic AgBr under visible light: The roles of oxidizing species. *Chemosphere* 76: 1185-1191.

Li, J.M., Shimizu, K., Sakharkar, M., Utsumi, M., Zhang, Z.Y., Sugiura, N. (2011) Comparative study for the effects of variable nutrient conditions on the biodegradation of microcystin-LR and concurrent dynamics in microcystin-degrading gene abundance. *Bioresour. Technol.* 102: 9509-9517.

Li, Y.H., Wang, Y., Yin, L.H., Pu, Y.P. (2009b) Using the nematode *Caenorhabditis elegans* as a model animal for assessing the toxicity induced by microcystin-LR, *J. Environ. Sci.-China* 21: 395-401.

Liang, P., Qin, Y.C., Hu, B., Li, C.X. (2000) Study of the adsorption behavior of heavy metal ions on nanometer-size titanium dioxide with ICP-AES. *Fresenius J. Anal. Chem.* 368: 638-640.

Lin, H., Huang, C.P., Li, W., Ni, C., Ismat Shah, S., Tseng, Y.H. (2006) Size dependency of nanocrystalline TiO_2 on its optical property and photocatalytic reactivity exemplified by 2-chlorophenol. *Appl. Catal. B: Environ.* 68: 1-11.

Liou, J.W., Chang, H.H. (2012) Bactericidal effects and mechanisms of visible light-responsive titanium dioxide photocatalysts on pathogenic bacteria. *Arch. Immunol. Ther. Exp.* 60: 267-275.

Litter, M.I. (1999) Heterogeneous photocatalysis transition metal ions in photocatalytic systems. *Appl. Catal. B: Environ.* 23: 89-114.

Liu, I., Lawton, L., Robertson, P.K.J. (2003) Mechanistic studies of the photocatalytic oxidation of microcystin-LR: An investigation of byproducts of the decomposition process. *Environ. Sci. Technol.* 37: 3214-3219.

Liu, Y.L., Guo, L.J., Yan, W., Liu, H.T. (2006) A composite visible-light photocatalyst for hydrogen production. *J. Power Sources* 159: 1300-1304.

Liu, Y.G., Ohko, Y., Zhang, R.Q., Yang, Y.N., Zhang, Z.Y. (2010) Degradation of malachite green on Pd/WO_3 photocatalysts under simulated solar light. *J. Hazard. Mater.* 184: 386-391.

Liu, W.S., Peng, Y.H., Shiumg, C.E. (2012a) The effect of cations on the aggregation of commercial ZnO nanoparticle suspension. *J. Nanopart. Res.* 14:1259.

Liu, Y.P., Fang, L., Lu, H.D., Liu, L.J., Wang, H., Hu, C.Z. (2012b) Highly efficient and stable Ag/Ag_3PO_4 plasmonic photocatalyst in visible light. *Catal. Commun.* 17: 200-204.

Lora, E., Fleming, Carlos R. (2002) Blue green algal (cyanobacterial) toxins, surface drinking water and liver cancer in Florida. *Harmful Algae* 1: 157-168.

Meng, S.G., Li, D.Z., Sun, M., Li, W.J., Wang, J.X., Chen, J., Fu, X.Z., Xiao, G.C. (2011) Sonochemical synthesis, characterization and photocatalytic properties of a novel cube-shaped $CaSn(OH)_6$. *Catal. Commun.* 12: 972-975.

Miao, H.F., Qin, F., Tao, G.J., Tao, W.Y., Ruan, W.Q. (2010) Detoxification and degradation of microcystin-LR and -RR by ozonation. *Chemosphere* 79: 335-361.

Morimoto, T., Suzuki, K., Torikoshi, M., Kawahara, T., Tada, H. (2007) Ag(core)-AgCl(shell) standard microelectrode-loaded TiO_2. *Chem. Commun.* 4291-4293.

Mouchet, P., Bonn ́aye, V. (1998) Solving algae problems: French expertise and world-wide applications. *J. Water Supply Res. T.* 47: 125-141.

Newcombe, G., Nicholson, B. (2004) Water treatment options for dissolved cyanotoxins. . *J. Water Supply Res. T.* 53: 227-239.

Oberholster, P.J., Botha, A.M., Grobbelaar, J.U. (2004) *Microcystis aeruginosa*: Source of toxic microcystins in drinking water. *Afr. J. Biotechnol.* 3: 159-168.

Okano, K., Maseda, H., Sugita, K., Saito, T., Utsumi, M., Maekawa, T., Kobayashi, M., Sugiura, N. (2006) Biochemical characteristics of microcystin LR degradation by typical protease. *Jpn. J. Water Treat. Biol.* 42: 27-35.

Paerl, H.W. (2006) Assessing and managing nutrient-enhanced eutrophication in estuarine and coastal waters: Interactive effects of human and climatic perturbations. *Ecol. Eng.* 26: 40-54.

Parmar, A., Singh, N.K., Pandey, A., Gnansounou, E., Madamwar, D. (2011) Cyanobacteria and microalgae: A positive prospect for biofuels. *Bioresour. Technol.* 102(22): 10163-10172.

Patsios, S.I., Sarasidis, V.C., Karabelas, A.J. (2013) A hybrid photocatalysis–ultrafiltration continuous process for humic acids degradation. *Sep. Purif. Technol.* 104: 333-341.

Pelaez, M., de la Cruz, A., O'She, K., Falaras, P., Dionysiou, D.D. (2011) Effects of water parameters on the degradation of microcystin-LR under visible light-activated TiO_2 photocatalyst. *Water Res.* 45: 2787-3796.

Pelaez, M., Falaras, P., Likodimos, V., Kontos, A.G., de la Cruz, A.A., O'shead, K. Dionysiou, D.D. (2010) Synthesis, structural characterization and evaluation of sol–gel-based NF-TiO_2 films with visible light-photoactivation for the removal of microcystin-LR. *Appl. Catal. B: Environ.* 99: 378-387.

Pelaez, M., Falaras, P., Kontos, A.G., de la Cruz, A.A., O'shea, K., Dunlop, P.S.M., Byrne, J.A., Dionysiou, D.D. (2012a) A comparative study on the removal of cylindrospermopsin and microcystins from water with NF-TiO_2-P25 composite films with visible and UV–vis light photocatalytic activity. *Appl. Catal. B: Environ.* 121-122: 30-39.

Pelaez, M., Nolanb, N.T., Pillai, S.C., Seery, M.K., Dionysiou, D.D. (2012b) A review on the visible light active titanium dioxide photocatalysts for environmental applications. *Appl. Catal. B: Environ.* 125: 331-349.

Piscopo, A., Didier, R., Victor, W.J. (2001) Influence of pH and chloride anion on the photocatalytic degradation of organic compounds Part I. Effect on the benzamide and *para* hydroxybenzoic acid in TiO_2 aqueous solution. *Appl. Catal. B: Environ.* 35: 117-124.

Pouria, S., de Andrade, A., Barbosa, J., Cavalcanti, R.L., Barreto, V.T.S. (1998) Fatal microcystin intoxication in haemodialysis unit in Caruaru, Brazil. *The Lancet* 352: 21-26.

Rahman, M.M., Khan, S.B., Marwanil H.M., Asiri, A.M., Alamry K.A. (2012) Selective Iron (III) ion uptake using CuO-TiO_2 nanostructure by inductively coupled plasma-optical emission spectrometry. *Chem. Cent. J.* 6: 158-168.

Reckhow, D.A., Platt, T.L., MacNeill, A.L. (2001) Formation and degradation of dichloroacetonitrile in drinking waters. *J. Water Supply: Res. Technol.-Aqua.* 50: 1-13.

Rodr ǵuez, E., Majado, M.E., Meriluoto, J., Acero, J.L. (2007) Oxidation of microcystins by permanganate: Reaction kinetics and implications for water treatment. *Water Res.* 41: 102-110.

Rodr ǵuez, E.M., Acero, J.L., Spoof, L., Meriluoto, J. (2008) Oxidation of MC-LR and -RR with chlorine and potassium permanganate: Toxicity of the reaction products. *Water Res.* 42: 1744-1752.

Sellner, K.G., Doucette, G.J., Kirkpatrick, G.J. (2003) Harmful algal blooms: Causes, impacts and detection. *J. Ind. Microbiol. Biotechnol.* 30: 383-406.

Sharma, V.K., Triantis T.M., Antoniou M.G. (2012) Destruction of microcystins by conventional and advanced oxidation processes: A review. *Sep. Purif. Technol.* 91: 3-17.

Shephard, G.S., Stockenstrom, S., de Villiers, D., Engelbrecht, W.J., Wessels, G.F.S. (2002) Degradation of microcystin toxins in a falling film photocatalytic reactor with immobilized titanium dioxide catalyst. *Water Res.* 36: 140-146.

Shibuya, M., Miyauchi, M. (2009) Site-selective deposition of metal nanoparticles on aligned WO_3 nanotrees for super-hydrophilic thin films. *Adv. Mater.* 21: 1373-1376.

Sushi, K.K., Navjeet, K., Sukhmehar, S. (2009) Photocatalytic degradation of two commercial reactive dyes in aqueous phase using nanophotocatalysts. *Nanoscale Res. Lett.* 4:709-716.

Tran, T.H., Nosaka, A.Y., Nosaka, Y. (2006) Adsorption and photocatalytic decomposition of amino acids in TiO_2 photocatalytic systems. *J. Phys. Chem. B* 110: 25525-25531.

Triantis, T.M., Fotiou, T., Kaloudis, T., Kontos, A.G., Falaras, P., Dionysiou, D.D., Pelaezd, M., Hiskia, A. (2012) Photocatalytic degradation and mineralization of microcystin-LR under UV-A, solar and visible light using nanostructured nitrogen doped TiO_2. *J. Hazard. Mater.* 211- 212: 196-202.

Tsuji, K., Naito, S., Kondo, F., Ishikawa, N., Watanabe, M.F., Suzuki, M., Harada, K.I. (1994) Stability of microcystins from cyanobacteria: Effect of light on decomposition and isomerization. *Environ. Sci. Technol.* 28: 173-177.

Wang, P., Huang, B.B., Qin, X.Y., Zhang, X.Y., Dai, Y., Wei, J.Y., Whangbo, M.H. (2008) Ag@AgCl: A highly efficient and stable photocatalyst active under visible light. *Angew. Chem. Int. Ed.* 47: 7931-7931.

Wang, P., Huang, B.B., Zhang, X.Y., Qin, X.Y., Jin, H., Dai, Y., Wang, Z.Y., Wei, J.Y., Zhan, J., Wang, S.Y., Wang, J.P., Whangbo, M.H. (2009) Highly efficient visible-light plasmonic photocatalyst Ag@AgBr. *Chem. Eur. J.* 15: 1821-1824.

Wang, H.J., Chen, X.Y. (2011a) Kinetic analysis and energy efficiency of phenol degradation in a plasma-photocatalysis system. *J. Hazard. Mater.* 186: 1888-1892.

Wang, X., Hao, C.B., Feng, C.P., Yang, Y.N. (2011b) Inhibition of the growth of two blue-green algae species (*Microsystis aruginosa* and *Anabaena spiroides*) by acidification treatments using carbon dioxide. *Bioresour. Technol.* 102: 5742-5748.

Wei, J., Li, H.Y., Mao, S.C., Zhang, C., Xu, Z., Dkhil, B. (2012) Effect of particle morphology on the photocatalytic activity of $BiFeO_3$ microcrystallites. *J. Mater. Sci: Mater. Electron.* 23: 1869-1874.

Welker, M., Steinberg, C. (2000) Rates of humic substance photosensitized degradation of microcystin-LR in natural waters. *Environ. Sci. Technol.* 34: 3415-3419.

WHO, (1998) Guidelines for Drinking-water Quality. Addendum to Volume 2, Health Criteria and Other Supporting Information, second ed. World Health Organization, Geneva.

WHO, (2003) Algae and cyanobacteria in fresh water. In Guidelines for safe recreational water environments. Organization, W.H. (ed). Geneva, pp.136-158.

Xia, X.X., Xu, J.L., Ying, Y. (2002) Effects of common inorganic anions on the rates phtocatlalytic degradation of sodium dodecylbenzenesulfonate over illuminated titanium dioxide. *J. Environ. Sci.* 14: 188-194.

Xu, B. (2010) Adsorption behavior of metal cations on gold nanoparticle surfaces studied by isothermal titration microcalorimetry. *J. Chin. Chem. Soc.* 57: 309-315.

Xue, G., Hiu, H.H., Chen, Q.Y., Hills, C. (2011) Synergy between surface adsorption and photocatalysis during degradation of humic acid on TiO_2/activated carbon composites. *J. Hazard. Mater.* 186: 765-772.

Yang, J.K., Lee, S.M. (2006) Removal of Cr(VI) and humic acid by using TiO_2 photocatalysis. *Chemosphere* 63: 1677-1684.

Yao, W.F., Zhang, B.C., Huang, P., Ma, C., Song, X.L., Xu, Q.J. (2012) Synthesis and characterization of high efficiency and stable Ag_3PO_4/TiO_2 visible light photocatalyst for the degradation of methylene blue and rhodamine B solutions. *J. Mater. Chem.* 22: 4050-4055.

Yi, Z.G., Ye, J.H., Kikugawa, N., Kako, T., Ouyang, S.X., Stuart-Williams, H. (2010) An orthophosphate semiconductor with photooxidation properties under visible-light irradiation. *Nature Materials* 9: 559-564.

Yin, M.C., Li, Z.S., Kou, J.H., Zou, Z.G. (2009) Mechanism investigation of visible light-induced degradation in a heterogeneous TiO_2/eosin Y/rhodamine B system. *Environ. Sci. Technol.* 43: 8361-8366.

Yu, J.G., Dai, G.P., Huang, B.B. (2009) Fabrication and characterization of visible-lightdriven plasmonic photocatalyst $Ag/AgCl/TiO_2$ nanotube arrays. *J. Phys. Chem. C* 113: 16394-16401.

Yu, J.G., Qi, L.F., Jaroniec, M. (2010) Hydrogen production by photocatalytic water splitting over Pt/TiO_2 nanosheets with exposed (001) facets. *J. Phys. Chem. C* 114: 13118-13125.

Yun, H.J., Lee, H., Kim, N.D., Yi, J. (2009) Characterization of photocatalytic performance of silver deposited TiO_2 nanorods. *Electrochem. Commun.* 11: 363-366.

Zanella, R., Giorgio, S., Henry, C., Louis, C.J. (2002) Alternative methods for the preparation of fold nanoparticles supported on TiO_2. *Phys. Chem. B* 106: 7634-7642.

Zang, Y.J., Farnood, R. (2008) Photocatalytic activity of $AgBr/TiO_2$ in water under simulated sunlight irradiation. *Appl. Catal. B: Environ.* 79: 334-340.

Zhang, W., Luo, Y.P., Hu, Z.C., Zhang, C.P. (1998) The investigation of interaction on catalase with silver (I) ion. *Chin. J. Spectrosc. Lab.* 2: 14-21.

Zhang, N., Liu, S.Q., Fu, X.Z., Xu, Y.J. (2011) Synthesis of $M@TiO_2$ (M = Au, Pd, Pt) core_shell nanocomposites with tunable photoreactivity. J. *Phys. Chem. C* 115: 9136-9145.

Zhu, X., Castleberry, S. R., Nanny, M. A., Butler, E. C. (2005), Effects of pH and catalyst concentration on photocatalytic oxidation of aqueous ammonia and nitrite in titanium dioxide suspensions, *Environ. Sci. Technol.* 39: 3784-3791.

Acknowledgements

. First and foremost, I would like to express my sincere appreciation to my advisor, Professor Norio Sugiura, for providing me the opportunity to study in Tsukuba University and undertake my research. His enthusiasm, amicability, and generosity make me feel warm in Japan, and his erudition and encouragement always guide me forward. I also would like to express my sincere appreciation to my co-supervisor, associate professor Motoo Utsumi, for his profound expertise, dedication, and patience during my doctor study. He has enlightened me how to conduct a good scientific work through his wide knowledge and rigorous scholarship.

I also wish to express my appreciations to professor Zhenya Zhang and professor Yingnan Yang for their supports, invaluable guidance and advices on my research.

I would also like to express my great appreciation to my thesis committee members, Professor Norio Sugiura, Motoo Utsumi, Zhenya Zhang, Yingnan Yang and Zhongfang Lei for their patient reading and listening, numerous suggestions and comments. All their instructors provided great help for the improvement of my dissertation and future study.

I would also like to thank Professor Chuanping Feng for the recommendation and the support for my abroad study. He taught me the truth in life, and I will remember it all my life.

I also want to express my great appreciation to China Scholarship Council for support me to study in Doctoral Program of Graduate School of Life and Environmental Sciences, University of Tsukuba.

Then I would like to thank Kazuya Shimizu, Xiaowei Tian, Dawei Li, Yu Gao and Jieming Li Shenghao Wang and Weijie Du who often discuss with me and I learned a lot of experiment design and data analysis methods from them. I would also like to thank Lili Hou, Yingxin Zhao,

Qintong Li, Hailong Cui, Yoshiteru Hamatani, Mariko Hirokawa for their help in my study and life. I also wish to thank my friends of Shengjiong Yang, Nan Xiang, Mawen Chao, Chie Amano, Shintaro Yamaguchi and many others for being with me for my beautiful life in Tsukuba.

Finally, I would like to thank my dearest family members, my parents, Qiguang Wang and Qionge Fu, my sisters and brothers. I would also like to express my appreciation to my friend, Ban Wang. This dissertation would not have been completed without their love and support.